To the Graduate Council:

I am submitting herewith a dissertation written by John Henry Blackson entitled "Phase Contrast Transmission Electron Microscopy Using Phase Plates." I have examined the final copy of this dissertation for form and content and recommend that it be accepted in partial fulfillment of the requirements for the degree of Doctor of Philosophy, with a major in Zoology.

David C Joy.
Dr. David C. Joy, Major Professor

We have read this disseration
and recommend its acceptance:

Raymond A. Buchana
Dr. Raymond Buchanan

David P. Gerard
Dr. David Gerard

John R Kennedy
Dr. John Kennedy

Accepted for the Council:

C.W. Minkel
Associate Vice Chancellor and
Dean of The Graduate School

PHASE CONTRAST TRANSMISSION ELECTRON MICROSCOPY USING PHASE PLATES

A Dissertation

Presented for the

Doctor of Philosophy

Degree

The University of Tennessee, Knoxville

John Henry Blackson

December 1995

DEDICATION

This dissertation is dedicated to

my loving wife, Marcia,

who has been my helper and

companion for over 20 years.

ACKNOWLEDGMENTS

I would like to thank the Dow Chemical Company for its financial support and for Dow management's willingness to allow me to pursue this degree. Specifically, I would like to acknowledge Ray Chrisman, my Research Manager at the start of this program, for helping make it possible. Don Beaman, my mentor and friend has provided support, encouragement and an example throughout my Dow career for which I am truly grateful.

I would like to thank my committee, Dr. Raymond Buchanan, Dr. David Gerard, Dr. John Kennedy and my major professor Dr. David Joy for their guidance and willingness to serve in this capacity. I also would like to thank Dr. Joy for his insight and patience throughout this process.

David Susnitzky's and Don Beaman's willingness to edit this manuscript is also gratefully acknowledged. Xiao Zhang's helpful collaboration during electron holography experiments was the start of what has become a good friendship. Charlie Wood was a tremendous help during the modeling experiments. He willingly shared his knowledge of computers making this part of the study a success.

I would also like to acknowledge the Oak Ridge National Laboratory High Temperature Materials Lab for the use of their microscopy facilities for a portion of this study.

Finally and most of all, the loving support of my son, Joshua, daughters, Johanna and Jeanette and my wife, Marcia, who have sacrificed much to make this possible, including having to pick up and move from Michigan to Tennessee for a school year, is gratefully acknowledged. Marcia's willingness to type this

manuscript and her love, understanding and support are appreciated more than words can describe.

ABSTRACT

Transmission electron microscopy of weakly scattering materials like thin sections of cells and polymers often leads to poor image contrast and poor transfer of information with a spatial frequency lower than around 2 nm. In addition, the information contained in the phase of the specimen exit wave is often lost due to an inability to directly record phase changes. Electron Holography, which is difficult and expensive to practice has proven ineffective at significantly improving image contrast in many cases. Another method for generating phase contrast involves the use of phase plates that until now were not practical for routine transmission electron microscopy (TEM). This work describes two phase plates, one employing a contamination spot and the other an electrically compensated electrostatic phase plate that can be routinely used in modern TEM to enhance contrast. This method should prove to be particularily useful where heavy metal stains are ineffective or where they must be avoided to preserve the sample integrity. Examples of the use of these plates to improve images of polymers, biological cells and catalysts are presented. Results show significant contrast improvement for features greater than 2 nm in dimension.

TABLE OF CONTENTS

LIST OF TABLES

LIST OF FIGURES

LIST OF SYMBOLS

R_{min}	.....	minimum periodicity (resolution limit)
R	.....	spatial frequency = 1/s
$R_c(\mathbf{r})$	.....	spatial carrier frequency
d_o	.....	diameter of the specimen
α_i	.....	illumination aperture angle
λ	.....	wavelength
dz	.....	specimen thickness
V_i	.....	internal potential (including mean inner potential and magnetic and electric fields)
V_a	.....	accelerating potential
$\Phi(\mathbf{r})$	.....	object phase shift
$A(\mathbf{r})$	.....	object amplitude
$\varphi(\mathbf{r})$	.....	image wave phase
$\mathbf{r}$	.....	position vector
η	.....	refractive index
$\mathbf{u}$	.....	undiffracted wave vector
$\mathbf{d}$	.....	diffracted wave vector
$\mathbf{p}$	.....	object wave vector
τ	.....	transmittance of phase plate

Δz	.....	objective lens defocus
α	.....	scattering angle
t	.....	film thickness
C	.....	contrast
I_p	.....	intensity on a particle
I_b	.....	intensity of the background
Θ	.....	aperture angle
b	.....	$0.9788 \times 10^{-6}\ V^{-1}$
k	.....	a correction parameter for the lens field surrounding a sculptured phase plate
r	.....	radius
f or f_o	.....	focal length of the objective lens
m	.....	integer
ε_o	.....	permittivity in vacuum
e	.....	charge on an electron
q	.....	positive charge units on the phase plate
K	.....	$-e/8\ \pi E_o V_a$
$U(\mathbf{r})$ or $U_o(\mathbf{r})$	.....	exit wave or modified wave front
$U_o^{cc}(\mathbf{r})$	.....	complex conjugate of U_o
U_{op}	.....	optimum image contrast
$a(\mathbf{r})$	.....	image amplitude

$\gamma(\alpha)$	.....	total phase shift when using an electrostatic phase plate
S	.....	periodic spacing in the object
FT	.....	Fourier transform
C_c	.....	coefficient of chromatic abberation
C_s	.....	coefficient of spherical aberration
$I(\mathbf{r})$	.....	image intensity distribution
$I_{hol}(\mathbf{r})$	.....	image intensity distribution in the hologram
$\chi(R)$	.....	phase factor
N	.....	phase plate absorption factor
S_{min}	.....	minimum periodicity (resolution limit)
Ψ	.....	phase plate phase shift

CHAPTER ONE

INTRODUCTION

Electron microscopy impacts the lives of all members of civilized society and it represents an indispensable tool of the scientist and engineer. It contributes to the development of modern materials, failure analysis, advances in medicine, forensic science and to the exploration of geological materials and it increases our understanding of plant and animal anatomy and physiology.

The two major classes of electron microscopes, scanning electron microscopy (SEM) and transmission electron microscopy (TEM) have historically provided unique types of information. The SEM uses backscattered and emitted electrons to reveal surface information while the TEM uses elastically and inelastically transmitted electrons to show the structure of thin (electron transparent) materials. This distinction is not as clear in modern instruments where SEMs equipped with transmitted electron detectors and TEMs equipped with scanning attachments and secondary and backscattered electron detectors overlap in function.

This work will concentrate on the problems associated with the direct examination of weakly scattering, low contrast, organic materials by transmission electron microscopy. As in light microscopy, prior to the development of phase contrast optics, organic materials, both man made and natural, required differential staining with high scattering components to impart image contrast. In electron microscopy, these stains have included OsO_4, RuO_4, salts of lead and uranium and phosphotungstic acid. Phase contrast light microscopy revolutionized the biological sciences by making it possible to view living

materials without the need for chemical stains that generally caused cell death. Electron microscopy is moving in a similar direction to expedite the examination of biological materials in a near living state. Current trends include cryogenic techniques to preserve antigenicity of cellular components and to prevent the loss and/or movement of ionic species (Shi et al. 1994). The former is necessary to take advantage of developments in immuno-labeling and the latter for undisturbed elemental analysis using high spatial resolution energy dispersive x-ray microanalysis (EDS) or parallel detection electron energy loss spectroscopy (PEELS). Both of these techniques require observation of sections unaltered by chemical fixatives and heavy metal staining; however, in the absence of stains, etc., it is difficult to identify cellular structure due to lack of contrast. Synthetic polymers are also often difficult to image and in some cases, there are no known heavy metal stains.

Several attempts (Agar et al. 1949; Locquin 1954; Kanaya et al. 1957; Faget et al. 1960a, b; 1962; Johnson and Parsons 1967; 1970; 1973; Parsons 1976; Parsons and Johnson 1972; Willasch 1975; Thon and Willasch 1970; 1971a, b; 1972; Badde and Reimer 1970; Reimer and Badde 1970; Unwin 1971; 1972; 1973; 1974; Krakow and Siegel 1975; Balossier and Bonnet 1981) have been made during the last forty years to realize the electron equivalent of Zernike phase contrast light optics to use the phase information lost in traditional electron microscopy. For weakly scattering biological materials the phase information potentially contains more contrast than the amplitude information. Attempts to convert electron wave phase differences to amplitude differences have included various designs of phase plates, objective lens defocusing and electron holography. The shortcoming of defocus contrast has been the limited region of usable contrast transfer due to zeros and contrast inversions, while the

use of electron holography is limited due to the need for a bright, highly coherent electron source that has only recently become commercialized through the development of modern field emission gun transmission electron microscopes (FEGTEM). Many researchers do not have access to FEGTEM because of the high cost (greater than $1,000,000). In addition, the most widely practiced mode of electron holography, off axis electron holography, requires *aposteriori* reconstruction of the hologram (Tonomura et al. 1968) making it less desirable as a contrast enhancing mechanism for morphological characterization prior to elemental analysis that requires in-situ imaging. Phase contrast enhancement using phase plates, at least in theory, offers a viable alternative. The ideal situation would be a $\pi/2$ phase shifting device that would enable constructive and destructive interference and that would attenuate the unscattered electron wave while retaining the microscopes resolving power. The device would also be stable over long periods of use, and could be retrofitted to most conventional TEMs. In practice such a device has not been realized either due to design constraints or instrument limitations such as limited beam brightness, vacuum cleanliness, and a precise centering holder. Modern instruments have overcome many of these limitations through improved vacuum technology incorporating ion and magnetically levitated turbomolecular pumps, higher accelerating voltage, LaB_6 emitters and precise aperture translators. The goal of this current investigation is to develop a practical, efficient, phase plate with long useful life and to compare it with other methods of phase contrast enhancement.

A review of the literature revealed the development of two main types of phase plates. One uses a single fine filament made partially conductive and suspended across an aperture on which a point charge develops as a result of the non-scattered transmitted electron beam (Unwin 1971; 1972; 1973; 1974).

This electrostatic device's major short comings have been: contamination during prolonged use, which changes the electrostatic properties; low brightness imaging conditions that result from controlling the electrostatic field by adjusting the illumination intensity; and an asymmetric electrostatic field that leads to image distortion.

In the second class of phase plates, thin foils preferentially shift the phase of the scattered wave front. These devices have had many of the same short comings as the electrostatic devices including contamination and operation under low brightness conditions. In addition, these films further scatter the already weak scattered wave front and have not incorporated a method for attenuating the intensity of the unscattered wave front that is necessary for maximum contrast realization.

Initially, experiments of previous workers (Agar et al. 1949; Unwin 1971; 1972; 1973; 1974) were duplicated in an attempt to gain experience with these devices on a modern electron microscope. Next, attempts were made to improve these devices with the goal of developing an effective direct phase contrast device that could be used in most modern commercial TEMs without significant alteration and with long term stability.

All phase plate experiments were performed on a Topcon 002B, 200 keV high resolution TEM equipped with a LaB_6 emitter, Gatan model 676 high resolution video camera and a Gatan Model 690 384 x 576 pixel slow scan CCD camera. The slow scan CCD camera coupled with Gatan's Digital Micrograph software enables direct digital image recording. At Scherzer defocus (38.8 nm), optimum contrast transfer on this microscope is limited to spatial frequencies between 0.8 nm and 0.2 nm (Figure 1.1). Many organic materials have important details with spatial frequencies larger than 0.8 nm that are not

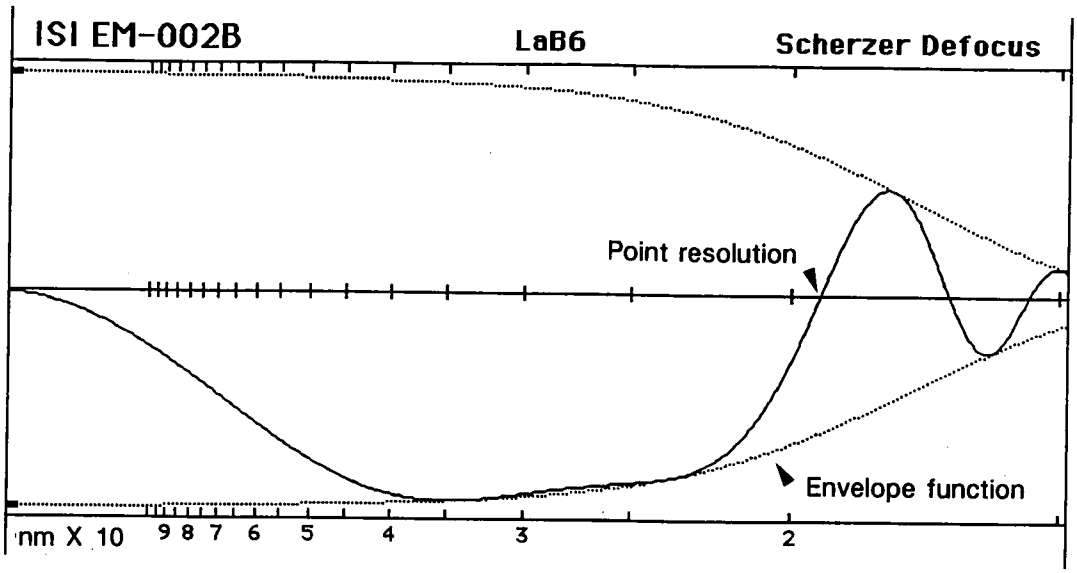

Accelerating voltage=200keV
Thickness= 10 nm

C_s=0.4 mm
Illumination semi-angle= 1.0 mRad

Figure 1.1. Contrast transfer function for a Topcon 002B at Scherzer defocus (-38.8 nm).

efficiently transferred. Contrast can be enhanced at these spatial frequencies by defocusing the objective lens but only at the expense of contrast inversions and zeros at other needed spatial frequencies (Figure 1.2).

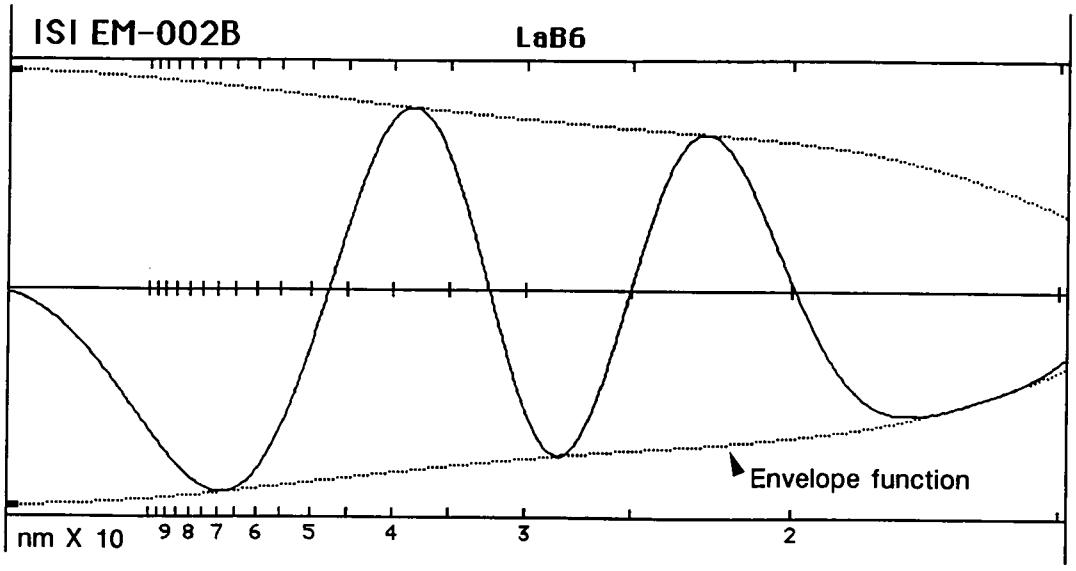

Accelerating voltage= 200 keV
Thickness= 10 nm

C_s= 0.4 mm
Illumination Semi-angle= 1.0 mRad

Figure 1.2. Contrast transfer function for a Topcon 002B at a defocus of -100 nm.

CHAPTER TWO

IMAGE THEORY

A primary use of transmission electron microscopy is to reveal structure of an object at a resolution better than that available with light microscopy. Uniform information transfer from the largest features to the resolution limit of the TEM would usually be desirable.

The theory of image formation for electron microscopy has many similarities to light microscopy. A point source of radiation defocused by a condenser lens forms a near parallel beam. A condenser aperture defines the illuminating beam and limits the radiation passing through the periphery of the lens. The incident beam then strikes the sample perturbing some of the radiation causing it to be diffracted to an angle that increases as the object dimensions decrease. The collimated, undiffracted, transmitted beam enters the objective lens that focuses it at the back focal point of the objective lens. This is typically the plane of the objective aperture in the transmission electron microscope. The image of the object appearing at the image plane is a result of the interference of the diffracted and undiffracted beams. Two contrast variables describe the lens transfer function, $U(\mathbf{r})$, the amplitude contrast, $a(\mathbf{r})$, formed by differential transfer of the scattered wave and in practice defined by the objective aperture size and $\varphi(\mathbf{r})$ the contribution due to the phase shift or path difference between the scattered and unscattered wave (Pluta 1989; Lichte 1991).

$$U(\mathbf{r}) = a(\mathbf{r}) \exp [i\varphi(\mathbf{r})] \quad (2.1)$$

where: $\mathbf{r}$ = (x,y) a position vector

$a(\mathbf{r})$ = wave amplitude

$\varphi(\mathbf{r})$ = wave phase

Typically for thin, non-crystalline, materials the intensity of the diffracted beam is small in comparison to the undiffracted beam and the phase shift is too small for significant constructive or destructive interference. In electron microscopy, the objective lens aberrations further modify the exit wave front by a function $\chi(R)$. The phase factor $\chi(R)$ was first described by Scherzer (1949).

For an object with a periodic spacing R, pure phase contrast exists if $\chi(R)$ equals an odd multiple of $\pi/2$ as described by the phase contrast transfer function:

$$PCTF = 2 \sin (\chi(R)) \quad (2.2)$$

Pure amplitude contrast occurs if $\chi(R)$ equals an even multiple of $\pi/2$ as described by the amplitude contrast transfer function:

$$ACTF = 2 \cos (\chi(R)) \quad (2.3)$$

where: $$\chi (R) = -\pi/\lambda (C_s \alpha^4 - 2 \Delta z \alpha^2) \quad (2.4)$$

and where: λ = wavelength

C_s = objective lens coefficient of spherical aberration

Δz = objective lens defocus

α = scattering angle generally limited by the objective aperture

R = the spatial frequency = 1/S where S = periodic spacing in the object

Shown in figure 2.1 are typical PCTF and ACTF. In principle, $\chi(R)$ acts as a phase plate to modify the object wave. The convolution of the object exit wave (Equation 2.1) and the lens aberrations (Equation 2.4) through a Fourier transform gives

$$FT\,[U(\mathbf{r})] = FT[U_o(\mathbf{r})]\,\exp\,[-i\chi(R)] \tag{2.5}$$

An inverse Fourier transform resulting from the action of the intermediate and projection lens results in the image wave $U(\mathbf{r})$.

$$U(\mathbf{r}) = FT^{-1}\{FT[U_o(\mathbf{r})]\,\exp\,i\chi(R)\} = a(\mathbf{r})\,\exp\,[i\varphi(\mathbf{r})] \tag{2.6}$$

The inverse Fourier transform may additionally alter the wave front due to a finite illumination aperture and the energy spread of the electron gun. The image phase $\varphi(\mathbf{r})$ and amplitude $a(\mathbf{r})$ do not agree with the object phase $\Phi(\mathbf{r})$ and amplitude $A(\mathbf{r})$ due to the lens imperfections. In conventional electron microscopy, only the intensity $|A^2(\mathbf{r})|$ is recorded and the phase information $\Phi(\mathbf{r})$ is lost giving image intensity $I(\mathbf{r})$.

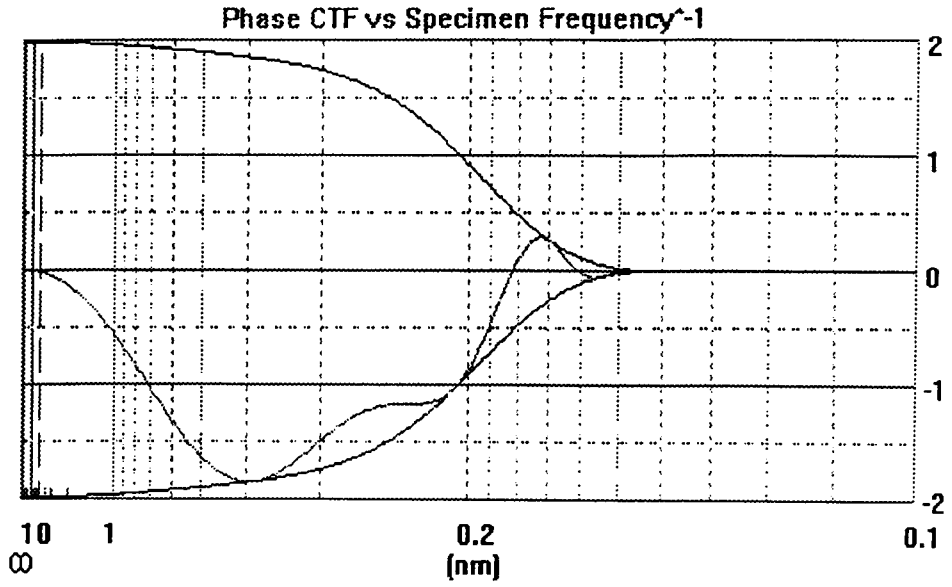

a

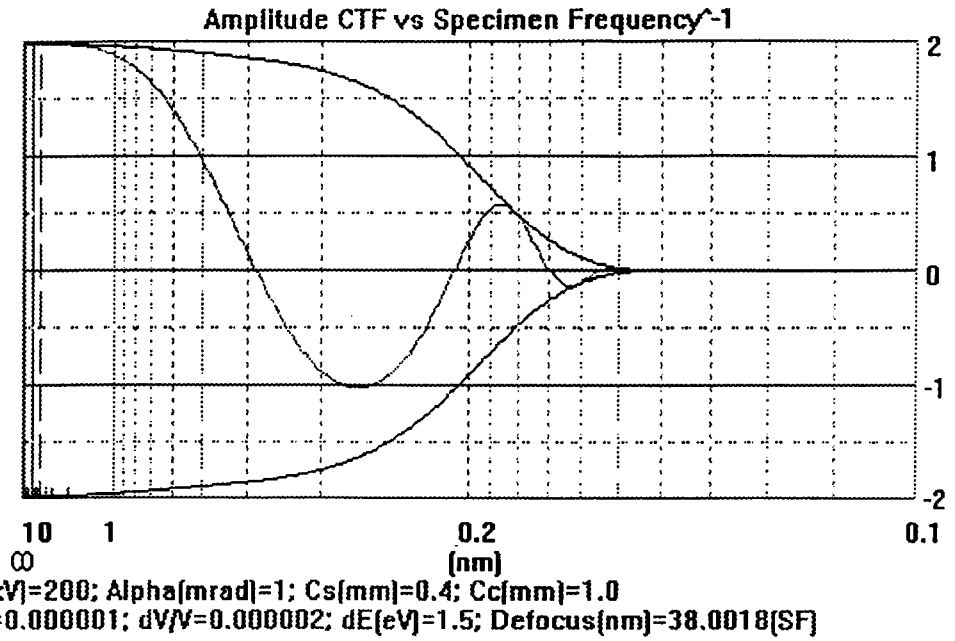

b

Figure 2.1. Typical (a) phase contrast transfer function and (b) amplitude contrast transfer function.

$$I(\mathbf{r}) = U_o(\mathbf{r})\, U_o^{cc}(\mathbf{r}) = |A^2(\mathbf{r})| \qquad (2.7)$$

where: U_o^{cc} is the complex conjugate of U_o

This results in an incomplete picture of the original object and one distorted by the lens aberrations.

In light optics, Fritz Zernike (1935a, b; 1942a, b) realized that the introduction of an additional phase shift of either the diffracted or undiffracted beam would result in a phase difference that could enhance image contrast. This phase shifting device, positioned at the back focal point of the objective lens, is called a phase plate. The introduction of an appropriate phase shift results in interference that transforms phase differences into amplitude (intensity) differences (Figure 2.2). Optimum image contrast (U_{op}) due to interference generated by a phase plate is when:

$$U_{op} = \pm 90^o + 1/2\varphi \qquad (2.8)$$

For a weak phase object where the object phase shift φ is close to zero the optimum phase plate is generally considered to be $\pm 90^o$ or $\pi/2$ which gives PCTF(R) = 2 for all spatial frequencies and the image intensity

$$I(\mathbf{r}) = 1\text{-}2\varphi(\mathbf{r}) \qquad (2.9)$$

uniquely represents the object phase shift.

When the light refractive index (η) of the object is greater than that of the medium, the object introduces a negative phase shift and is called phase

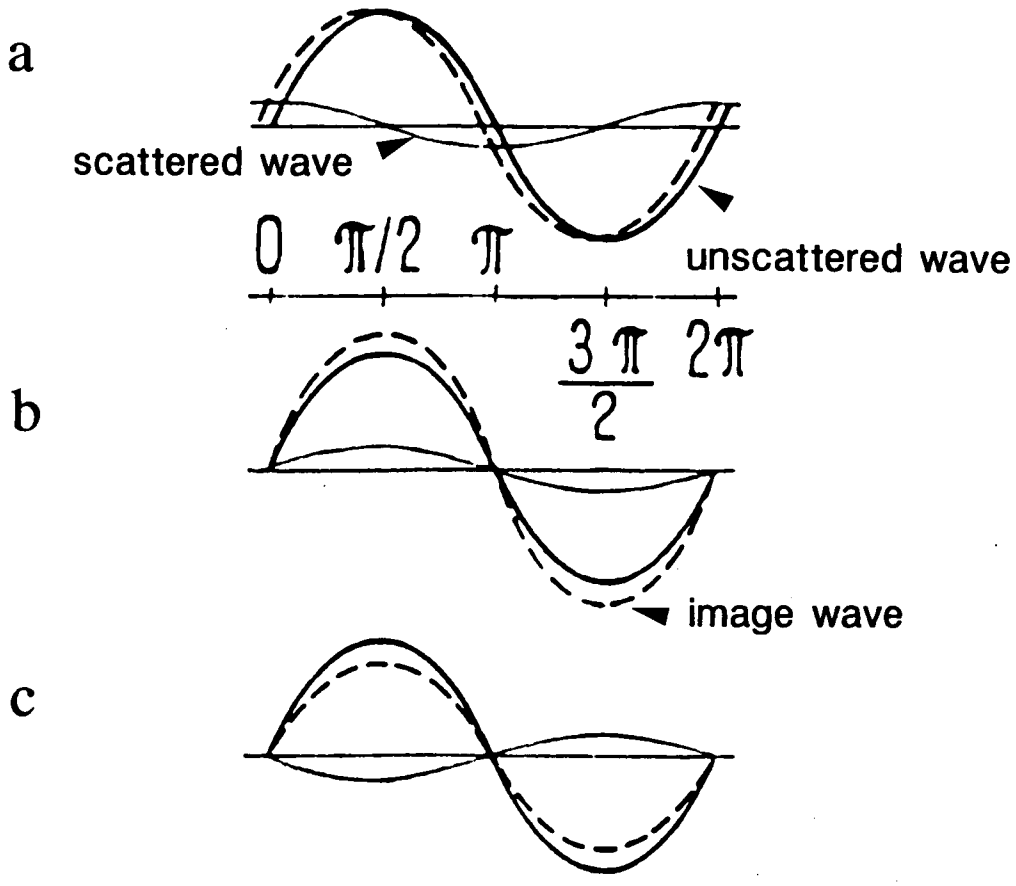

Figure 2.2. The transformation of a small phase shift into an amplitude difference (a) no phase plate (b) $\pi/2$ or $-3\pi/2$ phase plate (c) $-\pi/2$ or $3\pi/2$ phase plate.

Source: Adapted from Lenz F. 1963 Zonenplatten zur offnungsfehlerkorrektur und zur kontrasterholjhung, Z. Phys. **172**:498-502.

retarding. A +90° phase plate, that retards the diffracted wave front relative to the undiffracted wave front, incorporated in the optical path maintains the original contrast relationship, i.e., phase retarding objects will be dark in relationship to the background. A -90° phase plate that retards the undiffracted wave front relative to the diffracted wave front reverses the contrast. Likewise, if the refractive index of the object is less than that of the background then a +90° phase plate will cause the object to be lighter than the background and a -90° phase plate will cause the object to be darker than the background.

The use of a simple vector representation (Pluta 1989; Barer 1952a, b; 1953;1954;1955) is helpful in visualizing the phenomenon. The length of the vector represents the wave amplitude and the direction represents the angular phase shift (Figure 2.3). If **u** represents the undiffracted wave passing through the media and **d** the diffracted wave, then **p** defines the amplitude of the wave from the object. According to diffraction theory and Fourier optics, **p** is the sum of vectors **u** and **d**. The angle Φ represents U_{op} as defined by equation 2.8. This illustration assumes a weak phase object where the object phase shift (φ) is small. With the additional 90° phase shift (ψ) imparted by the phase plate $\mathbf{p}_1 = \mathbf{u}_1$ or $\mathbf{p}_2 = \mathbf{u}_2$. In both cases, the transformation of the small phase shift into an intensity difference between the object wave (**p**) and the wave passing through the background (**u**) occurs.

The contrast, C, can be calculated mathematically where:

$$C = \frac{|\mathbf{u}_X|^2 - |\mathbf{p}_X|^2}{|\mathbf{u}_X|^2} \qquad (2.10)$$

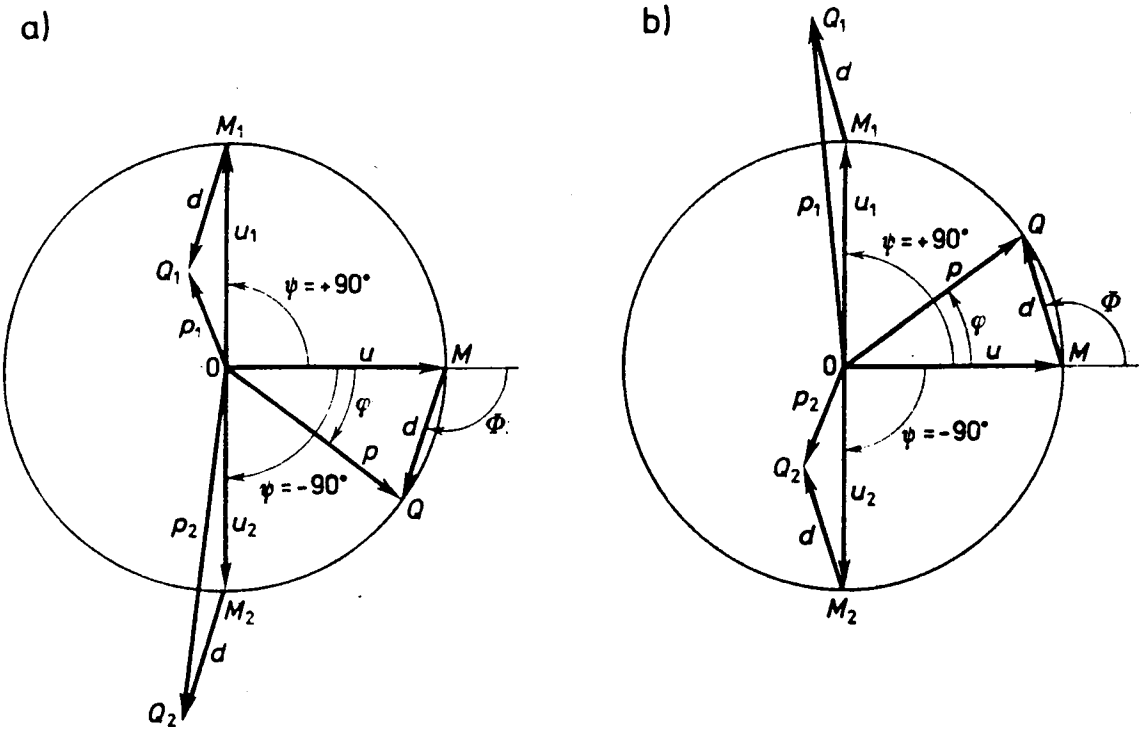

Figure 2.3. The phase contrast method, a vector representation: (a) phase retarding object, (b) phase advancing object. **u**=undiffracted wave, **d**= diffracted wave, **p**=image wave amplitude

Source: Pluta M. 1989 *Advanced Light Microscopy*, Polish Scientific Pub., Amsterdam, **2**:5.

Contrast is approximated by $C \sim \pm 2\varphi$. Attenuating the unscattered intensity results in additional contrast that can be approximated by:

$$C' = C\,\tau^{-1/2} \qquad (2.11)$$

where: τ is the transmittance and $\tau = 1/N$ where N is the amount by which the intensity of the direct undiffracted wave is divided.

A phase plate transmitting only 1/2 of the intensity of a transparent phase plate improves contrast by an additional factor of 1.4. Modern phase contrast light microscopes typically have a transmittance τ of 10-25%.

As the object phase shift increases, contrast can change sign. The contrast follows a sine function as illustrated in figure 2.4 for a $\pi/2$ phase plate with 100% transmittance. The range of unreversed contrast decreases with a reduction in the transmittance (Figure 2.5). In light optics, dielectric films are employed to phase shift and thin metallic films are used to attenuate the light intensity. In actual practice, the phase contrast light microscope employs an annular diaphragm at the focal point of the condenser lens and a ring shaped phase plate at the focal point of the objective lens (Figure 2.6). The light transmitted through the transparent condenser annulus and not diffracted by the object comes to focus on the ring of the phase plate which either retards or advances the direct beam in relationship to the diffracted beam. Typically different strength objectives use different diameter annuli and rings. A turret holds the condenser annuli for ease of selection. The diameter of the annulus and the ring must match.

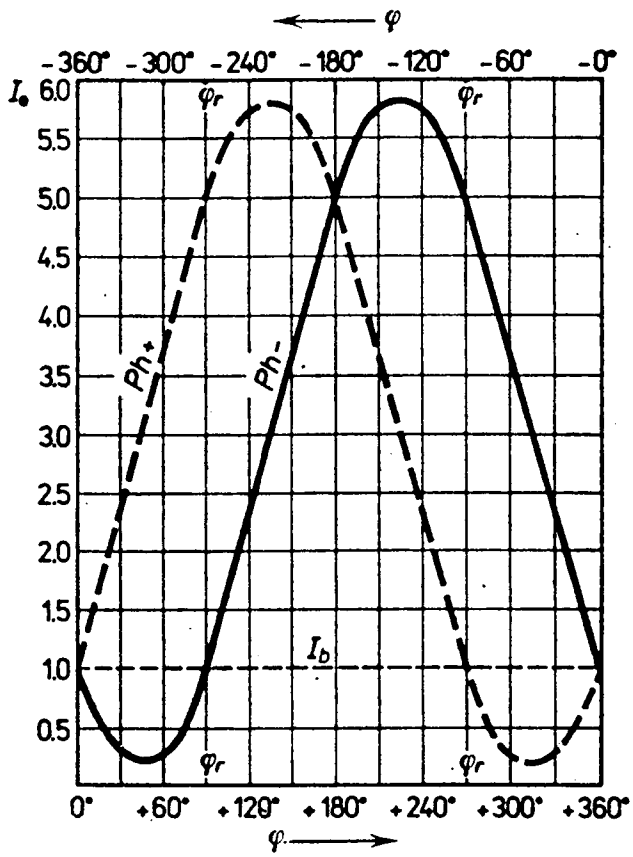

Figure 2.4. The relationship between the object intensity (I_o), and the object phase shift (φ), for a non-absorbing positive (Ph+) and negative (Ph-) quarter wavelength phase plate.

Source: Pluta M. 1989 *Advanced Light Microscopy*, Polish Scientific Pub., Amsterdam, **2**:9.

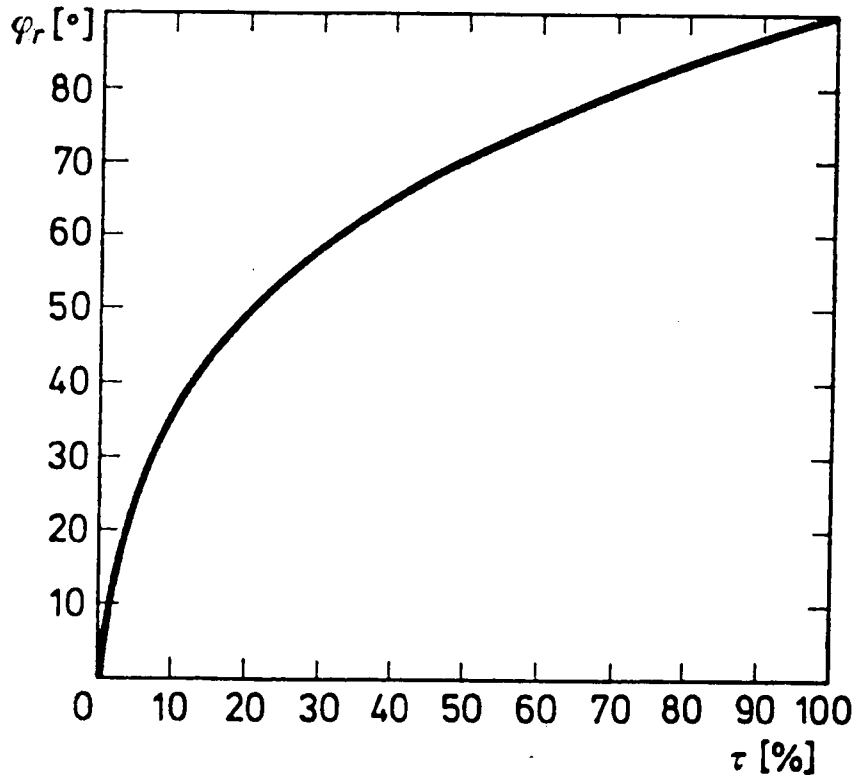

Figure 2.5. The relationship between the range of unreversed contrast (φ_r) and the transmittance (τ) of a quarter wavelength phase plate.

Source: Pluta M. 1989 *Advanced Light Microscopy*, Polish Scientific Pub., Amsterdam, **2**:10.

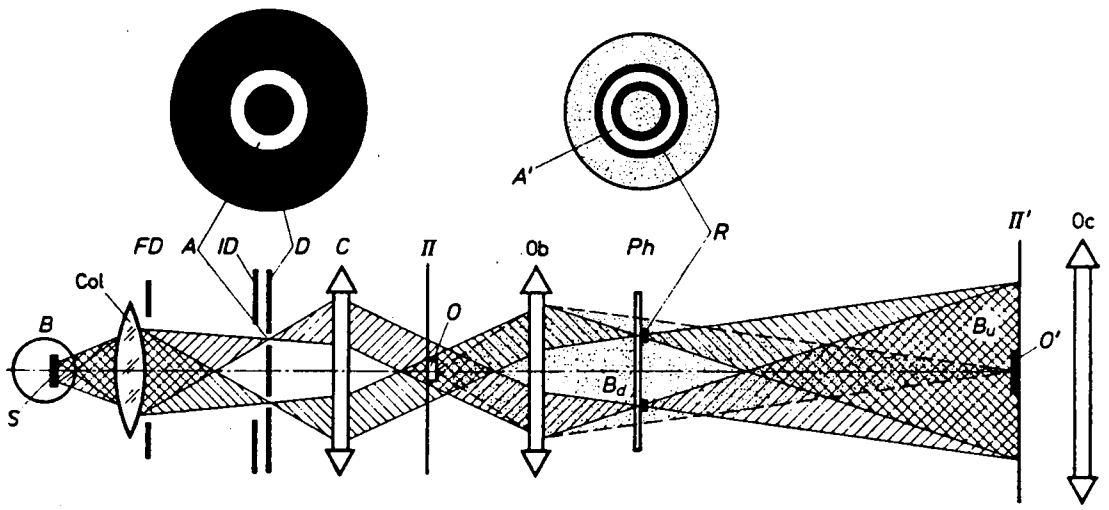

Figure 2.6. Schematic diagram of a typical light phase contrast microscope where: S = source, C = collector lens, FD = field diaphragm, A = condenser annulus, O = object, Ob = objective lens, Ph = phase plate, O' = image plane, Oc = ocular.

Source: Pluta M. 1989 *Advanced Light Microscopy*, Polish Scientific Pub., Amsterdam, **2**:10.

In 1941, C. Zeiss Jena constructed the first phase contrast microscope for light optics based on Zernike's design. The first commercially produced microscopes were marketed in 1946 and Zernike was awarded the Nobel Prize for Physics in 1953 for this work. These instruments proved most valuable to researchers in biology and the medical sciences. Cell biologists benefited greatly by the ability to study live cells using the enhanced contrast made available by the phase shifting optics. Previously,staining methods were necessary to provide sufficient contrast but these also caused cell death.

For transmission electron microscopes defocusing is the method most often used for introducing an additional phase shift. Scherzer (1949) showed that a converging lens, like the axially symmetric lens used in electron microscopy, used alone could not be made free of spherical aberration. In light microscopy, diverging lens correct for spherical aberration but their equivalent does not exist for electron microscopy. Methods proposed to compensate for spherical aberration (Scherzer 1949) have not been successfully applied to high resolution microscopy (Lichte 1991). The effects of defocus and objective lens spherical aberration on the phase factor $\chi(R)$ as described by Scherzer (1949) are defined in equation 2.4. The aim is to generate a uniform, non-oscillating transfer over a wide range of spatial frequencies. Phase enhancement using defocus is limited to a small range of spatial frequencies, introduces contrast inversion due to oscillations in the CTF, and the intensity of the unscattered beam masks the interference effects.

Additional work by Scherzer (1949) showed an improvement in resolution by properly balancing spherical aberration and defocus.

$$\Delta z = -2.5(C_s\lambda/2\pi)^{1/2} \qquad (2.12)$$

This condition has since been called Scherzer focus. The approximately three fold improvement is a result of the addition of phase contrast into the image. At Scherzer focus the resolution R_{min} can be approximated as (Reimer 1993, Ruska 1966):

$$R_{min} = 0.43(C_s\lambda^3)^{1/4} \qquad (2.13)$$

The point resolution limit of the microscope is generally considered to be the first zero of the PCTF. The lattice resolution of a microscope which is generally better than the point resolution is defined by the envelope function. The envelope function is limited by the chromatic aberration of the objective lens (C_c) and the incoherence of the illuminating electrons (Figure 1.1). The range of useful information transfer is generally limited to a region bounded by S = 1 nm and S = 0.2 nm (the point resolution). Spacings S>1 nm, that contain the large scale thickness contrast, are strongly damped and spacings S < 0.2 nm are difficult to interpret due to contrast inversions and zeros even though they may be transferred with high contrast. Modern field emission gun transmission electron microscopes with lower C_c objective lens and a more coherent electron source have improved the envelope function; however they have not improved the point resolution over that available in comparable low C_s objective lens TEMs equipped with thermionic emitters (Cowley 1988; Brock et al. 1992).

Electron holography can separate the phase and amplitude contrast elements of the CTF enabling phase contrast enhancement and improved instrument resolution. Electron holography was first described by Denis Gabor (1948, 1949, 1951) as a method to overcome the limitations of the then primitive TEM by storing the electron wavefront and subsequently reconstructing it

optically. He was awarded the Nobel Prize in Physics in 1971 for this work. Gabor initially credits Lawrence Bragg and his work with x-ray microscopes as his inspiration for his work on holography because the x-ray microscope used a similar two step imaging process. He later noted that the work of Mieszyslaw Wolfke predated the work of Bragg by 20 years and stated in a letter dated January 1968: "I have now read Wolfke's paper, and see that the priority for the double Fourier transformation must go to him, not to W. L. Bragg." (Shushurin 1971). Wolfke (1920) was apparently the first to describe the two step Fourier transformation of image formation. Wolfke, like Bragg, used a conventional diffraction pattern that did not contain phase information. Gabor's recognition of the need for and his ability to record phase differences for the complete image of the object was unique. Both holography and Zernike's phase contrast microscopy are rooted in Abbe's two step imaging theory (diffraction and recombination of the diffracted beams resulting in interference and image formation); however, in holography the two steps are separate (Abbe 1873). The interference pattern is produced by interference of the inelastically scattered wave front from the sample and the undiffracted wave front from the background. The interference fringes are recorded either on photographic film or more recently using digital methods incorporating a slow scan CCD camera. This interferogram or hologram is then reconstructed, *aposteriori*, by passing a coherent beam of light through the hologram or more recently by digital reconstruction using computers. This results in an image of the original object. The term hologram was coined by Gabor because the photographic record contains both amplitude and phase information. Hologram is derived from the Greek holos, whole or total and gamma, record (Pluta 1989). Gabor's original hope was to improve the resolving power of the electron microscope to less than

0.5 nm by using light optics to off set the imperfections of the TEM's objective lens.

Gabor's method of in-line holography also known as Fresnel or projection method holography uses a focused beam of electrons to illuminate the sample. The beam diameter determines the resolution of the image (Tonomura 1987). An object placed in the path of the wave front close to the point focus produces a spherical scattered wave. The scattered wave front and the unscattered part of the reference wave interfere and produce concentric fringes. The process works best when the reference wave contains a large fraction of the original beam intensity. During reconstruction, the hologram acts as a diffraction grating or Fresnel zone lens. The two diffracted waves or sidebands come to focus, one on each side of the hologram. Fresnel holography therefore has the disadvantage that a twin image is formed (Figure 2.7).

If the distance between Q and Q' is small, both images will be near focus when viewed but if a defocused image is used the distance between the reconstructed image and its conjugate can be increased. This method was employed to generate the first experimental electron holographs (Haine and Mulvey 1952). The disadvantage of this technique is that the three waves i.e., the two sidebands and the transmitted, overlap resulting in zero intensities for defocus values $\Delta z = nS^2/\lambda$ where n = integer.

Fraunhofer in-line holography employs a collimated electron beam to illuminate the object and is a method that circumvents some of the problems present in Fresnel holography. The hologram is formed in the far field diffraction region. In this case, the conjugate image is formed far enough away so as not to influence the reconstructed image. Another advantage is that this technique prevents contrast inversions in the image because the transfer function is the

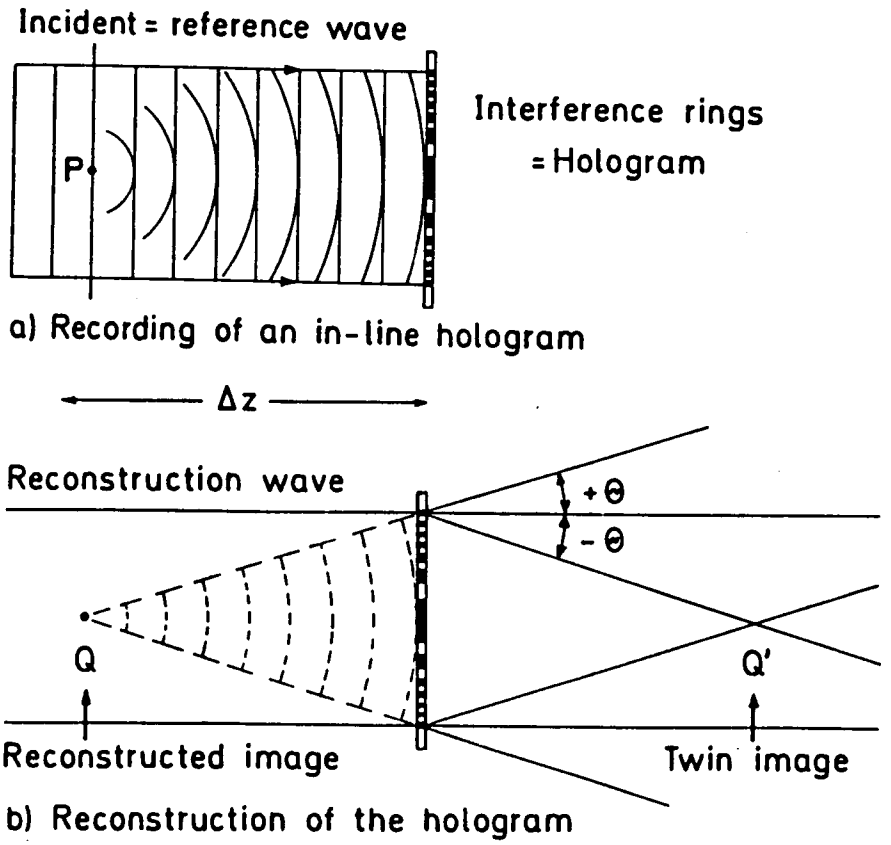

Figure 2.7 In-line holography (a) recording and (b) reconstruction.

Source: Reimer L. 1993 *Transmission Electron Microscopy Physics of Image Formation and Microanalysis*, Springer-Verlag, 239.

square of what it is for an electron lens (Tonomora 1987). A disadvantage of Fraunhofer holography is that the large defocus causes blurring, limiting the resolution of the image (Tonomura et al. 1968; Munch 1975). Further the image only contains amplitude information unless a phase plate is used during reconstruction, in which case the image will contain only the phase component (Hanszen 1973). For the best resolution, it is necessary to decrease the sample diameter while reducing the illumination angle. The resolution limit S can be calculated using the following relationship:

$$S_{min} = \frac{\alpha_i \, d_o^2}{\lambda} \qquad (2.14)$$

where: S_{min} = minimum periodicity (resolution limit)

d_o = diameter of the specimen

It is also important to have the sample on a thin electron transparent background. Image resolution down to approximately 0.7 nm has been reported using a FEGTEM (Bonnet et al. 1978).

A third approach to in-line holography avoids contrast transfer gaps by using only one of the diffracted side bands for image reconstruction. This is frequently accomplished by using a half plane objective aperture (Hoppe et al. 1970; Haydon and Lemons 1972; Downing and Siegel 1973; 1975; Cullis and Maher 1974a, b; 1975; Nakahara et al. 1975; Nakahara and Cullis 1977; Scales 1974; Hanszen 1969; 1970; Hanszen and Morgenstern 1965). In this case, the image of the phase component is shifted by $\pi/2$. The phase contrast obtained is asymmetric with bright contrast on one side of a feature and dark contrast on the

other and the amplitude component is unaffected. The amplitude component can be separated from the phase component by taking the sum or difference of two holograms taken with complementary half plane apertures (Downing and Siegel 1975). The electron wave aberration can also be corrected during the light optical reconstruction by using a lens with appropriate spherical aberration and defocus.

The use of a half plane aperture also generates topographical contrast that can be explained by diffraction. Electrons that enter a region on the sample that has a negative cross sectional slope will be deflected to the left and those regions of the sample with a positive slope will cause electrons to scatter to the right. Electrons deflected towards the solid half of the aperture will be blocked and this face of the object will appear dark. Those electrons deflected towards the semi-circular hole will be transmitted and these regions of the object will be bright (Haydon and Lemons 1972). In this way, sample contours are highlighted. Draw backs of this approach include charge build up on the aperture with increasing contamination and the difficulty in alignment of the complementary half plane apertures.

Off axis holography, first introduced by Leith and Upalnieks (1962), combines an unaltered reference wave and the transmitted wave altered by the sample and further modified by the electrostatic biprism. The electrostatic biprism was first described by Möllenstedt and Ducker (1956). A new appreciation of Gabor's theory, Möllenstedt's biprism, and the development of reliable field emission guns for transmission electron microscopy have generated a flurry of activity in off-axis holography in recent years. The FEG has higher brightness, lower energy spread and higher coherence than conventional thermionic emitters (Table 2.1). Coherent electron waves are

Table 2.1. A comparison of conventional thermionic electron emitters and field emission sources.

	W Hairpin	Single crystal LaB_6	Thermally assisted FEG	Cold FEG
energy spread (eV)	~2	~1	~0.5	~0.3
source size	50 μm	5 μm	10 nm	10 nm
brightness ($A/cm^2/sr/eV$)	1	20-50	100-500	100-1000

Source: Joy D.C., Maher, D.M. 1977 Sensitivity limits for thin specimen x-ray analysis, *Proceedings of the Workshop on Analytical Electron Microscopy IIT Research Institute, Chicago, Ill.*, edited by O. Johari1:325-334.

necessary to generate interference effects. Two aspects of coherence are important, spatial coherence and time coherence. The spatial coherence length is related to the source size, convergence angle and gun brightness. The time coherence length is related to the energy spread of the electron source and effects the contrast of the interference fringes while the spatial coherence more strongly effects fringe formation (Lichte 1991). In practice, the illuminating beam is made elliptical using the condenser stigmators to increase the spatial coherence while maintaining reasonable brightness. The direction of elongation is perpendicular to the biprism filament. The fringe spacing can be controlled by adjusting the potential on the biprism. The resolution attainable is approximately three times the fringe spacing created by the biprism for strong phase objects and two times the fringe spacing for weak phase structures. Fringe spacings as small as 0.03 nm have been achieved with the use of a FEGTEM (Völkl and Lichte 1990) making it possible to spatially resolve detail below 0.1 nm (Orchowski et al. 1995). An illustration of the electron biprism is shown in figures 2.8 and 2.9.

In the hologram, the amplitude $a(\mathbf{r})$ is recorded as the typical contrast modulation and the phase information $\varphi(\mathbf{r})$ is captured as a deflection of the fringes (Figure 2.10). The phase shift is proportional to the mean inner potential, magnetic potential and sample thickness. The combined specimen potential accelerates the electron beam slightly shortening the wavelength. The interference fringes are only formed by coherently scattered electrons, therefore the image represents an energy filtered image not blurred by inelastically scattered electrons (Zhang 1992). If two of the three factors influencing the phase shift, φ, are constant then the lines can be used to calculate the

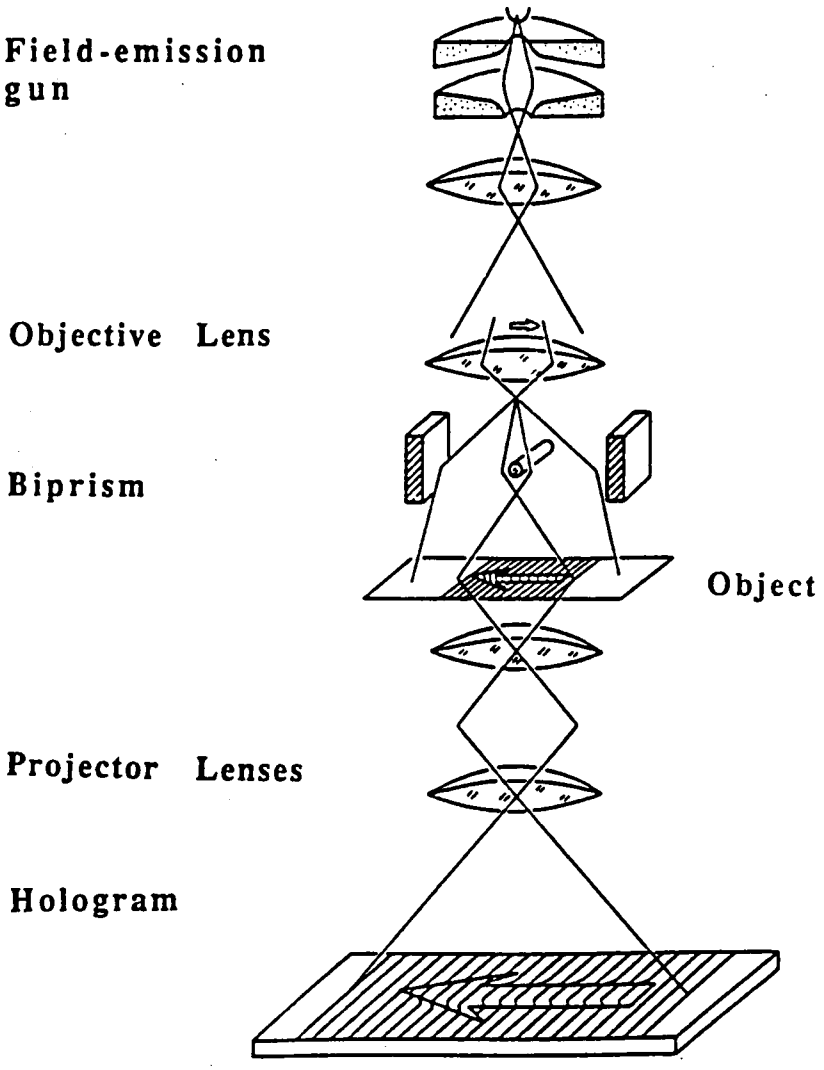

Figure 2.8. Schematic representation of a field emission gun TEM equipped with an electron biprism.

Source: Adapted from Zhang X. 1992 New electron beam methods for materials microcharacterization, *Dissertation Univ. of Tennessee Knoxville*, 100.

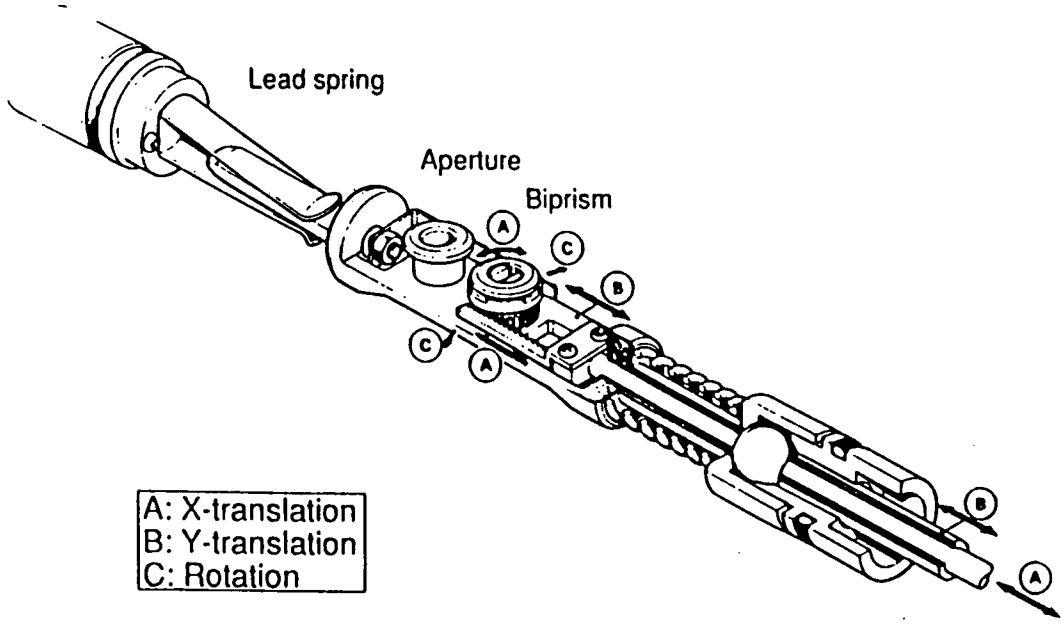

Figure 2.9. A rotatable electron biprism.

Source: Zhang X. 1992 New electron beam methods for materials microcharaterization, *Dissertation Univ. of Tennessee Knoxville,* 145.

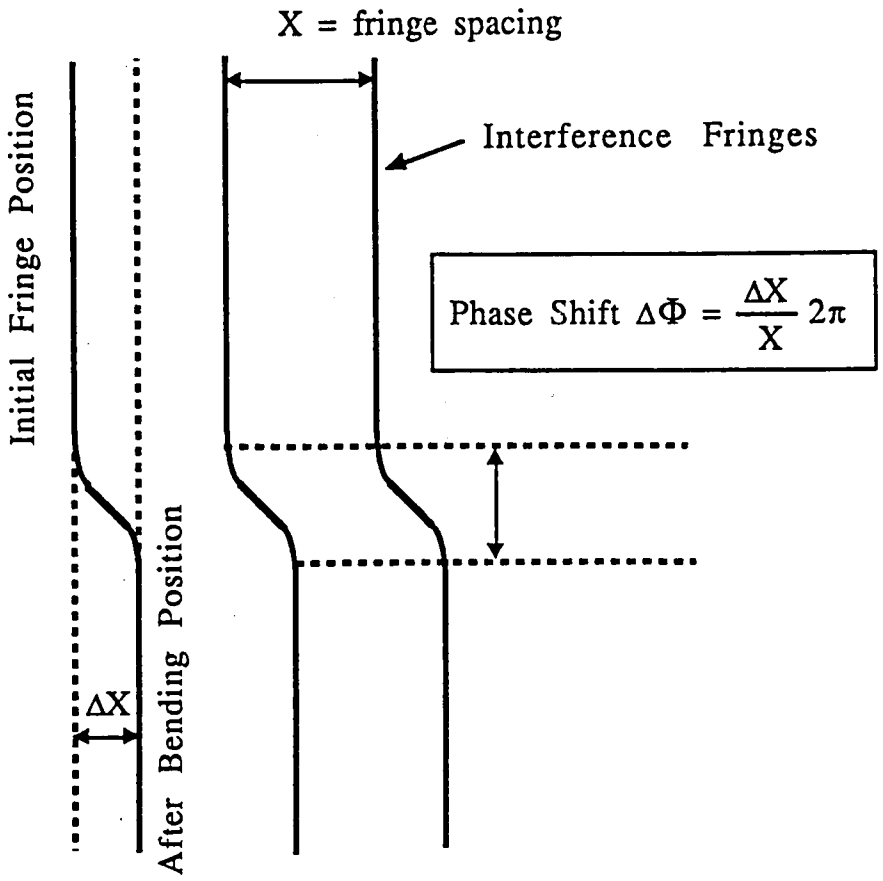

Figure 2.10. The phase shift as measured from the hologram fringe pattern.

Source: Adapted from Zhang X. 1992 New electron beam methods for materials microcharacterization, *Dissertation Univer. of Tennessee Knoxville*, 223.

magnitude of the remaining parameter using the following relationship (Vanzi 1984).

$$\varphi = 2\pi t V_i/(\lambda V_a) \qquad (2.15)$$

where: φ = phase change

t = film thickness

V_a = acceleration voltage

V_i = mean inner potential

The electron biprism modifies the object wave (Equation 2.1) by a phase factor $U_R(\mathbf{r})$.

$$U_R(\mathbf{r}) = \exp [i\, 2\pi\, R_c(\mathbf{r})] \qquad (2.16)$$

where: $R_c(\mathbf{r})$ is the spatial carrier frequency

When an object is placed into the beam path, part of the biprism shadow is occupied by the image wave $U(\mathbf{r})$ and the remainder by the reference wave. When a positive voltage is applied to the biprism, the two waves are deflected towards each other causing interference. The intensity distribution in the hologram $I_{hol}(\mathbf{r})$ is

$$I_{hol}(\mathbf{r}) = I + a^2(\mathbf{r}) + 2a(\mathbf{r}) \cos(2\pi R_c(\mathbf{r}) + \varphi(\mathbf{r})) \qquad (2.17)$$

$R_c(\mathbf{r})$ is modulated in position and contrast by the phase $\varphi(r)$ and amplitude $a(\mathbf{r})$.

The image wave can be reconstructed from the hologram through a series of Fourier transformations. A Fourier transformation of the hologram intensity distribution (Equation 2.17) gives the zero beam and auto correlation which contain amplitude information and two side bands, an image wave and its conjugate. If R_c is high enough, (small fringe spacing) the sidebands will be well resolved from the auto correlation (Lichte 1991).

$$FT(I_{hol}(\mathbf{r})) = R_{min}(R) \quad \text{zero beam} \tag{2.18}$$

$$+ FT(a^2(\mathbf{r})) \quad \text{auto correlation} \tag{2.19}$$

$$+ FT\left(a(\mathbf{r}) \exp\left(i\varphi(\mathbf{r})\right)\right) * R_{min}(R + R_c) \quad \text{sideband (+1)} \tag{2.20}$$

$$+ FT\left(a(\mathbf{r}) \exp\left(-i\varphi(\mathbf{r})\right)\right) * R_{min}(R - R_c) \quad \text{sideband (-1)} \tag{2.21}$$

If one side band is chosen and an inverse Fourier transform is performed, amplitude and phase information can be reconstructed. Reconstruction can either be accomplished using coherent light (Figure 2.11) or by numerical reconstruction. An advantage of holographic reconstruction is the ability to manipulate the Fourier spectrum light optically as opposed to making these manipulations directly in the electron microscope. Some of the alterations possible during reconstruction include: spatial frequency filtering, dark field, single sideband imaging, defocusing to obtain Fresnel diffraction, application of a $\lambda/4$ phase plate to obtain Zernike phase contrast and the use of an interferometer to superimpose the reference wave on the reconstructed wave for the purpose of generating a contour map with lines of equal phase (Lichte 1991; Tonomura 1987).

Numerical reconstruction of a digital hologram, obtained either directly using a slow scan CCD camera or by scanning a photographically produced

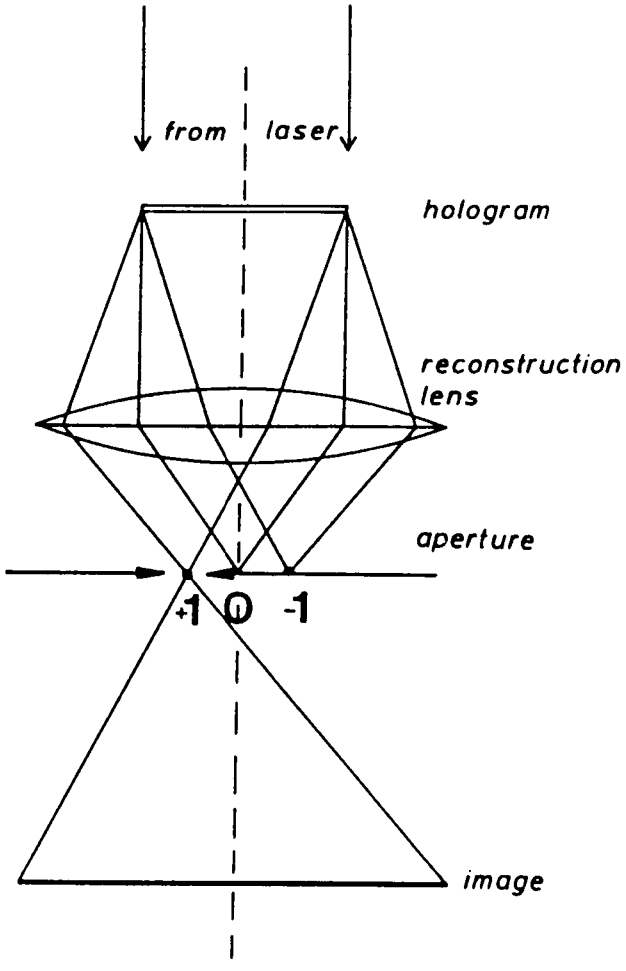

Figure 2.11. Schematic diagram of light optical reconstruction of an electron hologram.

Source: Lichte H. 1991 Electron image plane off-axis holography of atomic structure, *Advances in Optical and Electron Microscopy* **12**:37.

hologram into a computer, has several advantages when compared to the optical method. The nonlinearity of the photographic emulsion can be corrected for or avoided by using a CCD camera; the manipulations performed optically are easier to apply as the quality of the optical elements and their alignment are avoided; and, pixel by pixel manipulation is available for the correction of complex aberrations. Several software packages are now available for numerical reconstructions (Joy and Bunn 1993). During reconstruction, a single first order side band is chosen in diffraction space to eliminate the twin image. The reconstructed image has a fully restored amplitude with the correct sign; however the phase information is lost. If an interferometer is used in reconstruction, the phase information is represented as fringes or bands having equal phase shift.

CHAPTER THREE

THE HISTORY OF PHASE PLATES FOR ELECTRON MICROSCOPY

The use of phase plates in electron microscopy has not met with the success that it has for light microscopy. Several methods have been proposed and will be summarized here.

It appears that the first phase contrast electron microscope employing a phase plate was made by Agar, et al. in 1949. Following the advice of Boersch (1947) and Gabor (1948), they constructed a phase plate consisting of a thin formvar film with a glass fiber pierced 1 μm hole at its center. They determined the optimum film thickness (d) necessary for a $\pi/2$ phase delay using

$$t = \lambda(\eta-1)/ 4 \qquad (3.1)$$

$$\eta = [(V_a + V_i)/V_a]^{1/2} \qquad (3.2)$$

where:

η = effective refractive index of the film for electrons

This relationship later appeared in a more general form (Heidenreich 1964).

$$\varphi = (\pi V_i t)/(\lambda V_a) \qquad (3.3)$$

Using a mean inner potential of 7.8 volts for evaporated carbon, the film thickness would have been approximately 17 nm for their 50 keV microscope. Contamination build up on the phase plate and low image brightness under near

parallel illuminating conditions caused difficulty in focusing and photography required long exposure times (90 seconds typically). No images were included or discussed, presumably due to the difficulties mentioned above.

Locquin (1954) was the first to propose the use of an electrostatic charge to retard the unscattered beam. He constructed 6 separate devices in total, two having sharp points of tungsten wire or quartz filament suspended half way across an aperture, two with beam stop like characteristics either of quartz or tungsten, an aperture with thin margins and finally, an aperture covered with a thin polymer film having a hole in it approximately three quarters the size of the apertures inside diameter. The aperture with thin edges was made of platinum or silver using either two microballs, one on either side of the foil pressed together to thin the central region or by using electrical thinning procedures. The latter approach was found to be preferable.

The devices using the conductive tungsten wire were ineffective at enhancing phase contrast due to the absence of a point charge. When the central unscattered beam was focused on the beam stop like tungsten filament, an image resembling an annular dark field image resulted. The equivalent device made using a quartz filament gave inferior dark field contrast. The device employing the sharp tungsten wire again did not result in useful phase contrast; however the equivalent quartz filament gave strong phase contrast with partial absorption of the unscattered beam. The phase contrast was said to be due to an isolated point charge on the filament. The major difficulty noted with this arrangement was the asymmetry caused by the suspended filament.

Locquin (1954) preferred the use of the marginally thinned aperture to the electrostatic methods due to the symmetry of the technique, and all the published results presented were produced using this method. Careful alignment and control of electron optical conditions was necessary to insure optimum contrast enhancement. Images in figure 3.1 represent the first published phase plate enhanced electron micrographs.

Kanaya et al. (1957) also employed both positive and negative phase plates. They applied a different approach to the production of a positive phase plate from that used previously. They introduced holes (5-50 μm in diameter) in collodion (nitrocellulose) films by spraying the films with fine droplets of water during the casting of the films. The bubbles formed were then burned out using a gas burner. The negative phase plate was initially made from a folded collodion film, but was later improved by placing a section of a lacy carbon grid (microgrid) over a 50 μm aperture (Tochigi et al. 1970). The original experiments were performed on a microscope with an accelerating voltage of 50 keV and contrast improvement was reported for both devices demonstrating that the concept was sound. Several difficulties were noted such as phase plate contamination, inability to accurately control plate thickness and position and incoherencies in the illuminating system (Kanaya et al. 1957). Later some of the difficulties were overcome through the use of an improved 100 keV (C_s = 0.9 mm C_c = 1 mm) TEM and an anticontamination device (Tochigi et al. 1970) although no images or discussion of results were included.

Faget and colleagues (Faget et al. 1960a, b; Faget et al. 1962) improved on the Agar et al. (1949) design by employing an evaporated carbon film, containing a central hole, that was heated to +200° C to prevent

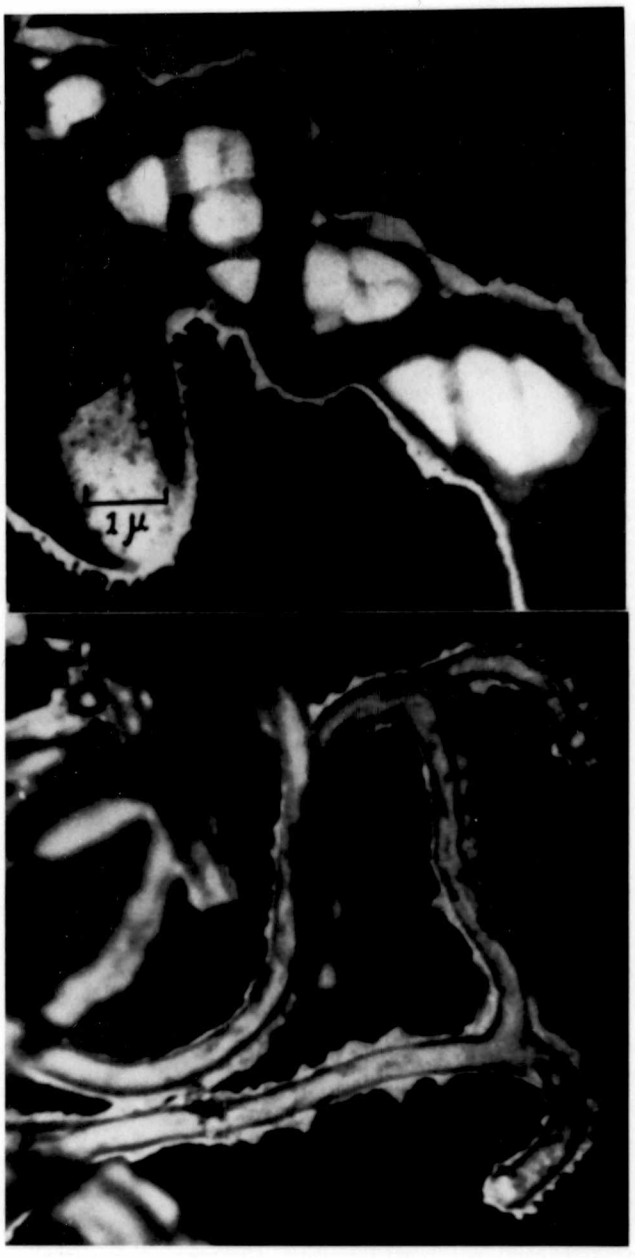

Figure 3.1. Images produced by Locquin that are believed to be the first electron micrographs produced using a phase plate.

Source: Locquin M. 1954 L'influence des modifications pupillaires de l'objectif sur les contrastes en microscopie electroniques *Proc. 3rd Inf. Conf. on EM, London,* edited by R. Ross Royal Microscopy Society, London, 285-289.

contamination build up. They placed their device in the back focal plane of the intermediate lens which provided more room to accommodate the heated holder. They presented micrographs of a collodion film comparing the normal image to the phase contrast image. The phase contrast micrograph showed a dramatic increase in contrast using their positive phase plate.

Faget et al. (1960a, b), unlike other researchers, not only modified the post specimen wave front but also, as according to Zernike's technique for light microscopy, modified the illumination wave by using a condenser aperture with a 10 to 20 μm wide slit in it. This, they proposed, would give them a more coherent illuminating wave front. The phase plate was made using a 0.3 μm spider filament suspended over a collodion film. Carbon or boron was evaporated onto the film to a thickness of approximately 15 nm to give a phase delay equal to $\pi/2$. After evaporation, the filament was removed leaving a narrow gap in the carbon or boron film. The phase plate was mounted between the intermediate and projector lens of a 100 keV TEM and heated to 200° C to reduce contamination. Careful alignment of the phase plate with respect to the band of illumination was critical. Fringes due to Fresnel diffraction were observed to aid in alignment and proper cross over of the source image slightly above or below the device. The authors concluded that when properly adjusted a uniform (across the field of view) phase contrast image could be obtained that was comparable to the contrast effects seen in phase contrast light microscopy.

Johnson and Parsons (1967; 1970; 1973; Parsons 1976; Parsons and Johnson 1972) quantitated the contrast of an object with and without a phase plate to characterize the improvement in contrast. They employed a Faraday cage to measure the electron intensity on and off the sample and employed the following relationship to determine contrast:

$$C = \Delta I/I = (I_p - I_b)/I_b \quad (3.4)$$

where: I_p = intensity of the particle

I_b = intensity of the background.

The phase shifting devices characterized were a dynamic self building contamination spot deposited on a 100 nm thick film supported on a 100 mesh copper grid. No additional objective aperture was employed. Using this device to examine 88 nm polystyrene latex spheres, they concluded that no significant improvements in contrast were realized as compared to an image formed using a small objective aperture. The other device was similar to earlier approaches using a carbon film supported over an aperture with a small central hole formed by a laser microscope. A 30 μm aperture was used to support the film. The object in this case was a thin carbon film. Images using this positive phase plate showed increased contrast of specimen detail having a spacing in the range of 0.8 - 2 nm. The overall contrast obtained between the film and background was not as great as that obtained using a 10 μm objective aperture. This was believed to be due to the attenuation of the elastically scattered component due to further scattering by the phase plate and the limited spatial frequency of uniform contrast transfer (Johnson and Parsons 1973). They also concluded that the phase plate did not significantly enhance the contrast of biological specimens because the detail was overwhelmed by the structure present in the support film. They recommended a lower C_s objective lens, a reduction in the amplitude of the non-scattered beam, a non-scattering phase shifting device, an energy filter and optical bench processing of micrographs, as necessary for further progress in enhancing phase contrast.

Another approach using sculptured or profiled phase plates made by electron beam micro-recording techniques (Müller 1970; Müller and Rindfleisch 1971) was used by a number of German researchers working in collaboration. Müller (1970) used a modified Siemens Elmiskop 101 fitted with magnetic deflection plates for beam positioning. An electron probe with a FWHM width as small as 1 nm was scanned across a thin carbon foil resulting in carbon deposition due to contamination build up. With constant beam intensity, the thickness of the contamination spot was varied by controlling the dwell time. Controlling beam sweep velocity with a flying spot photometer enabled the recording of miniature (5x5 μm) half tone images (Figure 3.2). By directing the beam in a circular manner, profiled phase plates were made (Müller 1976). Thickness was controlled by instantaneously monitoring electron scattering cross sections. A two collector system, one having a smaller radius and placed above the second larger radius collector, was used to ratio the intensity of wide angle scattered electrons I_2 to the intensity of small angle scattered electrons I_1. This ratio, I_2/I_1 was found to vary linearly with carbon thickness (Müller 1976). The ratio was compared to a computer stored value to accurately control the radial deposition of carbon.

Willasch (1975) determined the radial thickness variation for a phase plate designed to correct for spherical aberration that results in oscillations of the contrast transfer function giving random positive and negative contrast changes and gaps in information transfer at some spatial frequencies (Equation 2.4). The phase plate design was optimized for a pure weak phase object. For small aperture angles, α, α is related to object spatial frequency R by the following relationship:

Figure 3.2 Focused electron beam induced contamination used to create a micro-recorded half-tone image.

Source: Müller K.H. 1970 Micro-recording by use of the Elmiskop 101 *Proceedings 7th International Congress on Electron Microscopy, Grenoble,* edited by Favard Soc. Francaise de Microsc. Electronique, **1**:183-184.

$$\alpha = \lambda \; R \tag{3.5}$$

The radial thickness distribution D(**r**) based on the PCTF (equation 2.2) is given as:

$$D(\mathbf{r}) = \frac{V_a \quad 1 + bV_a}{2\,V_i \;\; 1 + 2\,b\,V_a} \quad \left[\frac{C_s k^4 \;\; r^4 - 2 \quad \Delta z\, k^2 \;\; r^2}{f^4 \qquad\qquad f^2} \right]$$

$$- \frac{\lambda_a}{2V_i} \; \frac{1-\alpha V_a}{1+2\alpha V_a} \quad (4m - 1) \tag{3.6}$$

where: $b = 0.9788 \times 10^{-6} / V_a$

k = a correction parameter for the lens field surrounding the plate

r = radius

f = focal length of the objective lens

m = integer

Using this relationship and Müllers micro-recording device, phase plates were fabricated having a central hole of 5 μm. (Thon and Willasch 1970; 1971a, b; 1972; Willasch 1975; Badde and Reimer 1970; Reimer and Badde 1970) Thicknesses at high spatial frequencies were kept to a minimum to reduce the influence of chromatic aberration due to scattering in the plate that results in a reduction of contrast transfer. Experimentally Willasch (1975) showed that resolution decreases with increasing plate thickness as determined using uniform thickness carbon films as phase plates (Table 3.1). By using increased defocus values, the information envelope can be extended to higher spatial frequencies but with a sacrifice of uniform contrast transfer. By employing a profiled phase plate it was hoped that the contrast inversions and zeros would be avoided thus giving interpretable information transfer over a large range of

Table 3.1. Reduction of inverse spatial frequency, S, as a function of film thickness D for a uniform thickness phase plate with 8 μm central hole.

D(nm)	S
0	0.35-0.4
20	0.4
50	0.45
100	0.5

Source: Willasch D. 1975 High resolution electron microscopy with profiled phase plates, *Optik* **44(1)**:17-36.

spatial frequencies. A profiled phase plate was fabricated for the specific set of experimental operating conditions (Figure 3.3).

In practice, several errors were possible. The mean inner potential used in the calculation of D(**r**) was determined for evaporated carbon films which is likely different for electron deposited contamination, especially since silicon was detected in the films. Errors in the thickness of deposited carbon were possible, positioning of the phase plate would also be critical, and astigmatism must be made minimal. Even then, a phase plate would be optimized only for a single defocus. Contamination was kept to a minimum through the use of anticontaminators. Willasch (1975) concluded that the quality of the results obtained with the profiled phase plate (although not optimized) with a defocus of 128 nm are comparable to conventional micrographs taken at Scherzer defocus.

It was also concluded that further improvements would be possible with improved phase plate fabrication, to give thickness accuracies of better than 5% and precise knowledge of the mean inner potential and mass density of the contamination layer (Thon and Willasch 1972; Willasch 1975). Using profiled phase plates and advanced electron microscopes with field emission guns, (reduced chromatic aberration effects) Willasch (1975) estimated that point resolutions down to 0.1 nm should be possible.

A device similar to the sculptured phase plate was proposed initially for the compensation of objective lens spherical aberration (Hoppe 1963; 1970; 1971; Hoppe et al. 1970; Möllenstedt et al. 1968; Lenz 1963). This zone plate was fabricated having opaque rings of a specific diameter and width coinciding with the regions of the aperture that contribute to negative contrast transfer. These zone plates required precise alignment, astigmatism correction

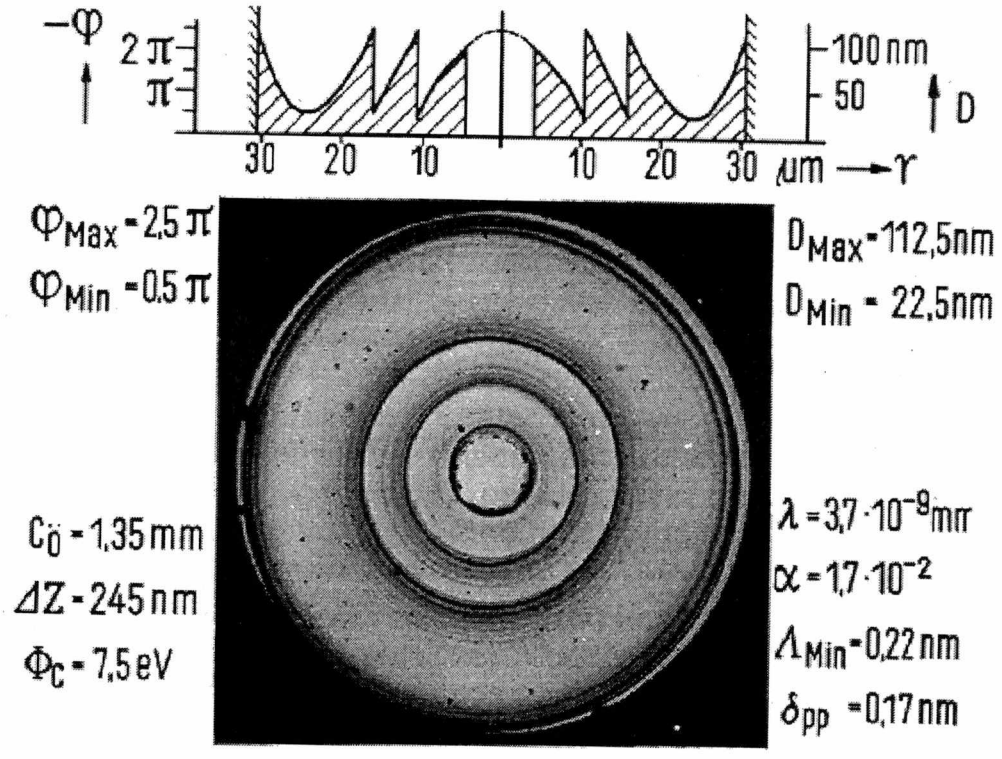

Figure 3.3. Sculptured phase plate as developed by Thon and Willasch using electron beam induced contamination.

Source: Thon F., Willasch D. 1971b A calibration method usable in the production of phase plates for high resolution electron microscopy, *Proceedings of the 29th Meeting of EMSA, Boston*, edited by J. Areneaux, Claitor's Publishing Division, 46-47.

and they were again designed for a specific defocus. Although the range of useful contrast transfer could be extended, some regions of spatial frequency information were not transferred. This problem could be overcome by combining two images of the same object taken at different defocus and employing different zone plates followed by optical reconstruction (Hanszen 1973). Although, this approach is sound in theory it has not been successfully demonstrated.

Möllenstedt et al. (1968) purposed a practical method of zone plate fabrication. They started with a 40 nm thick silver foil and used electron beam contamination to build up the negative areas of the plate. The device was then electroplated with gold which built up in the non-contaminated regions. The silver was etched away and the contamination layer dropped out leaving a self supporting zone plate. The difficulty of using the zone plate in practice in the TEM has led a number of authors to perform the zonal filtering subsequently on a light optical bench during reconstruction (Hoppe et al. 1970; Thon and Siegel 1970).

Unwin (1971; 1972; 1973; 1974) recognizing the deficiencies of defocus phase contrast, including contrast reversals and the high intensity of the unscattered beam, tried to build upon the success of Locquin (1954) by designing an electrostatic phase plate that would provide high resolution and improved contrast transfer. His device employed a 0.3 μm diameter poorly conducting filament placed across the diameter of a 30 μm thin metal aperture. The apertures were fabricated by placing 30 μm diameter latex spheres onto a convex glass surface, evaporating approximately 0.5 μm of silver onto the glass, and then blowing away the latex spheres leaving 30 μm apertures. A thin (0.3 μm diameter) spider thread was laid across the metal foil several times and an aperture with a thread traversing the diameter was selected, outline scored,

floated on distilled water and picked up on a single holed diaphragm. It was then glued in place with a conducting adhesive and finally coated with approximately 15 nm film of gold to impart partial conductivity to the filament (Unwin 1974).

The device was mounted in the back focal plane of the objective lens at the position of the objective aperture holder. A Philips EM 300 operated at 100 keV was used. The device was heated to 120°C and surrounded by an anticontaminator. It was determined, using interferometry that at an accelerating voltage of 100 kV the phase plate filament potential stabilizes at approximately + 1V. Due to the fact that the unscattered beam intersects the partially conducting filament at its midpoint the charge is primarily localized in this region. Unwin (1974) suggests that the charge is largely a result of secondary electron emission. The primary, unscattered electrons strike the filament causing secondary electron emission and since the net yield of electrons is greater than unity the filament charges positively. The positive charge is partially offset by leakage charge along the filament and by the collection of secondary electrons generated at the edge of the aperture. Unwin claimed that a balance is quickly obtained and the potential is adjusted to give maximum phase contrast by manipulating the illuminating system. Intersection of the primary beam and the filament also results in absorption, reducing the intensity of the unscattered signal. The amount of absorption is determined by the filament size and the size of the unscattered beam. The field generated was believed to shorten the path length of the scattered wave allowing it to interact constructively and destructively with the unscattered wave. At optimum illuminating conditions the phase shift would be $\pi/2$ (Unwin 1973).

Unwin (1974) utilized this device to image negatively stained T4 bacteriophages and tobacco mosaic viruses (TMV) and showed significant improvements in resolving fine detail in the tail region particularly in internal regions removed from the stain (Figure 3.4). Contrast transfer was more uniform over a wider range of spatial frequencies than that obtained using defocusing methods. A resolution limit of 0.5 nm was obtained with his experimental set up (Unwin 1973). He concluded that the negative stain was only needed for preservation purposes during electron irradiation and not for image contrast (Unwin 1972). The contrast enhancement was believed to be due both to phase contrast and improved amplitude contrast as a result of partial absorption of the unscattered beam. Unwin (1972) claimed that the "[electrostatic phase plate] enables the contrast to be increased several times over that attainable by the brightfield method". The useful transfer range was increased to include a range of bright contrast from 0.85 to 3.0 nm.

Unwin's (1972) device had several advantages over the thin film methods of previous investigators:

1) The amplitude of the scattered wave is mostly undisturbed
2) It provides absorption of the primary beam
3) It enables bright phase contrast versus dark phase contrast. (Dark phase contrast is more effective at enhancing contrast in high scattering materials than in weakly scattering materials)

In practice, the device was difficult to use because of the need for precise alignment and exact illuminating conditions for optimum effect. The lack of rotational symmetry of the field near the thread results in astigmatism in the image most noticeable at low spatial frequencies. Furthermore this device, unlike the contoured phase plate, is not effective at correcting spherical

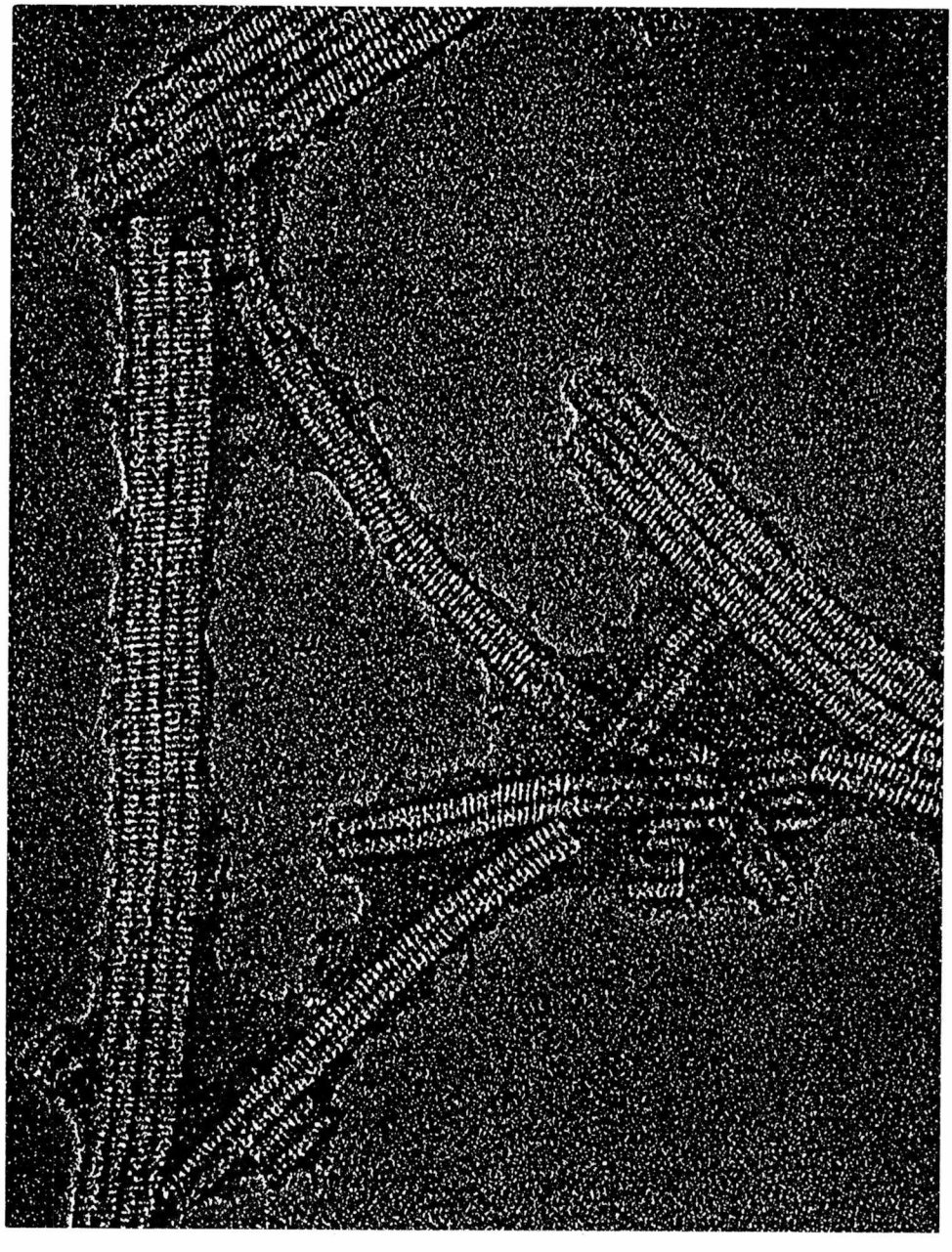

Figure 3.4. Transmission electron microscope phase contrast image of a 1% uranyl acetate stained tobacco mosaic virus protein. The rings of protein are ~2.5 nm thick by ~15 nm in diameter.

Source: Unwin P.N.T. 1971 Phase contrast and interference microscopy with electron microscope, *Phil. Trans. Roy. Soc. London* **B261**:95-104.

aberration, so the ultimate resolution is still limited by spherical aberration (Unwin 1971). Unwin (1974) also noted that even with the extra precautions taken to minimize contamination build up, the device was limited to approximately 30 hours of use before contamination became prohibitive.

Krakow and Siegel (1975) constructed an electrostatic phase plate similar in concept to that of Unwin (1971; 1972; 1973; 1974); however the construction was simpler. They used the 0.3-0.4 μm platinum wire core of a Wollaston wire after removing the silver sheath by wet chemical methods. The platinum wire was mounted across a platinum aperture and cemented in place with epoxy. The device was then coated with several tens of nanometers of evaporated gold.

They gave an equation for calculating the total phase shift $\gamma(\alpha)$ that results when using an electrostatic phase plate of this design

$$\gamma(\alpha) = \pi/\lambda \left(\tfrac{1}{2}C_s\alpha^4 - \Delta z\alpha^2 + 4Kq \ln\alpha\right) \qquad (3.7)$$

where: $K = - e/8\pi\varepsilon V_a$

q = positive charge units on the phase plate

e = charge of an electron

ε = permittivity in vacuum

Krakow and Seigel (1975) also noted that the phase shift that the unscattered beam experiences as it passes close to the wire must be considered. Under optimum operating conditions of the phase plate ($\Delta z = o$, $q = 68$), the effective resolution limits are 0.4 to 4.0 nm. Experimentally they were unable to reduce q below 200 and settled on $q = 235$ and $\Delta z = 450$ nm resulting in good contrast transfer from approximately 0.7 to 3.0 nm.

They noted that contamination of the wire causes excessive charging and spreads the charge along the length of the wire no longer giving a point charge. In conclusion, they demonstrated the usefulness of the device by imaging at high contrast, negatively stained ferritin. The image showed that high scattering materials become darker while weak phase objects become brighter.

The work of Balossier and Bonnet (1981) represents another attempt at utilizing a filament mounted over an aperture to produce an electrostatic phase plate. Although the filament material, a 0.4 μm diameter platinum wire, was employed, instead of Unwin's spider filament, the concept remains the same. Balossier mounted the platinum filament across a 100 μm diameter molybdenum aperture and coated the device with a 20 nm film of gold to stabilize the charge. Using a JEOL 100C operated at a Scherzer defocus and using a contrast threshold of $\pm$ 0.4, the transfer interval is from 0.26 nm to 1.85 nm. Using their electrostatic phase plate in the back focal plane of the objective lens, the transfer interval extended from 0.33 nm to 7 nm. In addition to the improvement in the contrast transfer interval for high spatial frequencies, it was noted that the contrast is positive for their phase plate versus the negative contrast that results at Scherzer defocus. Balossier and Bonnett (1981) also described the device's ability to generate topographical contrast similar to that obtained when using a half plane aperture. This effect became most pronounced when the filament was translated from its symmetrical position to a position where it stopped an asymmetrical part of the scattered wave front. This work appears to be the most recently published work on phase plates for the transmission electron microscope.

Dupouy et al. (1966; 1969) were able to increase image contrast in a 1000 keV TEM by blocking the electrons not diffracted by the object. They

proposed the use of a central opaque disk between 5 and 7 μm in diameter held in place by support wires anchoring the disk to the aperture. The device was found to be difficult to fabricate and maintain due to its delicate nature. Instead they employed a tungsten wire either stretched across the diameter of the aperture or its radius. Although this device did not result in increased phase contrast enhancement, it did result in an image comparable to an annular darkfield image like that obtained more recently in a scanning transmission electron microscope. They further refined their method in 1969 with the placement, at the condenser aperture plane, of a larger and more robust device than that originally proposed for the objective aperture. This generated a hollow cone of illumination that was blocked by an appropriate sized objective aperture unless the object caused electron scattering into the objective aperture. This resulted in a similar annular dark field image using a more robust and more easily fabricated device. As mentioned earlier, this device is not a phase plate; however it represents an additional method of contrast enhancement made possible by using either a non-conventional objective or condenser aperture.

CHAPTER FOUR

ELECTROSTATIC PHASE PLATE MODELING

The fields generated by electrostatic phase plates can be modeled using a computer spread sheet incorporating the Laplace equation (Bradley and Joy 1991, and Leclerc and Sanche 1990).

The Laplace equation when solved in 2 dimensions takes the form

$$\Phi(i,j) = \tfrac{1}{4}[\Phi(i + 1,j) + \Phi(i - 1,j) + \Phi(i,j+1) + \Phi(i,j-1)] \qquad (4.1)$$

This sets each point in the spread sheet to the average of the four points surrounding it. The computer can be set to continue solving the equation for each point in an iterative manner until a set precision is obtained.

Once the array is entered, potentials can be assigned to any point in the array and when all values have been entered the computer will calculate the field based on an exponential decay. Once the calculations are complete, minor alterations may be made and the array is automatically updated to reflect the change. In this experiment, a Macintosh computer running Microsoft Excel was used to develop a 27x27 grid that gives sufficient resolution without excessive computational times. Several phase plate designs incorporating a circular aperture were modeled to predict the symmetry of the electrostatic field. Figure 4.1 incorporates a central point charge and is the only design that generates a radially symmetrical field. The field strength in this case can be controlled either by increasing the potential at the center of the aperture or by altering the potential of the aperture. Rather than being at ground potential, the aperture

a

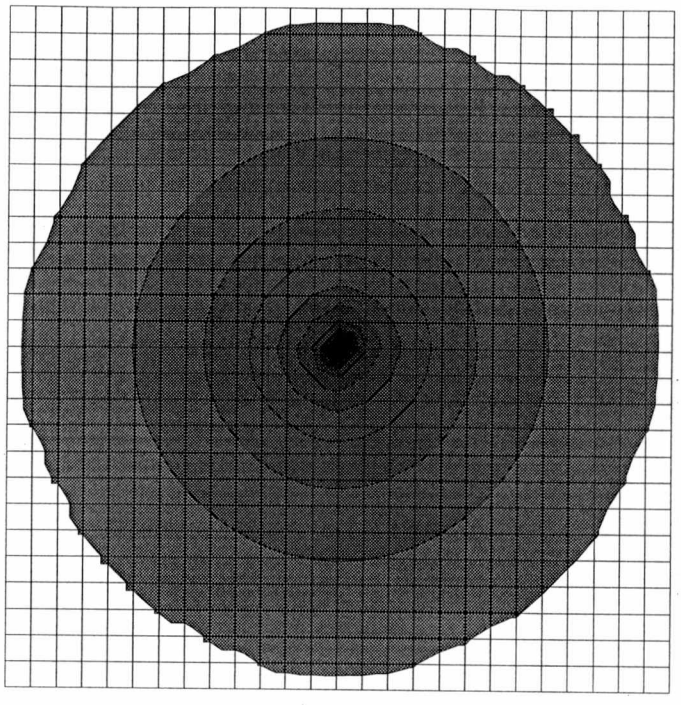

b

0	0	0	0	0	0	0	0	0	0	0	0	0	0	0	0	0	0	0	0	0	0	0	0	0	0
0	0	0	0	0	0	0	0	0	0	1	2	2	2	2	2	1	0	0	0	0	0	0	0	0	0
0	0	0	0	0	0	0	0	1	2	3	3	4	4	4	3	3	2	1	0	0	0	0	0	0	0
0	0	0	0	0	0	1	2	3	4	5	6	6	6	6	6	5	4	3	2	1	0	0	0	0	0
0	0	0	0	0	1	3	4	5	6	7	8	8	9	8	8	7	6	5	4	3	1	0	0	0	0
0	0	0	0	1	3	4	6	7	9	10	11	11	11	11	11	10	9	7	6	4	3	1	0	0	0
0	0	0	1	3	4	6	8	9	11	12	14	14	15	14	14	12	11	10	8	6	4	3	1	0	0
0	0	0	2	4	6	8	10	12	14	15	17	18	18	18	17	16	14	12	10	8	6	4	2	0	0
0	0	1	3	5	7	9	12	14	16	19	21	22	23	22	21	19	17	14	12	10	7	5	3	1	0
0	0	2	4	6	9	11	14	16	19	22	25	27	28	27	25	23	20	17	14	11	9	6	4	2	0
0	1	3	5	7	10	12	15	19	22	26	30	33	35	34	30	26	23	19	16	13	10	7	5	3	1
0	2	3	6	8	11	13	17	21	25	30	36	42	45	42	36	30	25	21	17	14	11	8	6	4	2
0	2	4	6	8	11	14	18	22	27	33	42	52	62	52	42	34	27	22	18	14	11	9	6	4	2
0	2	4	6	9	11	14	18	22	28	35	45	62	100	62	45	35	28	23	18	15	11	9	6	4	2
0	2	4	6	8	11	14	18	22	27	33	42	52	62	52	42	34	27	22	18	14	11	9	6	4	2
0	2	3	6	8	11	13	17	21	25	30	36	42	45	42	36	30	25	21	17	14	11	8	6	4	2
0	1	3	5	7	10	12	15	19	22	26	30	33	35	34	30	26	23	19	16	13	10	7	5	3	1
0	0	2	4	6	9	11	14	16	19	22	25	27	28	27	25	23	20	17	14	11	9	6	4	2	0
0	0	1	3	5	7	9	12	14	16	19	21	22	23	22	21	19	17	14	12	10	7	5	3	1	0
0	0	0	2	4	6	8	10	12	14	15	17	18	18	18	17	16	14	12	10	8	6	4	2	0	0
0	0	0	1	3	4	6	8	9	11	12	14	14	15	14	14	12	11	10	8	6	4	3	1	0	0
0	0	0	0	1	3	4	6	7	9	10	11	11	11	11	11	10	9	7	6	4	3	1	0	0	0
0	0	0	0	0	1	3	4	5	6	7	8	8	9	8	8	7	6	5	4	3	1	0	0	0	0
0	0	0	0	0	0	1	2	3	4	5	6	6	6	6	6	5	4	3	2	1	0	0	0	0	0
0	0	0	0	0	0	0	0	1	2	3	3	4	4	4	3	3	2	1	0	0	0	0	0	0	0
0	0	0	0	0	0	0	0	0	1	2	2	2	2	2	1	0	0	0	0	0	0	0	0	0	0
0	0	0	0	0	0	0	0	0	0	0	0	0	0	0	0	0	0	0	0	0	0	0	0	0	0

Figure 4.1. a) A two dimensional model for the electrostatic field generated by a point charge centered in an aperture at ground potential. b) Values used to generate the model.

can be isolated from ground and charged positive or negative. This design has the greatest appeal due to its radially symmetric field and the ability to control the field independently of the central charge (Figure 4.2). The construction of an actual device for use in an electron microscope based on this model would be the most difficult to realize in practice. Ideally the object used to generate the point charge would be suspended in vacuum in the center of an aperture. Since this does not appear to be physically possible, the object must be held in place by a supporting material such as a thin conductive film or a rigid peninsula or bridge of material that would effect the field distribution.

The latter approach is similar to the designs of Locquin (1954) who used a quartz finger following the radius of the aperture and Unwin (1971;1972) and later workers using a partially conductive filament suspended across the diameter of the aperture. In these cases, the primary high intensity unscattered beam striking the fiber generates a charge that can be at least partially carried across the filament. The fiber's conductivity and the balance between negative charging due to primary beam absorption and positive charging due to secondary electron emission are important in determining the total charge. If the charge on the filament is not stabilized and becomes too high, discharge will occur. If areas of intense diffraction occur, secondary charge centers are also possible. The main advantage of a filament type support is that it allows the remaining aperture field to be free of electron scattering materials.

The use of a conductive filament, also proposed by Locquin (1954), would fail to generate a localized charge especially if the filament diameter was sufficient to result in a low resistance. If the filament is floating, through attachment of the fiber to the aperture using an insulating material, then the charge built up on the filament due to secondary emission would be distributed

a

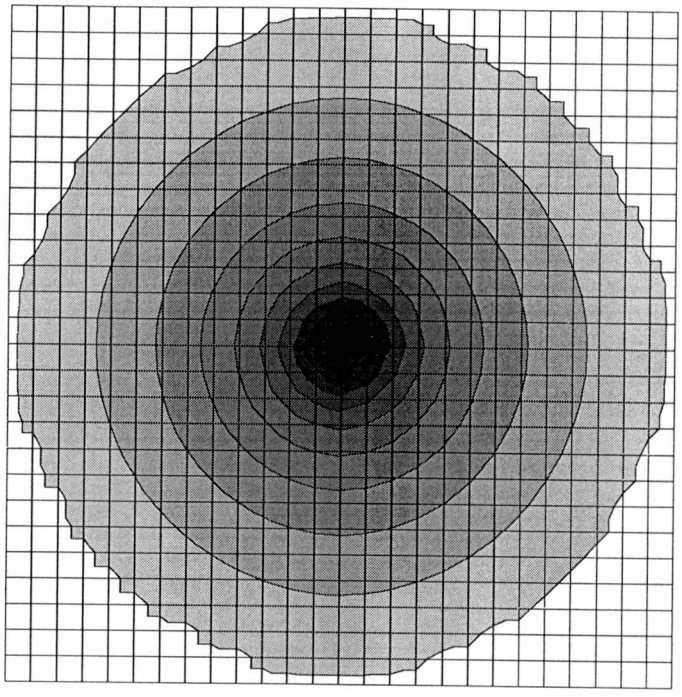

b

-50 -50 -50 -50 -50 -50 -50 -50 -50 -50 -50 -50 -50 -50 -50 -50 -50 -50 -50 -50 -50 -50 -50 -50 -50 -50 -50
-50 -50 -50 -50 -50 -50 -50 -50 -50 -50 -48 -48 -47 -47 -47 -48 -48 -50 -50 -50 -50 -50 -50 -50 -50 -50 -50
-50 -50 -50 -50 -50 -50 -50 -50 -48 -47 -45 -45 -44 -44 -44 -45 -45 -47 -48 -50 -50 -50 -50 -50 -50 -50 -50
-50 -50 -50 -50 -50 -50 -48 -47 -45 -44 -42 -41 -41 -41 -41 -41 -42 -44 -45 -47 -48 -50 -50 -50 -50 -50 -50
-50 -50 -50 -50 -50 -48 -46 -44 -42 -40 -39 -38 -37 -37 -37 -38 -39 -40 -42 -44 -46 -48 -50 -50 -50 -50 -50
-50 -50 -50 -50 -48 -45 -43 -41 -39 -37 -35 -34 -33 -33 -33 -34 -35 -37 -39 -41 -43 -46 -48 -50 -50 -50 -50
-50 -50 -50 -48 -46 -43 -41 -38 -35 -33 -31 -29 -28 -28 -28 -29 -31 -33 -35 -38 -41 -43 -46 -48 -50 -50 -50
-50 -50 -50 -47 -44 -41 -38 -35 -32 -29 -26 -24 -23 -22 -23 -24 -26 -29 -32 -35 -38 -41 -44 -47 -50 -50 -50
-50 -50 -48 -45 -42 -39 -35 -32 -28 -25 -21 -18 -16 -15 -16 -18 -21 -25 -28 -32 -35 -39 -42 -45 -48 -50 -50
-50 -50 -47 -44 -40 -37 -33 -29 -25 -20 -16 -12 -9 -7 -9 -12 -16 -20 -25 -29 -33 -37 -40 -44 -47 -50 -50
-50 -48 -45 -42 -39 -35 -31 -26 -21 -16 -10 -4 1 3 1 -4 -10 -16 -21 -26 -31 -35 -39 -42 -46 -48 -50
-50 -48 -45 -41 -38 -34 -29 -24 -18 -12 -4 4 13 18 13 4 -4 -12 -18 -24 -29 -34 -38 -41 -45 -48 -50
-50 -47 -44 -41 -37 -33 -28 -23 -16 -9 1 13 28 44 28 13 1 -9 -16 -23 -28 -33 -37 -41 -44 -47 -50
-50 -47 -44 -41 -37 -33 -28 -22 -15 -7 3 18 44 100 44 18 3 -7 -16 -22 -28 -33 -37 -41 -44 -47 -50
-50 -47 -44 -41 -37 -33 -28 -23 -16 -9 1 13 28 44 28 13 1 -9 -16 -23 -28 -33 -37 -41 -44 -47 -50
-50 -48 -45 -41 -38 -34 -29 -24 -18 -12 -4 4 13 18 13 4 -4 -12 -18 -24 -29 -34 -38 -41 -45 -48 -50
-50 -48 -45 -42 -39 -35 -31 -26 -21 -16 -10 -4 1 3 1 -4 -10 -16 -21 -26 -31 -35 -39 -42 -46 -48 -50
-50 -50 -47 -44 -40 -37 -33 -29 -25 -20 -16 -12 -9 -7 -9 -12 -16 -20 -25 -29 -33 -37 -40 -44 -47 -50 -50
-50 -50 -48 -45 -42 -39 -35 -32 -28 -25 -21 -18 -16 -16 -16 -18 -21 -25 -28 -32 -35 -39 -42 -45 -48 -50 -50
-50 -50 -50 -47 -44 -41 -38 -35 -32 -29 -26 -24 -23 -22 -23 -24 -26 -29 -32 -35 -38 -41 -44 -47 -50 -50 -50
-50 -50 -50 -48 -46 -43 -41 -38 -35 -33 -31 -29 -28 -28 -28 -29 -31 -33 -35 -38 -41 -43 -46 -48 -50 -50 -50
-50 -50 -50 -50 -48 -46 -43 -41 -39 -37 -35 -34 -33 -33 -33 -34 -35 -37 -39 -41 -43 -46 -48 -50 -50 -50 -50
-50 -50 -50 -50 -50 -48 -46 -44 -42 -40 -39 -38 -37 -37 -37 -38 -39 -40 -42 -44 -46 -48 -50 -50 -50 -50 -50
-50 -50 -50 -50 -50 -50 -48 -47 -45 -44 -42 -41 -41 -41 -41 -41 -42 -44 -45 -47 -48 -50 -50 -50 -50 -50 -50
-50 -50 -50 -50 -50 -50 -50 -50 -48 -47 -46 -45 -44 -44 -44 -45 -46 -47 -48 -50 -50 -50 -50 -50 -50 -50 -50
-50 -50 -50 -50 -50 -50 -50 -50 -50 -50 -48 -48 -47 -47 -47 -48 -48 -50 -50 -50 -50 -50 -50 -50 -50 -50 -50
-50 -50 -50 -50 -50 -50 -50 -50 -50 -50 -50 -50 -50 -50 -50 -50 -50 -50 -50 -50 -50 -50 -50 -50 -50 -50 -50

Figure 4.2. a) A two dimensional model for the electrostatic field generated by a point charge centered in an aperture held at a potential having the opposite sign. b) Values used to generate the model.

along the fiber length. In this case, the field would only be bilaterally symmetric (Figure 4.3 and 4.4). With an arrangement of this type, charge stabilization would be difficult to maintain due to discharging as the charge continued to build up. If the conductive filament were connected to ground using a conductive adhesive mounting material, a stabilized charge could be maintained using a thin wire with high resistivity. Due to the partial conductivity of the filament, the charge would be less localized (Figure 4.5).

Attempts to control the field shape by applying regions of charge around the aperture were not very productive. Modeling showed that although these regions were able to influence the field, they were too far from the central charged region to effect the field close to the center of the aperture (Figure 4.6). The modeling exercise suggests that field shaping to obtain a radially symmetric field from an initial non-radial charge center will not be completely successful. Without good radial symmetry, some degree of image distortion will exist. It therefore appears imperative to generate a central point charge for maximum image integrity.

a

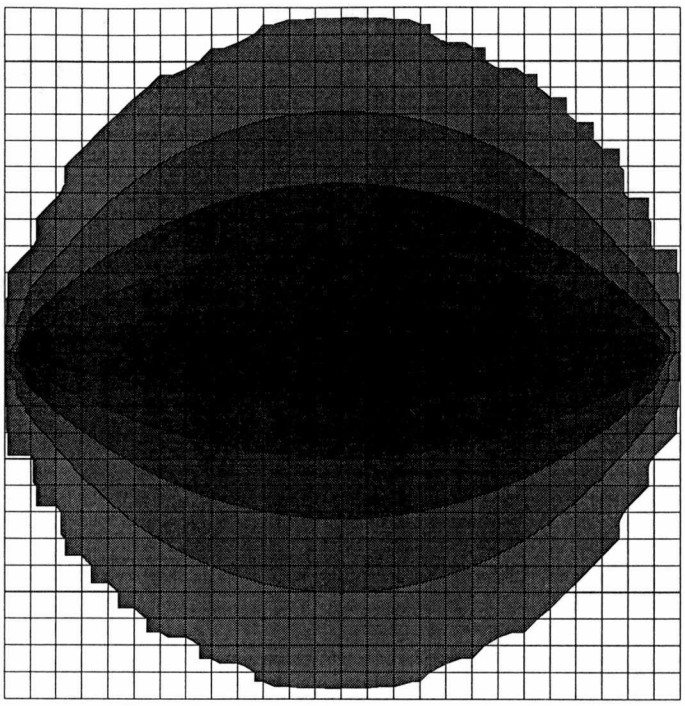

b

0	0	0	0	0	0	0	0	0	0	0	0	0	0	0	0	0	0	0	0	0	0	0	0	0
0	0	0	0	0	0	0	0	0	0	0	2	2	2	3	2	2	2	0	0	0	0	0	0	0
0	0	0	0	0	0	0	0	0	2	3	4	5	5	5	5	5	4	3	2	0	0	0	0	0
0	0	0	0	0	0	0	2	3	5	6	7	8	8	8	8	8	7	6	5	3	2	0	0	0
0	0	0	0	0	0	3	5	6	8	9	10	11	11	11	11	11	10	9	8	6	5	3	0	0
0	0	0	0	0	3	6	8	10	11	13	14	14	15	15	15	14	14	13	11	10	8	6	3	0
0	0	0	0	3	6	9	11	13	15	16	17	18	18	18	18	18	17	16	15	13	11	9	6	3
0	0	0	5	9	13	15	17	19	20	21	22	22	22	22	22	22	21	20	19	17	15	13	9	5
0	0	4	9	14	17	20	22	23	25	25	26	26	27	26	26	25	25	23	22	20	17	14	9	4
0	0	8	14	19	22	25	27	28	29	30	30	31	31	31	30	30	29	28	27	25	22	19	14	8
0	7	15	20	25	28	30	32	33	34	35	35	35	35	35	35	35	34	33	32	30	28	25	20	15
0	13	23	28	32	35	36	38	39	39	40	40	40	40	40	40	40	39	39	38	36	35	32	28	23
0	24	34	38	41	42	43	44	44	45	45	45	45	45	45	45	45	44	44	43	42	41	38	34	24
0	50	50	50	50	50	50	50	50	50	50	50	50	50	50	50	50	50	50	50	50	50	50	50	50
0	24	34	38	41	42	43	44	44	44	45	45	45	45	45	45	45	44	44	44	43	42	41	38	34
0	13	22	28	32	35	36	38	38	39	40	40	40	40	40	40	40	39	38	38	36	35	32	28	22
0	7	15	20	25	28	30	32	33	34	34	35	35	35	35	35	34	34	33	32	30	28	25	20	15
0	0	8	14	19	22	24	26	28	29	30	30	31	31	31	30	30	29	28	26	24	22	19	14	8
0	0	4	9	14	17	19	21	23	24	25	26	26	26	26	26	25	24	23	22	19	17	14	9	4
0	0	0	5	9	12	15	17	19	20	21	22	22	22	22	22	22	21	20	19	17	15	13	9	5
0	0	0	3	6	9	11	13	15	16	17	18	18	18	18	18	18	17	16	15	13	11	9	6	3
0	0	0	0	3	5	8	10	11	12	13	14	14	14	14	14	14	13	12	11	10	8	5	3	0
0	0	0	0	0	3	5	6	8	9	10	11	11	11	11	11	11	10	9	8	6	5	3	0	0
0	0	0	0	0	0	2	3	5	6	7	7	8	8	8	7	7	6	5	3	2	0	0	0	0
0	0	0	0	0	0	0	0	2	3	4	5	5	5	5	5	4	3	2	0	0	0	0	0	0
0	0	0	0	0	0	0	0	0	0	2	2	2	2	2	2	2	0	0	0	0	0	0	0	0
0	0	0	0	0	0	0	0	0	0	0	0	0	0	0	0	0	0	0	0	0	0	0	0	0

Figure 4.3. a) A two dimensional model for the electrostatic field generated by a uniformly charged filament suspended across the diameter of an aperture held at ground potential. b) Values used to generate the model.

a

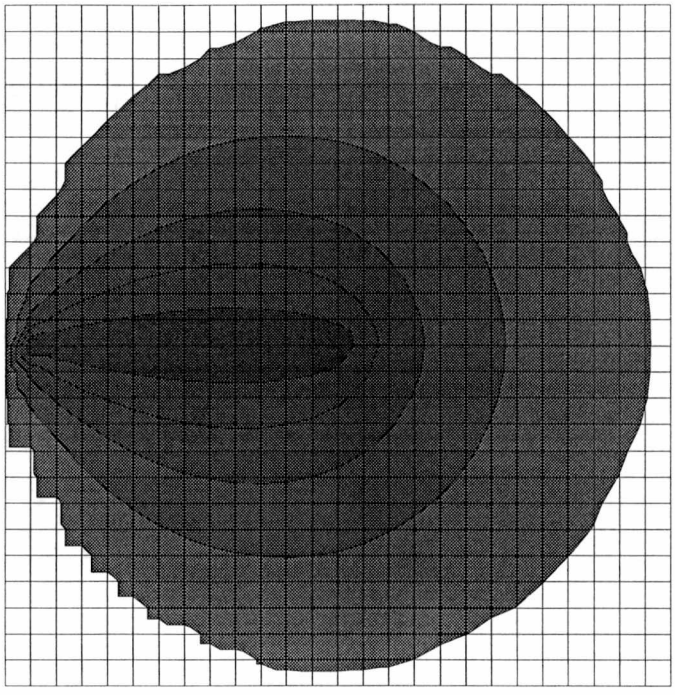

b

0	0	0	0	0	0	0	0	0	0	0	0	0	0	0	0	0	0	0	0	0	0	0	0	0
0	0	0	0	0	0	0	0	0	0	1	2	2	2	2	1	1	0	0	0	0	0	0	0	0
0	0	0	0	0	0	0	0	0	2	2	3	4	4	4	3	3	3	2	1	0	0	0	0	0
0	0	0	0	0	0	0	2	3	4	5	6	6	6	6	5	5	4	3	3	2	1	0	0	0
0	0	0	0	0	0	2	4	6	7	8	8	8	8	8	8	7	6	5	4	3	2	1	0	0
0	0	0	0	0	3	5	7	9	10	11	11	11	11	11	10	9	8	7	6	4	3	2	1	0
0	0	0	0	3	6	8	10	12	13	14	14	14	14	13	12	11	10	9	7	6	5	3	2	1
0	0	0	5	9	12	14	16	17	18	18	18	17	16	15	14	12	10	9	7	6	4	3	1	0
0	0	4	9	13	16	19	20	21	22	22	22	21	20	18	16	14	12	10	9	7	5	4	2	1
0	0	8	14	18	21	24	25	26	27	27	26	25	23	21	19	16	14	12	10	8	6	4	3	1
0	7	14	20	24	27	29	31	32	32	32	31	30	28	25	22	19	16	13	11	9	7	5	3	2
0	13	22	28	32	34	36	37	37	38	37	37	35	33	29	24	21	17	14	12	9	7	5	4	2
0	24	34	38	40	42	43	43	44	44	44	43	42	39	33	27	22	18	15	12	10	8	6	4	3
0	50	50	50	50	50	50	50	50	50	50	50	50	50	36	28	23	19	15	12	10	8	6	4	3
0	24	34	38	40	42	43	43	44	44	43	43	42	39	33	27	22	18	15	12	10	8	6	4	3
0	13	22	28	32	34	36	37	37	38	37	37	35	33	29	24	21	17	14	12	9	7	5	4	2
0	7	14	20	24	27	29	31	31	32	32	31	30	28	25	22	19	16	13	11	9	7	5	3	2
0	0	8	14	18	21	24	25	26	27	27	26	25	23	21	19	16	14	12	10	8	6	4	3	1
0	0	4	9	13	16	19	20	21	22	22	22	21	20	18	16	14	12	10	8	7	5	4	2	1
0	0	0	5	9	12	14	16	17	18	18	18	17	16	15	14	12	10	9	7	6	4	3	1	0
0	0	0	3	6	8	10	12	13	14	14	14	14	13	12	11	10	9	7	6	5	3	2	1	0
0	0	0	0	3	5	7	9	10	11	11	11	11	11	10	9	8	7	6	4	3	2	1	0	0
0	0	0	0	0	2	4	6	7	8	8	8	8	8	8	7	6	5	4	3	2	1	0	0	0
0	0	0	0	0	0	2	3	4	5	5	6	6	6	5	5	4	3	3	2	1	0	0	0	0
0	0	0	0	0	0	0	0	2	2	3	4	4	4	3	3	2	2	1	0	0	0	0	0	0
0	0	0	0	0	0	0	0	0	0	1	2	2	2	2	1	1	0	0	0	0	0	0	0	0
0	0	0	0	0	0	0	0	0	0	0	0	0	0	0	0	0	0	0	0	0	0	0	0	0

Figure 4.4. a) A two dimensional model for the electrostatic field generated by a uniformly charged filament suspended halfway across an aperture held at ground potential. b) Values used to generate the model.

a

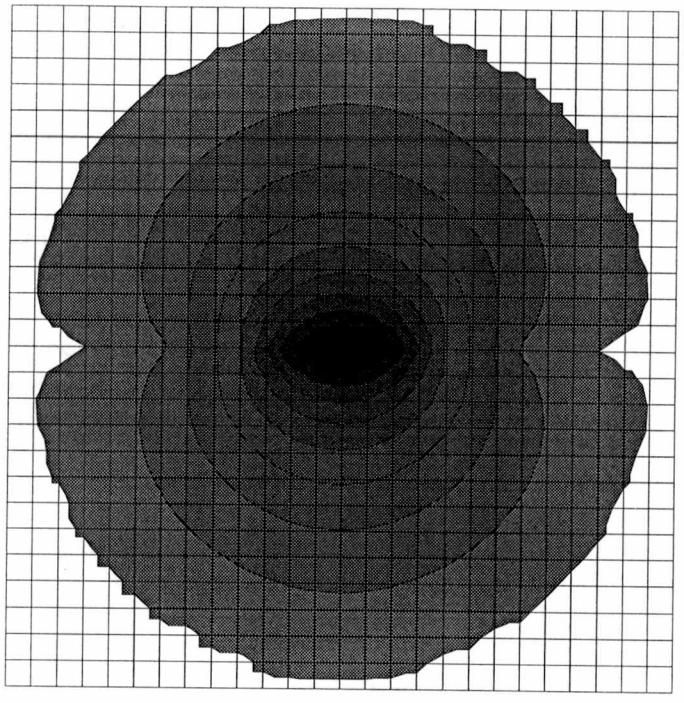

b

0	0	0	0	0	0	0	0	0	0	0	0	0	0	0	0	0	0	0	0	0	0	0	0	0	0
0	0	0	0	0	0	0	0	0	0	0	2	2	3	3	3	2	2	0	0	0	0	0	0	0	0
0	0	0	0	0	0	0	0	0	2	3	4	5	5	6	5	5	4	3	2	0	0	0	0	0	0
0	0	0	0	0	0	0	2	3	4	6	7	8	9	9	9	8	7	6	4	3	2	0	0	0	0
0	0	0	0	0	0	2	4	5	7	9	10	11	12	12	12	11	10	9	7	5	4	2	0	0	0
0	0	0	0	0	2	4	6	8	10	12	14	15	16	16	16	15	14	12	10	8	6	4	2	0	0
0	0	0	0	1	3	6	8	11	13	16	18	19	20	21	20	19	18	16	13	11	8	6	3	1	0
0	0	0	0	2	5	7	10	13	16	19	22	24	26	26	26	24	22	19	16	13	10	7	5	2	0
0	0	0	1	3	6	9	12	16	20	23	27	30	32	32	32	30	27	23	19	16	12	9	6	3	1
0	0	0	2	4	7	10	14	18	23	28	32	36	39	40	39	36	32	28	23	18	14	10	7	4	2
0	0	1	2	4	7	10	15	20	26	32	38	44	48	50	48	44	38	32	26	20	15	10	7	4	2
0	0	1	2	4	7	10	15	21	28	36	45	54	60	62	60	54	45	36	28	21	15	10	7	4	2
0	0	1	1	3	5	8	14	21	30	40	53	66	76	79	76	66	53	40	30	21	14	8	5	3	1
0	0	0	0	1	3	5	10	20	30	40	60	80	100	100	100	80	60	40	30	20	10	5	3	1	0
0	0	1	1	3	5	8	14	21	30	40	53	66	76	79	76	66	53	40	30	21	14	8	5	3	1
0	0	1	2	4	7	10	15	21	28	36	45	54	60	62	60	54	45	36	28	21	15	10	7	4	2
0	0	1	2	4	7	10	15	20	26	32	38	44	48	50	48	44	38	32	26	20	15	10	7	4	2
0	0	0	2	4	7	10	14	18	23	28	32	36	39	40	39	36	32	28	23	18	14	10	7	4	2
0	0	0	1	3	6	9	12	16	19	23	27	30	32	32	32	30	27	23	19	16	12	9	6	3	1
0	0	0	0	2	5	7	10	13	16	19	22	24	26	26	26	24	22	19	16	13	10	7	5	2	0
0	0	0	0	1	3	6	8	11	13	15	18	19	20	21	20	19	18	15	13	11	8	6	3	1	0
0	0	0	0	0	2	4	6	8	10	12	14	15	16	16	16	15	14	12	10	8	6	4	2	0	0
0	0	0	0	0	0	2	4	5	7	9	10	11	12	12	12	11	10	9	7	5	4	2	0	0	0
0	0	0	0	0	0	0	2	3	4	6	7	8	8	9	8	8	7	6	4	3	2	0	0	0	0
0	0	0	0	0	0	0	0	0	2	3	4	5	5	6	5	5	4	3	2	0	0	0	0	0	0
0	0	0	0	0	0	0	0	0	0	0	2	2	3	3	3	2	2	0	0	0	0	0	0	0	0
0	0	0	0	0	0	0	0	0	0	0	0	0	0	0	0	0	0	0	0	0	0	0	0	0	0

Figure 4.5. a) A two dimensional model for the electrostatic field generated by a centrally charged poorly conductive filament suspended across the diameter of an aperture held at ground potential. b) Values used to generate the model.

a

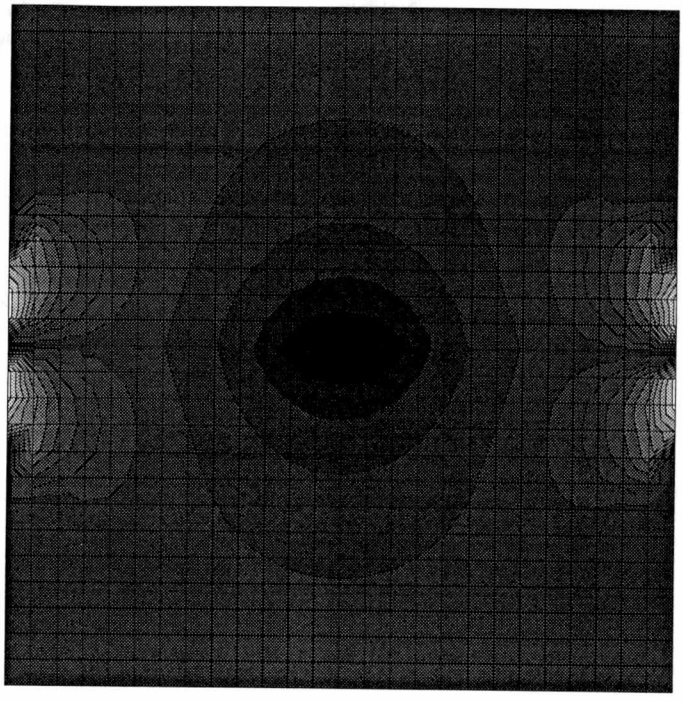

b

0	0	0	0	0	0	0	0	0	0	0	0	0	0	0	0	0	0	0	0	0	0	0	0	0
0	0	0	0	0	0	0	0	0	0	0	1	2	2	2	2	2	1	0	0	0	0	0	0	0
0	0	0	0	0	0	0	0	0	1	2	3	4	4	5	4	4	3	2	1	0	0	0	0	0
0	0	0	0	0	0	1	2	3	4	5	6	7	7	7	6	6	4	3	2	1	0	0	0	0
0	0	0	0	0	0	2	3	5	6	8	9	10	10	10	9	8	6	5	3	2	0	0	0	0
0	0	0	0	-1	0	2	4	6	9	11	12	13	14	13	12	11	9	6	4	2	0	-1	0	0
0	0	0	-3	-3	-1	2	5	8	11	14	16	17	18	17	16	14	11	8	5	2	-1	-3	-3	0
0	0	0	-8	-7	-3	1	6	10	14	18	21	22	23	22	21	18	14	10	6	1	-3	-7	-8	0
0	-50	-33	-23	-14	-7	0	7	13	18	23	26	28	29	28	26	23	18	13	7	0	-7	-14	-23	-33
0	-100	-60	-36	-20	-9	0	8	16	22	28	33	36	37	36	33	28	22	16	8	0	-9	-20	-36	-60
-150	-109	-69	-41	-22	-9	2	11	19	27	35	41	46	47	46	41	35	27	19	11	2	-9	-22	-41	-69
-200	-117	-67	-38	-19	-6	4	14	23	33	43	52	58	60	58	52	43	33	23	14	4	-6	-19	-38	-67
-200	-90	-45	-23	-10	-1	8	17	27	38	51	64	75	78	75	64	51	38	27	17	8	-1	-10	-23	-45
0	0	0	1	3	5	10	20	30	40	60	80	100	100	100	80	60	40	30	20	10	5	3	1	0
-200	-90	-45	-23	-10	-1	8	17	27	38	51	64	75	78	75	64	51	38	27	17	8	-1	-10	-23	-45
-200	-117	-67	-38	-19	-6	4	14	23	33	43	52	58	60	58	52	43	33	23	14	4	-6	-19	-38	-67
-150	-109	-69	-41	-22	-9	2	11	19	27	35	41	46	47	46	41	35	27	19	11	2	-9	-22	-41	-69
0	-100	-60	-36	-20	-9	0	8	16	22	28	33	36	37	36	33	28	22	16	8	0	-9	-20	-36	-60
0	-50	-33	-23	-14	-7	0	7	13	18	23	26	28	29	28	26	23	18	13	7	0	-7	-14	-23	-33
0	0	0	-8	-7	-3	1	6	10	14	18	21	22	23	22	21	18	14	10	6	1	-3	-7	-8	0
0	0	0	-3	-3	-1	2	5	8	11	14	16	17	18	17	16	14	11	8	5	2	-1	-3	-3	0
0	0	0	0	-1	0	2	4	6	9	11	12	13	14	13	12	11	9	6	4	2	0	-1	0	0
0	0	0	0	0	0	2	3	5	6	8	9	10	10	10	9	8	6	5	3	2	0	0	0	0
0	0	0	0	0	0	1	2	3	4	5	6	7	7	7	6	5	4	3	2	1	0	0	0	0
0	0	0	0	0	0	0	0	1	2	3	4	4	5	4	4	3	2	1	0	0	0	0	0	0
0	0	0	0	0	0	0	0	0	0	1	2	2	2	2	2	1	0	0	0	0	0	0	0	0
0	0	0	0	0	0	0	0	0	0	0	0	0	0	0	0	0	0	0	0	0	0	0	0	0

Figure 4.6. a) A two dimensional model for the electrostatic field generated by a centrally charged poorly conductive filament suspended across the diameter of an aperture having regions of charge of opposite sign placed around its inside diameter. b) Values used to generate the model.

CHAPTER FIVE

EXPERIMENTAL

Experimentation with phase contrast transmission electron microscopy began with an investigation of the applicability of off axis electron holography to the phase imaging of weakly scattering materials. Little has been published in this area and most work involving electron holography has revolved around the use of this technique for the imaging of magnetic materials and for improving high resolution imaging. Imaging conditions suitable for high resolution holography were not appropriate for the lower magnification requirements of this investigation due to the limited field of electron interference fringes. The optics of the Hitachi HF-2000 FEG TEM, operating at 200 keV and equipped with an electron biprism (Figure 2.8) are used in a non-standard mode to demagnify the object image in relationship to the interference fringes. The electron biprism was positioned before the intermediate lens. The objective lens is either turned off or weakly excited to reduce image magnification and the intermediate lens is more highly excited to increase the field of electron interference. This results in usable negative magnifications of around 60,000x with a region of electron interference greater than 1 micron.

To improve coherence, the illumination is made highly elliptical through the use of the condenser stigmators and the astigmatic beam is aligned with its long axis parallel to the filament of the electron biprism. The improved coherence in the direction perpendicular to the biprism improves fringe contrast. With sufficient contrast, the fringe spacing is altered by changing the potential on the biprism. Higher voltage results in finer fringe spacing (Figure 5.1).

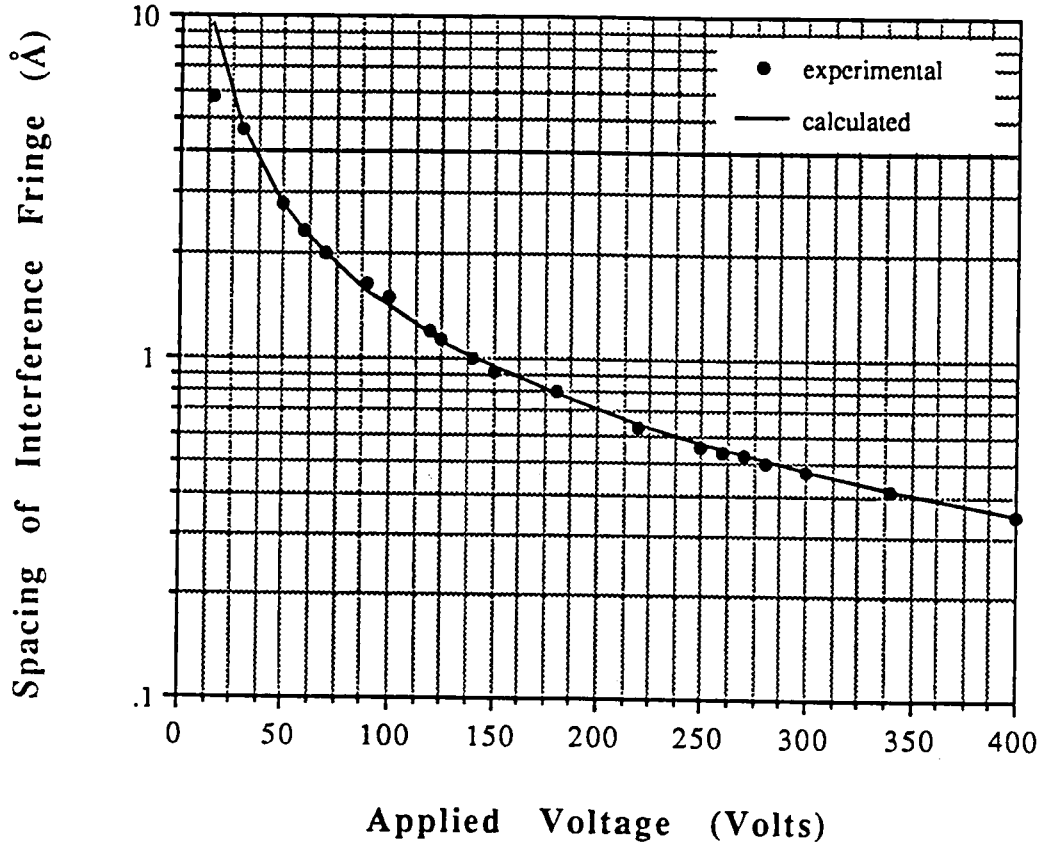

Figure 5.1. The relationship of interference fringe spacing versus biprism voltage for the Hitachi HF-2000 TEM operating at an accelerating potential of 200 keV.

Source: Zhang X. 1992 New electron beam methods for materials microcharacterization, *Dissertation Univ. of Tennessee Knoxville.*

The beam intensity striking the sample is kept low to prevent significant beam damage and was approximately 1000 $e^-/nm^2/sec$. Under these conditions, focusing using the fluorescent screen is difficult. Mitsubishi electron image film, push processed, was used instead of Kodak 4489 Electron Image Film because it is approximately three times more sensitive, but it still required exposure times in excess of 20 seconds. It became apparent that a more sensitive recording method is needed. At this time, the experiment was transferred from the University of Tennessee instrument to the system at the High Temperature Materials Laboratory of the Oak Ridge National Laboratory that is equipped with a Gatan 1000 x 1000 pixel slow scan CCD camera and a Gatan high resolution CCD camera. The high resolution CCD camera aids image focusing and electron biprism optimization and the slow scan CCD camera enables images to be recorded using two second exposures. The slow scan CCD camera, controlled by Gatan's Digital Micrograph software, has a more linear response function than photographic film and also aids computer reconstruction due to the direct recording of a digital image.

Image reconstruction was performed using a numerical reconstruction software package developed by Joy and Bunn (1993). After selecting a 256 x 256 pixel subset of the hologram, a Fourier transform is performed, followed by sideband selection, spectrum recentering, and an inverse Fourier transform. The numerical image wave that results is stored as a two dimensional array of complex numbers of which the real part contains the amplitude information and the imaginary part contains the phase information. The amplitude and phase images are displayed on the computer monitor with 256 gray levels. Phase amplification is done numerically.

The initial phase plate experiments attempted to duplicate previous work described in the literature. This was done to determine the advantages and disadvantages of the early style devices when used on a modern electron microscope. Based on the work of Kanaya et al. (1957), an amorphous film having a central hole was the first phase plate attempted.

A solvent cast collodion film (carbon stabilized) was used to cover a copper grid using a standard grid coating technique. A small drop of a 50% collodion[1], 50% amyl acetate solution was released onto a 100 x 190 mm culture dish over filled with Millipore deionized and filtered water. The first film was removed using a glass rod. This removes any surface debris and results in a cleaner second film. Precleaned single hole copper grids, 3 mm OD and 50 μm ID, were placed on the film after the solvent had evaporated. The copper grids serve as apertures and will be referred to as such. The apertures are picked up by coming down onto them with a precleaned screen, pushing the apertures under the water, and following a "U" motion to lift the grids from the culture dish. Once dry the apertures are stabilized with a thin evaporated film of carbon (approximately 2 nm) using a Blazer's turbomolecular pumped high vacuum evaporator. Total film thickness was estimated to be approximately 12 nm. The apertures were then sent to Precision Laser Services[2] for laser drilling to provide a 2-5 μm diameter hole. It was hoped that a laser could be used to accurately place a clean edged hole in the center of the aperture that would be superior to a fine probe punched hole. Attempts failed due to an

---

[1]Collodion USP (40 g nitrocellulose, 750 ml diethylether, 250 ml Isopropanol)

[2]Precision Laser Services, 314 East Wallace St., Fort Wayne, Indiana 46803

inability to laser drill without causing catastrophic film failure. Precision Laser Services suggested that the use of an eximer laser might be more successful.

After the initial failure to laser drill holes, electron beam thinning was attempted where it was thought that a high intensity focused electron beam could be used to thin a hole through the carbon stabilized collodion film. A VG 601 FEG scanning transmission electron microscope (STEM) operating with a nanoamp of current focused onto a region 4 nm square failed to provide any significant thinning even after 30 mins. of exposure. The experiment was repeated using a collodion film without the evaporated carbon coating. In this case the film proved to be unstable and easily ruptured even at lower magnifications (20,000x).

Further attempts to produce an amorphous film with a small central hole were abandoned when it was realized that a modification of a method proposed by Johnson and Parsons (1973) would likely generate a higher contrast image. They employed a contamination spot centered on an amorphous film that failed to improve contrast when compared to a normal objective aperture; however it is believed that their phase plate had several major shortcomings. First the amorphous film used was too thick, causing too much additional scatter of the already weak diffracted beam. The film was also not suspended over an aperture which failed to provide the normal aperture contrast and like most thick film phase plates of the day, this one also had a short useful life due to electron beam contamination. Johnson and Parson's (1973) attempts to image biological thin sections did result in additional contrast of the film used to support the sections but it was thought that it distracted from the image of the section. This type of negative phase plate was abandoned by them due to the above failures and was not revisited by other workers.

A device based on Johnson and Parsons' (1973) idea, but overcoming some of the difficulties, was constructed using the following procedure. Thin carbon films, 2.5 nm thick were purchased from Arizona Carbon Foil Co[1]. The carbon films are evaporated on freshly cleaved mica sheets. Film thickness of EM Ultra Smooth Carbon films from Arizona Carbon Foil are determined using surface density measurements and the accuracy of the thickness measurement is claimed to be ±10%. These films are extremely clean, fine structured and electron beam stable. To prepare the phase plate, a hose and clamp are attached to a Coors 60244, 114 mm porcelain funnel with a fixed perforated plate that is half filled with Millipore deionized and filtered water. A clean piece of filter paper is placed at the bottom of the flask upon which pre-cleaned single hole gold grids, 3 mm OD 75 μm ID are placed. Gold was chosen because of its inertness, higher atomic number, and because it will effectively stop 200 keV electrons. The carbon was removed from the mica by lowering the sheet of mica, carbon side up into the water at an angle of approximately 120°. The water level was then reduced while carefully guiding the carbon film over the gold apertures. Upon drying at room temperature, apertures were examined in a transmission electron microscope. The apertures with the best carbon films, those free of debris and cracks were chosen for use as phase plates. Contamination spots were grown on the film in a JEOL 6300 Scanning Electron Microscope. A test pattern of spots (Figure 5.2) showed that spots could be accurately positioned and that the thickness could be varied with time. Several problems were noted; it was difficult to focus on the substrate due to a lack of

---

[1]Arizona Carbon Foil Co. Inc., 2239 East Kleindale Road, Tucson, AZ 85719-2440.

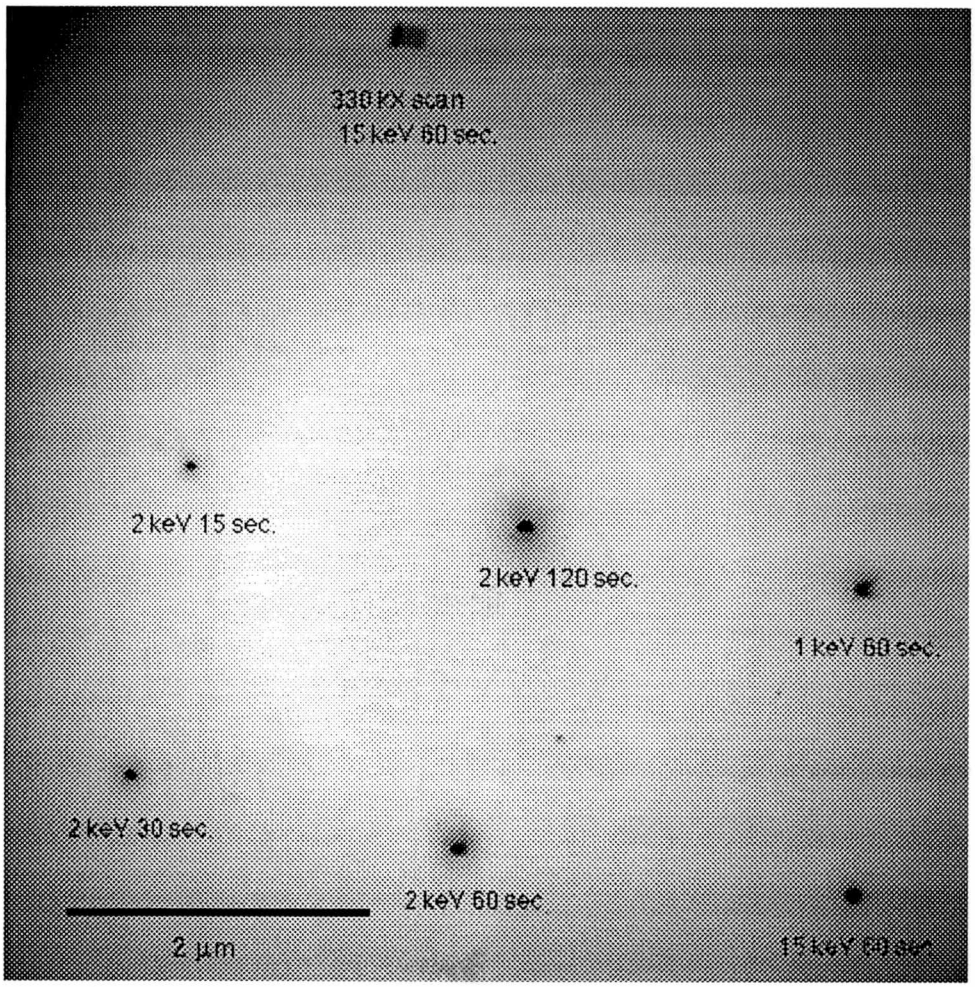

Figure 5.2. STEM micrograph of a series of contamination spots grown on a 2.5 nm thick carbon foil using a JEOL 6300F SEM.

structure, contamination spots were less than 100 nm in diameter after 300 sec. (5 keV, condenser lens coarse #7) and scan lines of contamination were noticeable at the left edge of the scanned area. Small increases in the contamination spot size could be made by reducing the condenser lens excitation; however the spots were still less than 100 nm in size.

A central contamination spot was grown in a Hitachi H-600 TEM using a 0.2 μm spot setting. This instrument was chosen as it was the "dirtiest" TEM available in our laboratory. Larger spots were produced, focusing was easier and contamination due to beam scanning was avoided in the H-600. Spots were accurately and easily placed in the center of the gold aperture. Only a few phase plates were made using this method so it is not known how easy it would be to get reproducible thicknesses. Ideally, a microscope fitted with an electron energy loss spectrometer could be used to in-situ monitor relative thickness for good reproducibility. An alternative method would be to monitor the scattered electrons using an annular dark field detector. In either case, standards of similar composition would be required to generate an absolute thickness. Carbon foils, available from Arizona Carbon Foil Co., range in thickness from 2.5 to 50 nm. Thicknesses are known to within 10% for thinner foils and to within 1 nm for thicker foils making them good thickness standards. Using the following equation (Heidenreich 1964) and solving for a $\pi/2$ phase shift the optimum film thickness t may be calculated:

$$t = \varphi \lambda V_a / \pi V_i \qquad (5.1)$$

For: V_i = 7.8 volts

V_a = 200,000 volts

λ = 0.002508 nm

φ = $\pi/2$

The deposited contamination t should be approximately 32.2 nm assuming that the mean inner ionization potential of the contamination material is close to that of evaporated carbon. Using a 2.5 nm foil would bring the total desired thickness at the contaminated region to 34.7 nm.

For the current experiment, no attempt to precisely control the thickness of the spot was made. It was believed that, for proof of concept, any reasonable phase shift would result in enhanced contrast even if it were not the optimum $\pi/2$ shift.

The diameter of the contamination spot produced using this method is about 0.75 μm (Figure 5.3). By tilting the film 60° in the TEM it was found that the contamination spot was about the desired thickness.

A phase plate similar in principle to that used by Unwin (1974) was also fabricated. Instead of employing Unwin's method of using a spider to produce a thin filament, a method similar to that used to make electron biprism filaments for off axis electron holography was used. An approximately 2 cm piece of a quartz fiber optic was drawn in the flame of a propane torch until the two halves separated. The finest filament at the end of the drawn area was carefully positioned to bisect the 75 μm hole in a single hole gold grid described above; excess material was trimmed using a sharp clean razor blade. A small wood dowel sharpened to a point was used to tease the fiber into position. When in the desired location, the ends were glued in place using collodion insuring that the resin was not placed any closer than 25 μm from the edge of the hole.

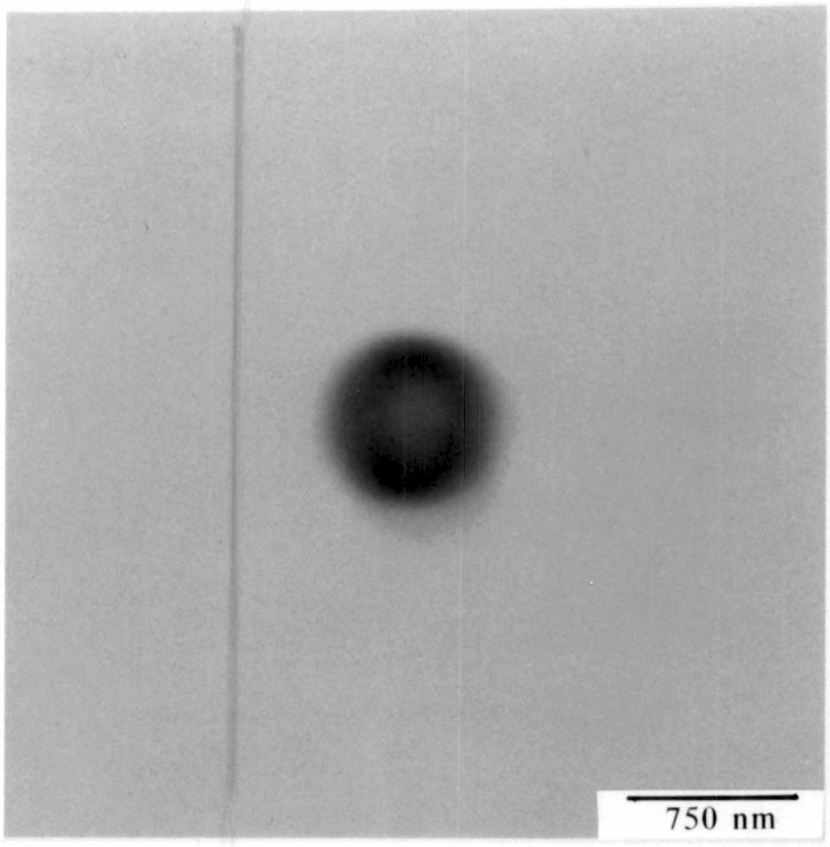

Figure 5.3. A contamination spot grown on a 2.5 nm thick carbon foil using a Hitachi H-600 TEM. The film was mounted over a 75 μm gold aperture.

Collodion proved to have the desired viscosity and drying time for the application. Fifty percent collodion in amyl acetate and 0.5% formvar in diethylchloride and cyanoacrylate resin were also tried, but either the drying time was too fast or too slow or the viscosity made it more difficult to work with the securing resin. All mounting operations were performed under a stereo microscope at 40X magnification. Both sides of the plate were coated with approximately 1 nm of sputtered chromium using a Denton Model DV502A high vacuum chromium sputter coater. Presputtering with the shutter closed for at least 60 sec at a current of 150 μA, removed the surface oxides from the target. Each 1 nm deposition was performed at a current of 30 μA using 99.995% argon and a pressure of 5 millitorr.

The two phase plates, the contamination spot and the quartz filament device (Figure 5.4), along with an unaltered 75 μm inside diameter gold aperture were mounted to a standard Topcon 002B platinum objective aperture strip modified by removing a 1 mm wide strip down the length of the region of the aperture strip containing the apertures. The phase plates and gold aperture were trimmed to fit the aperture strip and held in place at the edges by tacking with small quantities of conductive silver paint. An attempt was made to place these devices as close to the position of the original apertures as possible to facilitate positioning during use.

The modified aperture strip was placed in the standard, Topcon 002B objective aperture holder and inserted into the microscope. The conditions giving the best contrast were determined for each device and the results were compared to images taken using the 75 μm aperture.

During use, the filament phase plate was found to require a narrowly defined set of optimum operating conditions that resulted in low beam brightness

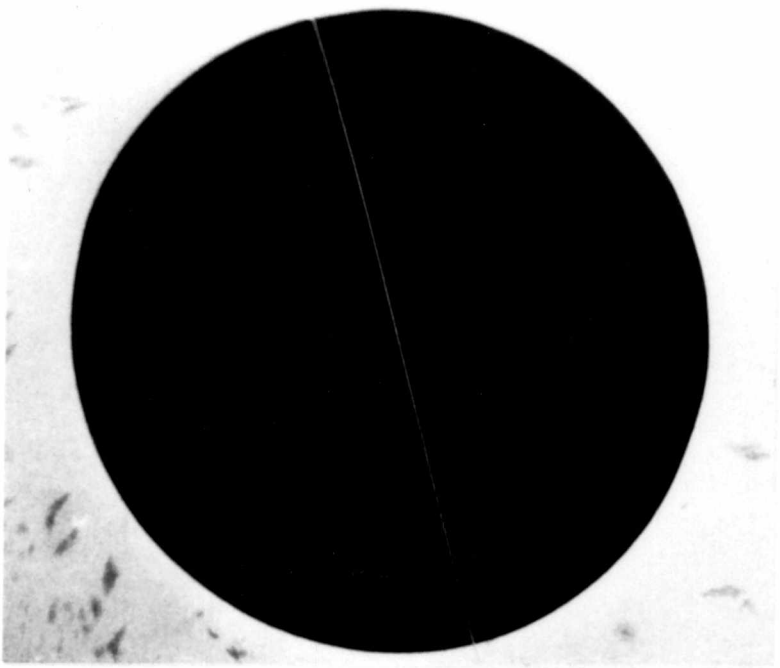

Figure 5.4. A SEM micrograph of a drawn quartz filament suspended across the diameter of a 75 μm gold aperture.

and longer than desired exposure times. If the charge on the filament, or more importantly the strength of the field, could be controlled independently of the illuminating conditions, this problem could be resolved.

In trying to produce a more ideal phase shifting device, it was decided to try charging the filament or charging the aperture using a variable power supply. The former approach was abandoned due to inability to make electrical contact with the filament while at the same time electrically floating the filament from the aperture. The following modifications were made in the latter approach. A quartz filament phase plate was made using the procedure described above. Prior to mounting the phase plate to the aperture holder, two approximately 1.5 x 2 min. pieces of perfluoroethylene tape were glued, using collodion, to both sides of the hole on the holder over which the aperture would be placed. The phase plate was then glued to the blocks, again using collodion, with the perfluroethylene keeping the phase plate electrically isolated from the holder. A 75 μm single hole gold aperture was mounted to another aperture position using conductive silver paint. A 0.001 inch diameter gold wire was attached to the phase plate using conductive silver paint. The gold wire was positioned down the length of the holder far enough to clear the objective pole piece and anchored in place using perfluoroethylene blocks as insulators and collodion as glue. It was found that it was necessary to reinforce the final anchor point by wrapping the holder with polyarimid fiber and sealing it with collodion. This was due to the stresses applied to the wire when making the electrical connection of the gold wire to the vacuum feed through. Even though the wire could be positioned initially without shorting, once a potential was applied the wire tended to drift. A length of perfluoroethylene tubing was placed around the gold wire to insulate it. A schematic representation of the set up is shown in figure 5.5. A

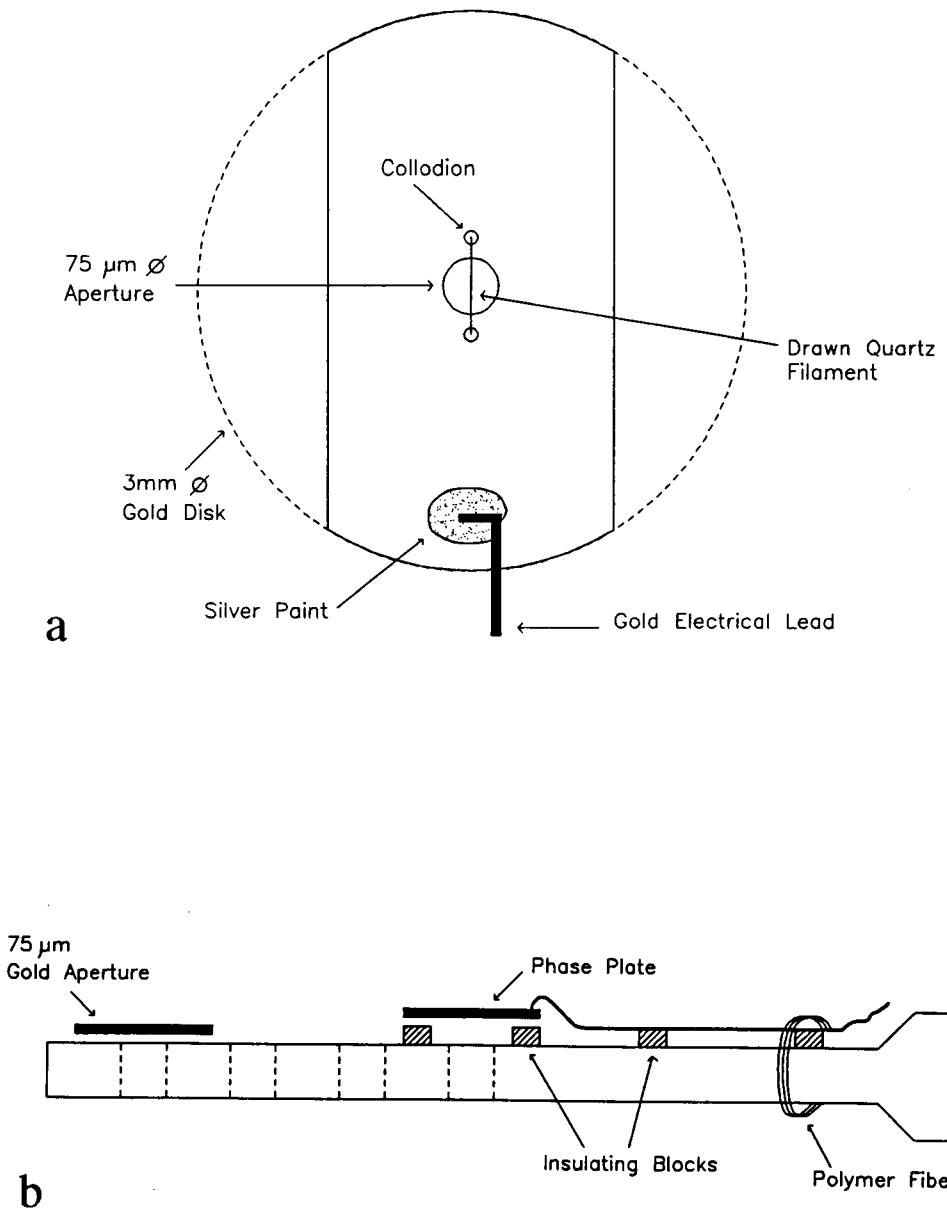

Figure 5.5. A schematic drawing showing a) the details of the compensated electrostatic phase plate and b) the aperture holder with the phase plate and standard 75 μm aperture attached (not drawn to scale).

photograph of the actual modification is shown in figure 5.6. A coax BNC 1 pin vacuum feed through[1] was used to provide the electrical connection. A clip type connector with a set screw wire clamp was modified to fit over the feed through post and a flange was fabricated to couple the vacuum feed through to the microscope column (Figure 5.7). A HP6516A DC power supply capable of delivering ± potentials up to 999.9 volts in 0.1 volt increments was connected to the vacuum feed through using a BNC connector cable.

All phase plate imaging experiments were performed on the Topcon 002B TEM using a LAB_6 emitter operating at 200 keV accelerating potential. The microscope was equipped with the standard ultra high resolution pole piece. Kodak Type 4489 Electron Image Film was used for all micrographs and was processed in a Richcolor automatic film processor using Kodak D-19 developer.

Contrast transfer functions were produced by digitizing the micrographs using a flat bed scanner and performing a 512 X 512 pixel Fourier transform using NIH Image software. An intensity line scan across a representative region of the micrographs was also made on the digitized images using NIH Image for comparison of image contrast.

---

[1]Insulator Seal Incorporated, Hayward, CA, model number 601A0379-2.

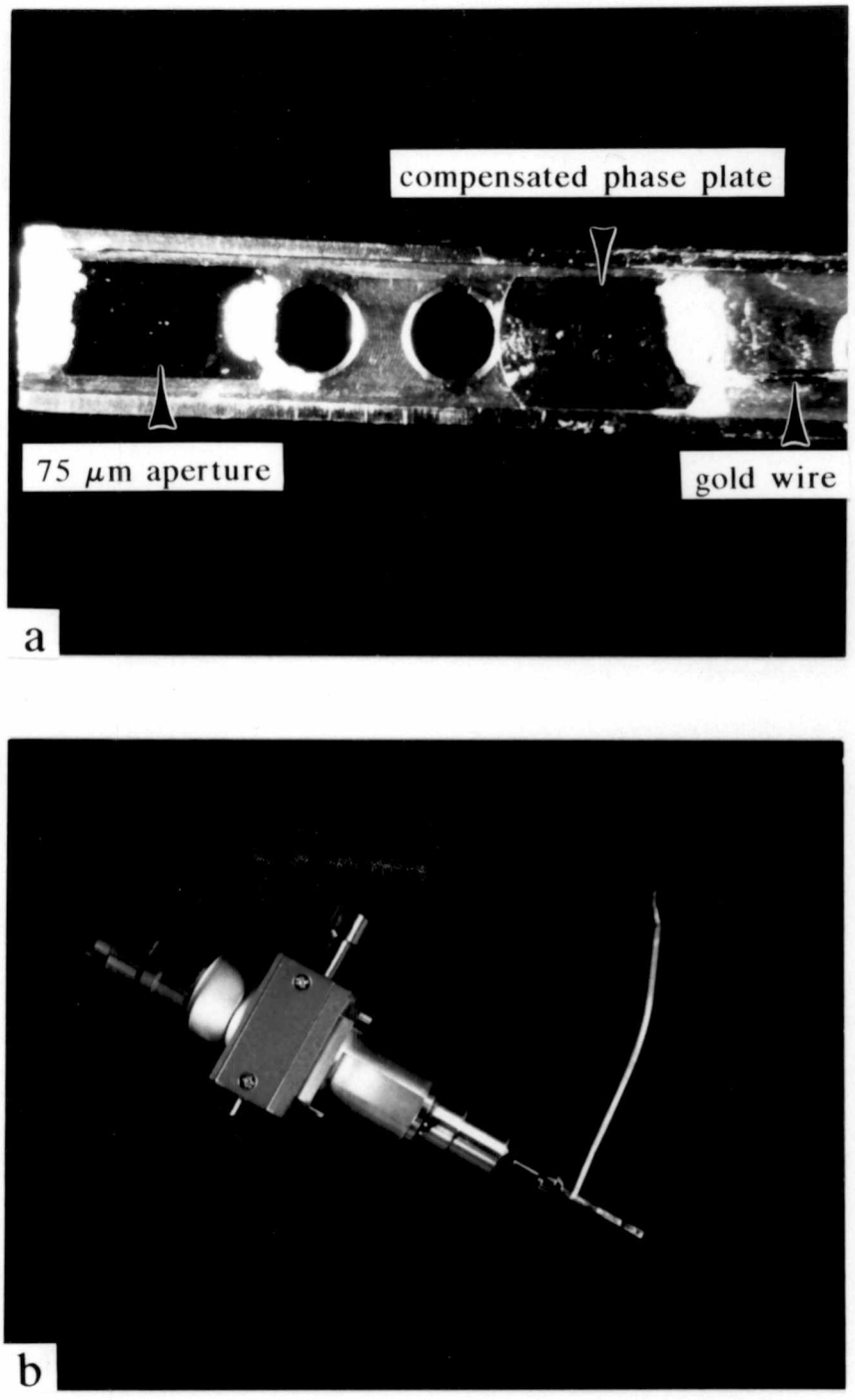

Figure 5.6. Photographs of the a) Topcon 002B objective aperture holder blade and b) aperture holder.

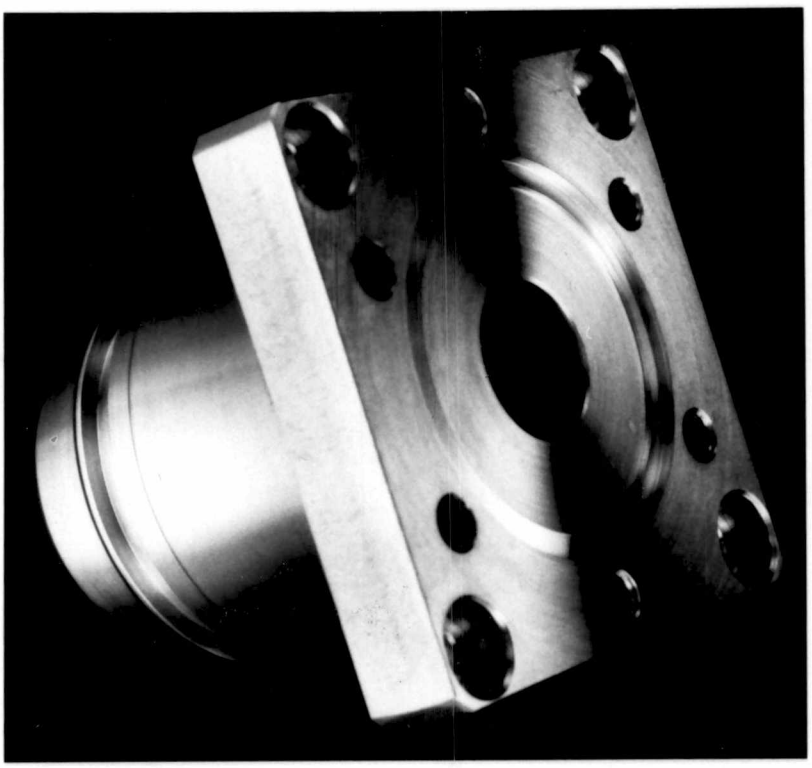

Figure 5.7. Photograph of a fabricated flange used to attach the vacuum feed through for the phase plate compensation circuit to the microscope column.

CHAPTER SIX

RESULTS AND DISCUSSION

Optimum contrast using the contamination spot or the quartz filament electrostatic phase plate was obtained when the condenser lens was adjusted to give parallel illumination with the objective lens focal point set to the objective aperture plane. This condition was established by first focusing on the object where focus was approximately Scherzer focus (-38.8 nm) as set using a 75 μm objective aperture. Defocus values of approximately -240 nm and 160 nm were also used to determine the effect that greater defocus has on image quality (Figure 6.1 and 6.2). The microscope was then switched to the selected area diffraction mode of operation, the 75 μm objective aperture was inserted, the aperture image was focused using the diffraction focus, centered and the C2 condenser lens was adjusted to give the smallest unscattered beam cross over. The phase plate was then inserted and centered using the X and Y aperture translators. The microscope was then switched back to the normal imaging mode where the maximum amount of the undiffracted beam intersected the phase shifting device which resulted in the maximum attenuation of this component.

Selection of the first condenser lens setting and condenser aperture size was less stringent for the contamination spot phase plate than for the electrostatic device. For the contamination spot, as the first condenser lens excitation was reduced and/or the condenser aperture size was increased, the apparent contrast was reduced due to a reduction in the amount of the

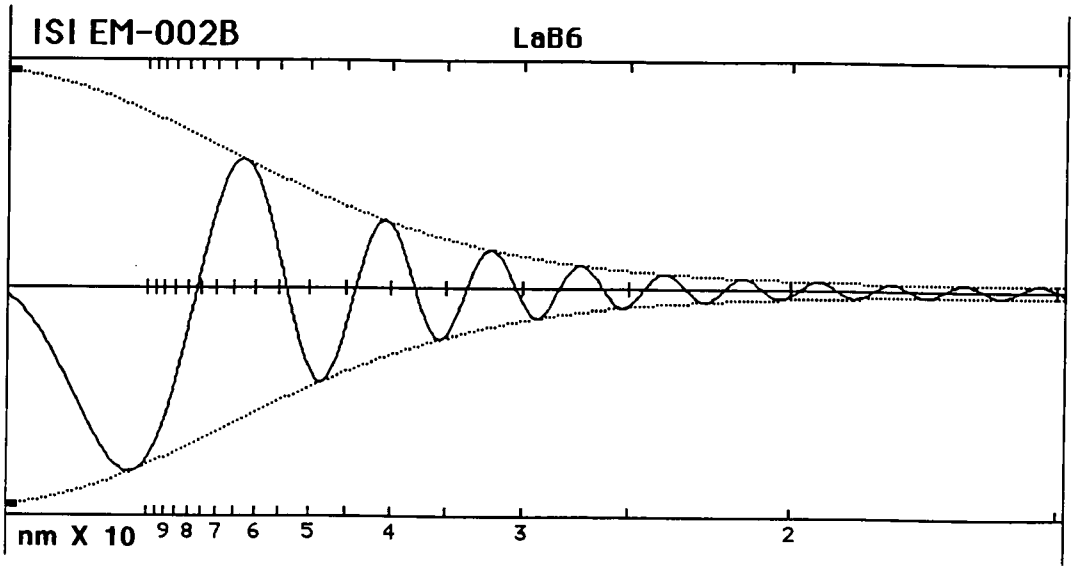

Accelerating voltage=200keV
Thickness= 10 nm

C_s=0.4 mm
Illumination semi-angle= 1.0 mRad

Figure 6.1. Contrast transfer function for a Topcon 002B at a defocus of -240 nm.

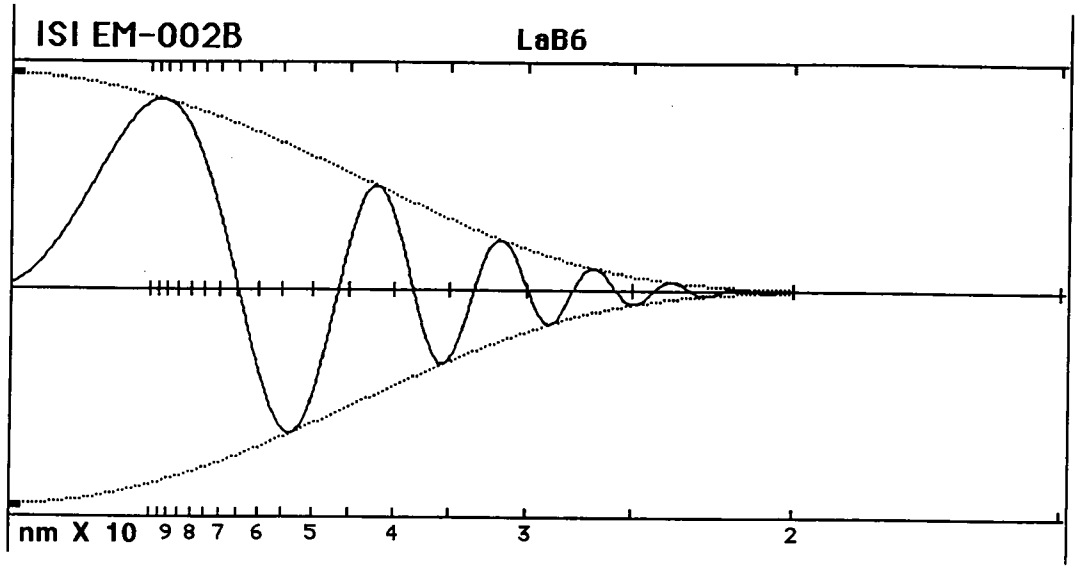

Accelerating voltage=200keV
Thickness= 10 nm

C_S=0.4 mm
Illumination semi-angle= 1.0 mRad

Figure 6.2. Contrast transfer function for a Topcon 002B at a defocus of 160 nm.

undiffracted beam passing through the contamination spot (Figure 6.3-6.6). This could be avoided through the use of a larger diameter contamination spot; however as the contamination spot is increased in size there is a greater chance that the high frequency information contained in the low angle scattered region will also be phase shifted and attenuated significantly reducing the contrast transfer of high frequency detail.

In the conventional TEM mode, exposure times ranged from 12 sec for a high (1) condenser lens excitation to 0.74 sec for the lowest (4) condenser lens excitation setting using a 30 μm C2 aperture. At 20,000 times negative magnification and these condenser lens settings, the field of view was limited by the condenser aperture. Using a 100 μm C2 aperture and a C1 lens setting of 4 resulted in contrast (Figure 6.7) similar to that obtained with the same C1 setting and a 30 μm aperture (Figure 6.6). No significant contrast improvement was seen in the phase plate images taken using a weakly excited C1 lens (Figures 6.6 and 6.7) when compared to an image taken with a conventional 75 μm objective aperture (Figure 6.8). The Topcon 002B illumination convergence angles for each combination of C2 aperture and C1 lens setting are listed in Table 6.1.

At higher magnifications, the same condenser conditions that result in parallel illumination must be maintained for optimum phase contrast. Using a 30 μm C2 aperture, a number 3 C1 lens setting and a negative magnification of 98,000 X, typical exposure times are increased to approximately 26 seconds. The long exposure times are not particularity problematic for non-beam sensitive materials as the microscope's stage has a low drift rate and specimen contamination is minimal; however, exposure times of less than 4 seconds would be preferable. The resultant image is similar to what is anticipated based on

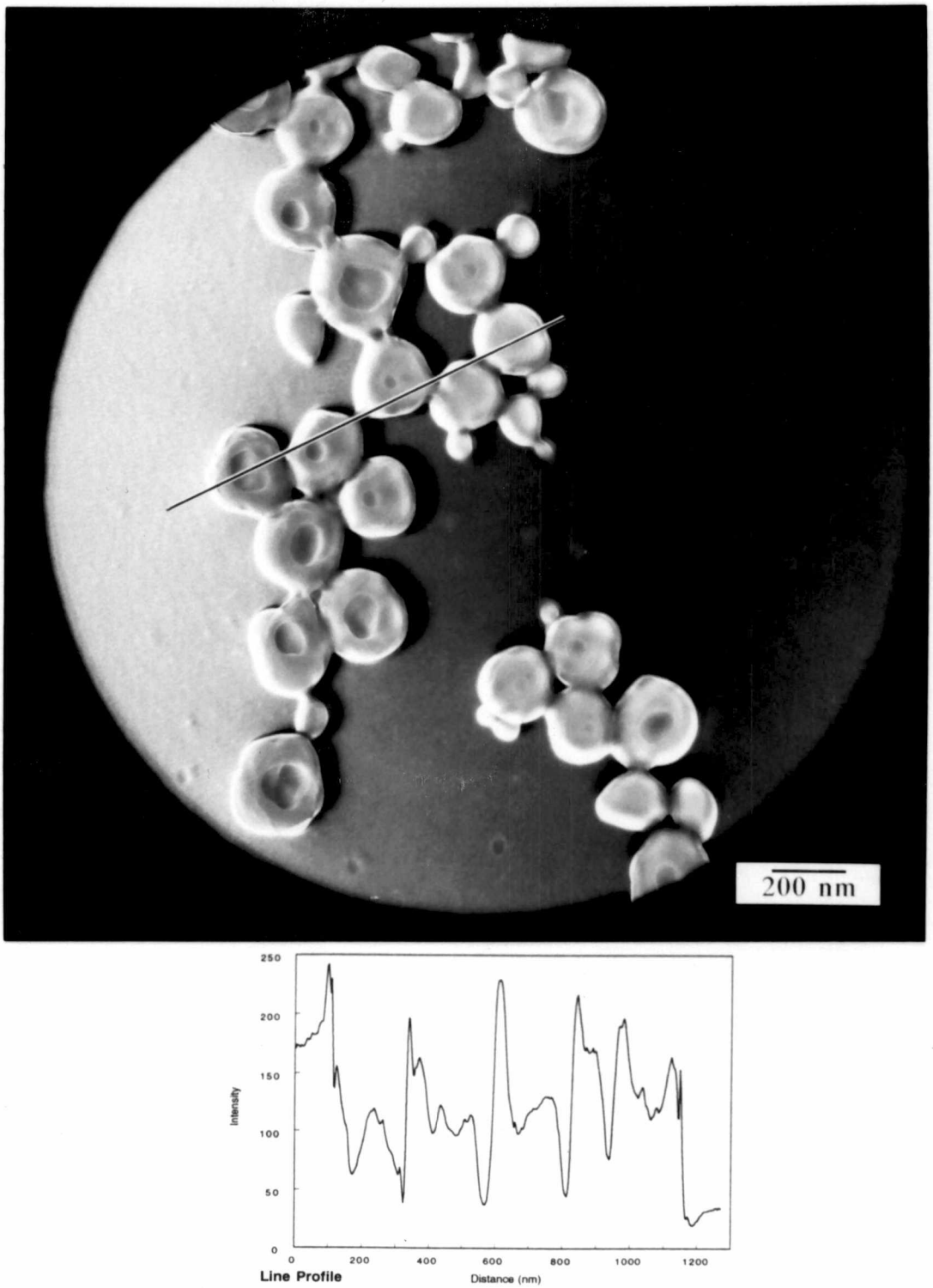

Figure 6.3. Phase contrast image of a porous latex taken using a contamination spot phase plate, a 30 μm condenser aperture and a #1 CL1 setting.

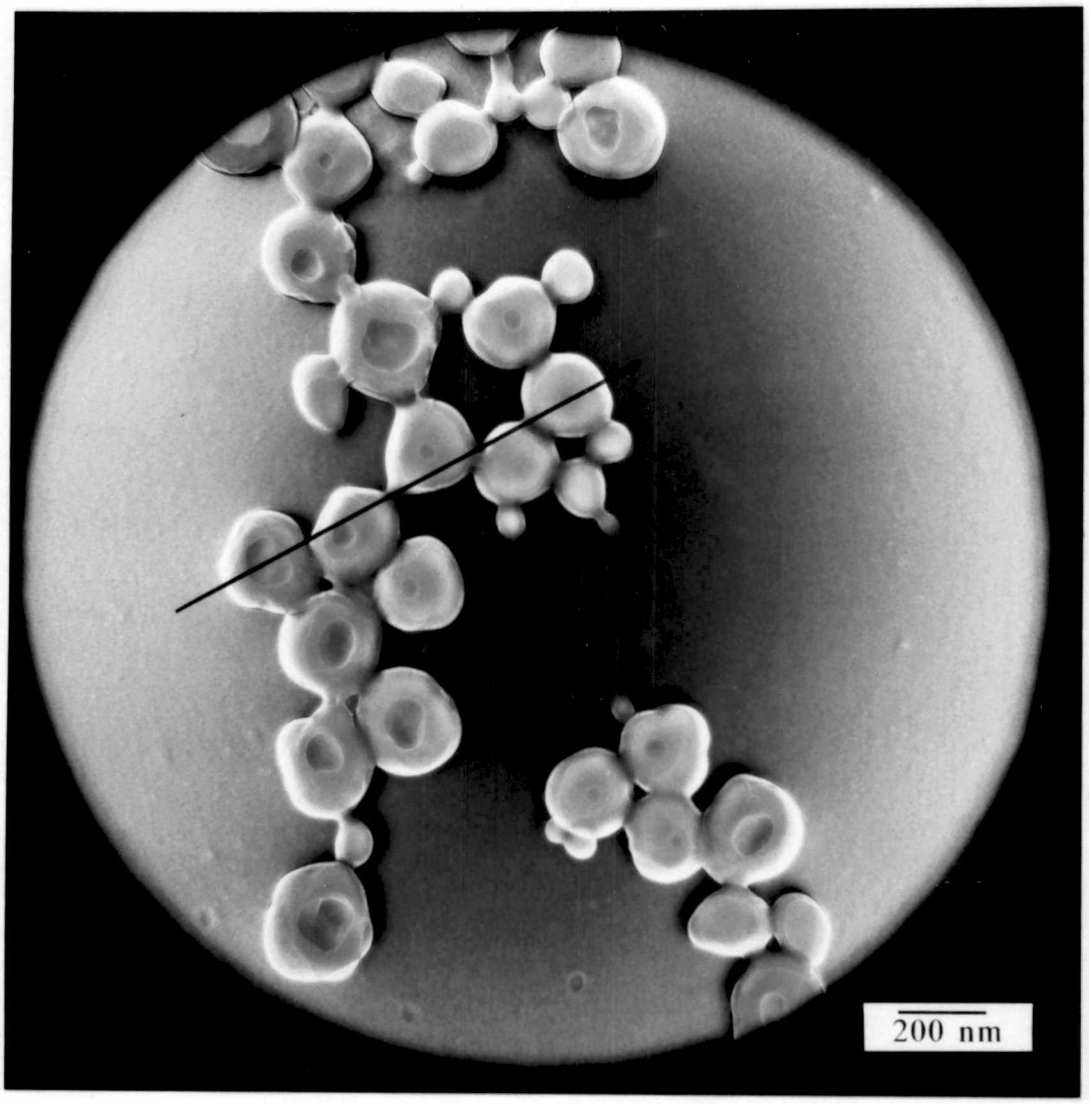

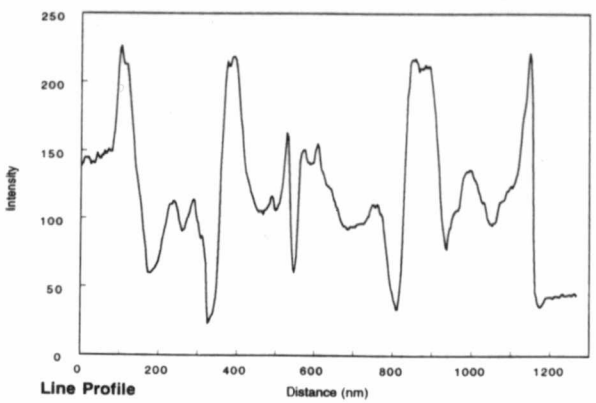

Figure 6.4. Phase contrast image of a porous latex taken using a contamination spot phase plate, a 30 μm condenser aperture and a #2 CL1 setting.

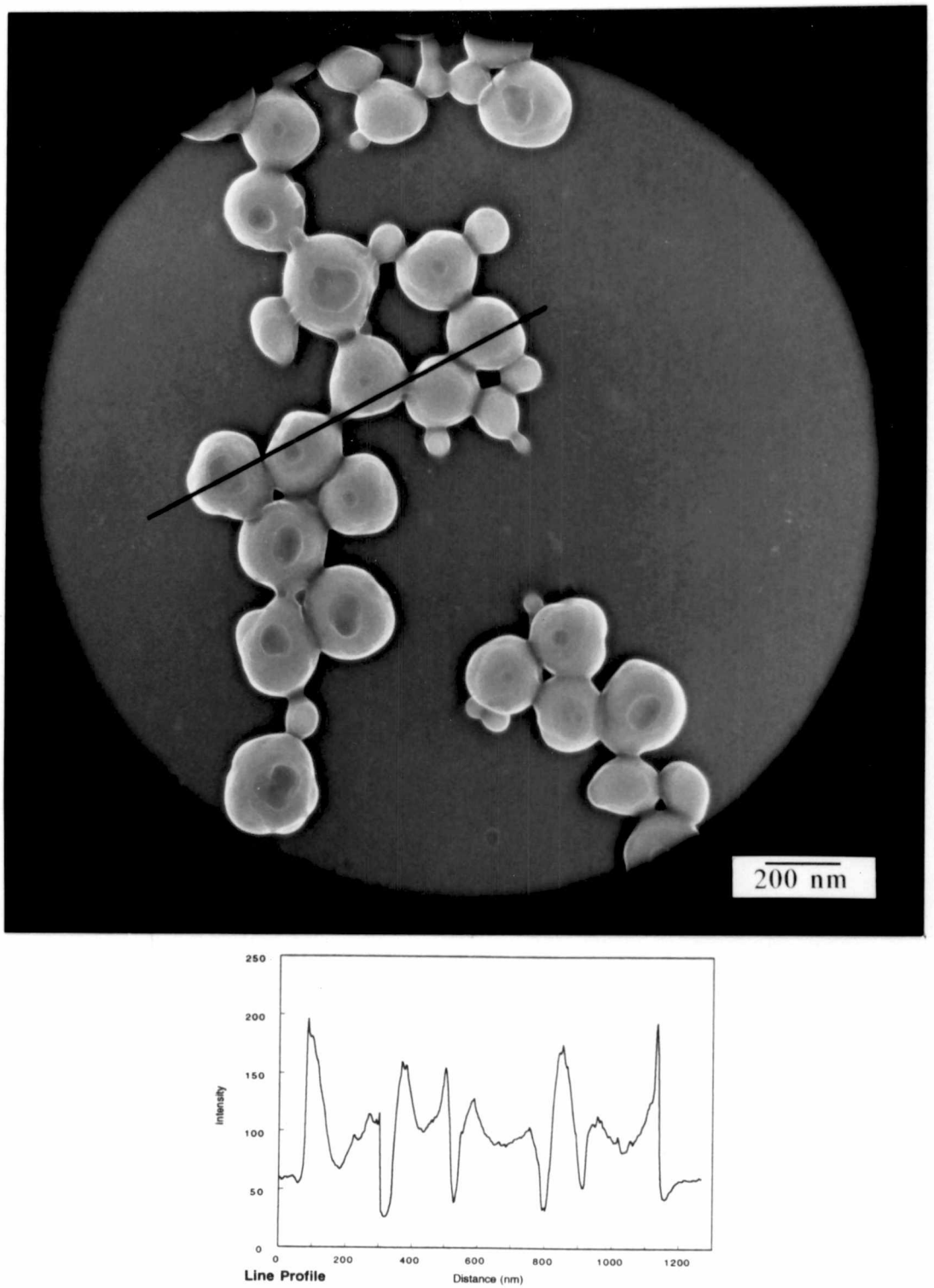

Figure 6.5. Phase contrast image of a porous latex taken using a contamination spot phase plate, a 30 μm condenser aperture and a #3 CL1 setting.

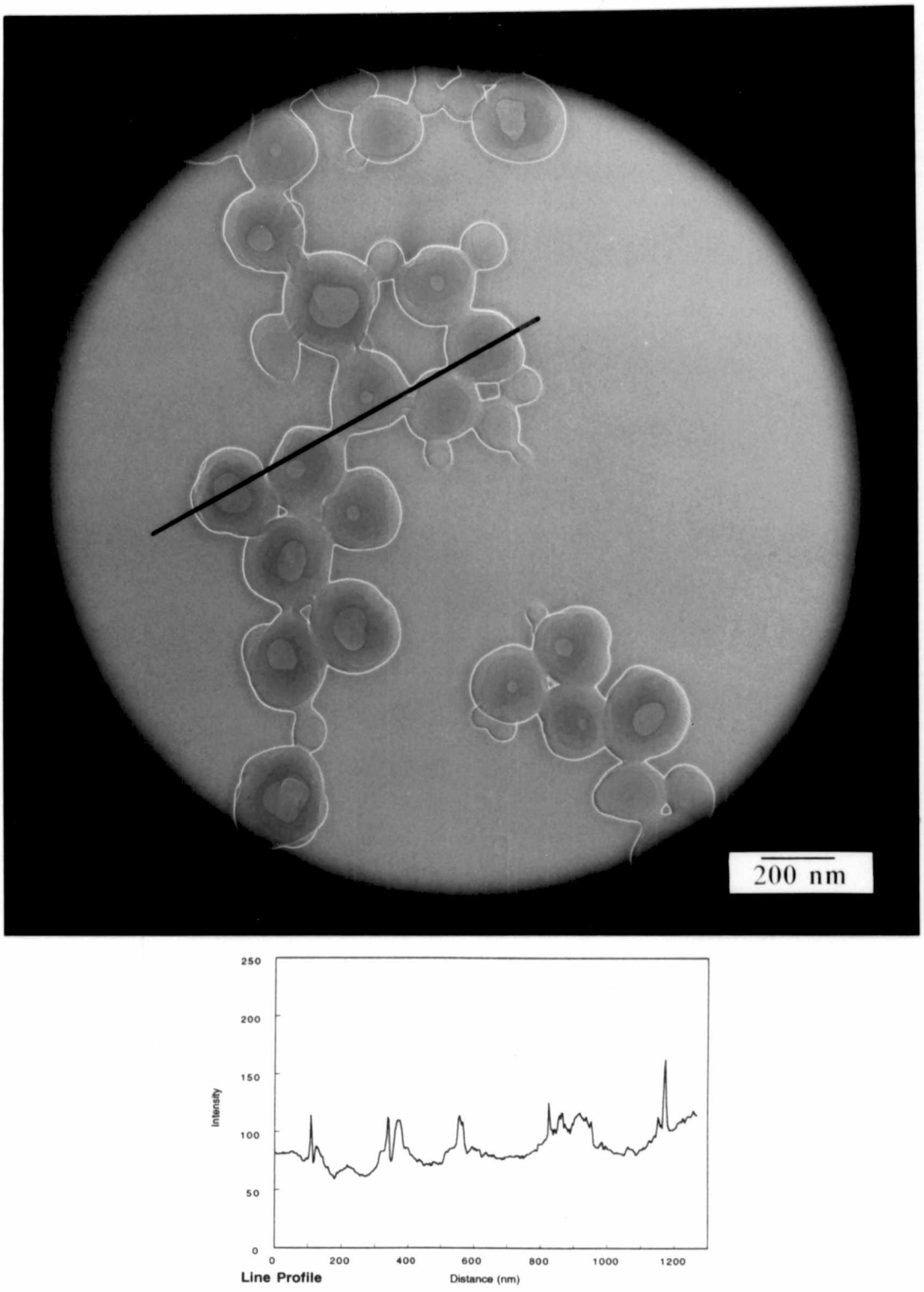

Figure 6.6. Phase contrast image of a porous latex taken using a contamination spot phase plate, a 30 μm condenser aperture and a #4 CL1 setting.

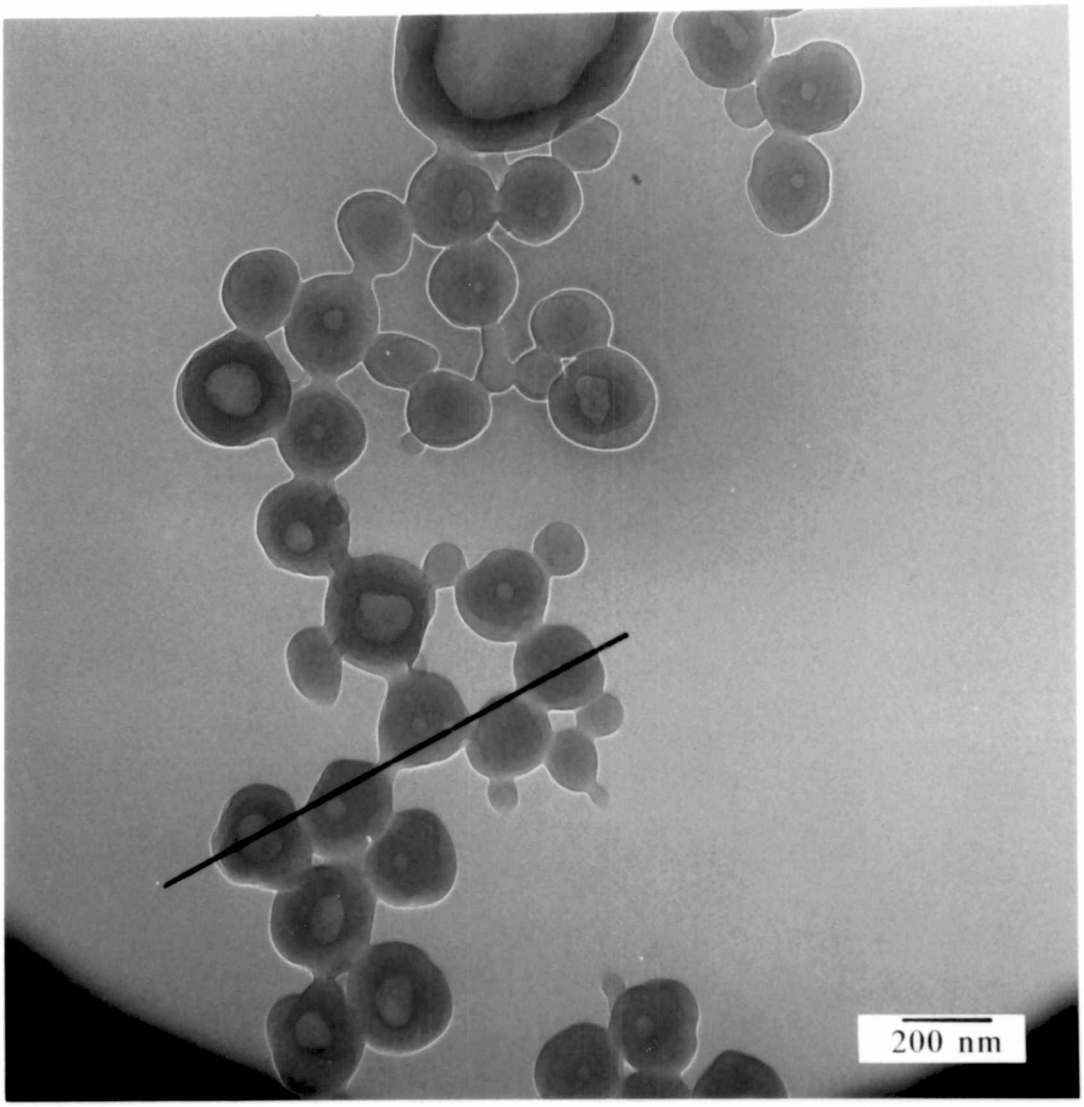

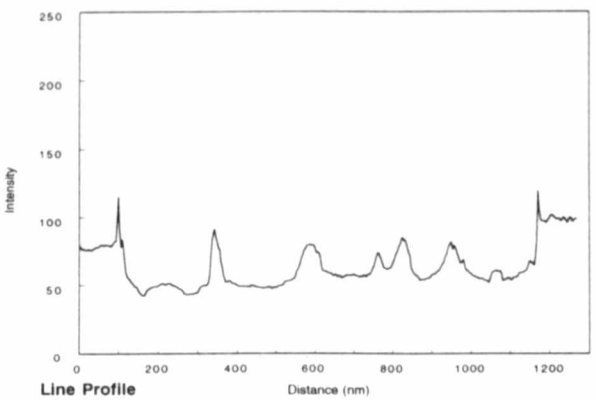

Figure 6.7. Phase contrast image of a porous latex taken using a contamination spot phase plate, a 100 μm condenser aperture and a #4 CL1 setting.

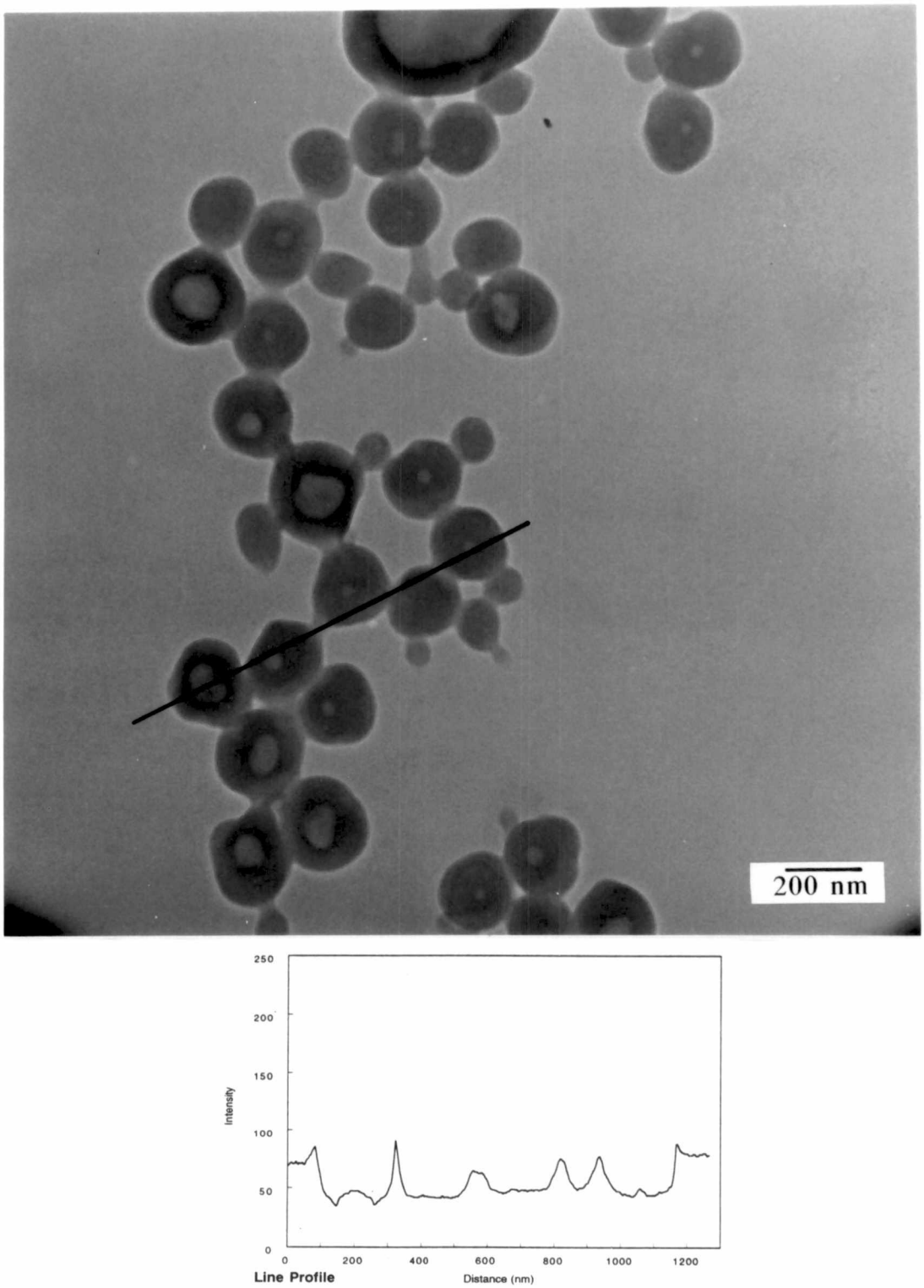

Figure 6.8. TEM micrograph of porous latex taken using a 75 μm objective aperture, a 100 μm condenser aperture and a #4 CL1 setting.

Table 6.1. Illumination convergence angles for the Topcon 002B for C1 lens settings of 0, 1, 2, 3 and 4.

C2 aperture	Convergence Angle
30 μm	1.8 mradians
100 μm	8.9 mradians

light microscopy when a phase retarding, unscattered beam attenuating phase plate is used. The more highly scattering elements of the object have higher intensity than the more weakly scattering components. In this case, the latex particles instead of being darker than the background support film, as expected from conventional bright field microscopy (Figure 6.9), appear lighter against a dark background (Figure 6.10). In addition, the particles have a bright edge that causes them to stand out from the background. A defocus of approximately -240 nm results in an image (Figure 6.11) very similar to the image taken at focus. A defocus of approximately -160 nm results in an image with similar contrast but with a slight loss of resolution (Figure 6.12). When a 75 μm objective aperture is used, instead of the phase plate, the results are quite different when the objective focus is changed to the same extent. The results are the usual lower contrast near focus (Figure 6.9) and higher contrast under (Figure 6.13) and over focus images (Figure 6.14). Fine detail is seen in the under focused image that is not apparent in the in focus or over focused micrograph. This is most dramatic in the marked region of figure 6.13.

Even in the under focused condition, the contrast both in fine and gross features is not as good as for the image taken using the contamination spot phase plate (Figure 6.10). The phase contrast image also takes on a three dimensional perspective that is not apparent using a standard objective aperture. The contrast transfer of features having a spatial frequency greater than approximately 2 nm is significantly increased (Figures 6.10 and 6.13). There are several advantages of the contamination spot phase plate: it is easy to use; the image focus is less critical than in standard imaging conditions, particularly if the image tends towards the under focused side of focus; significant contrast improvement and a three dimensional perspective is

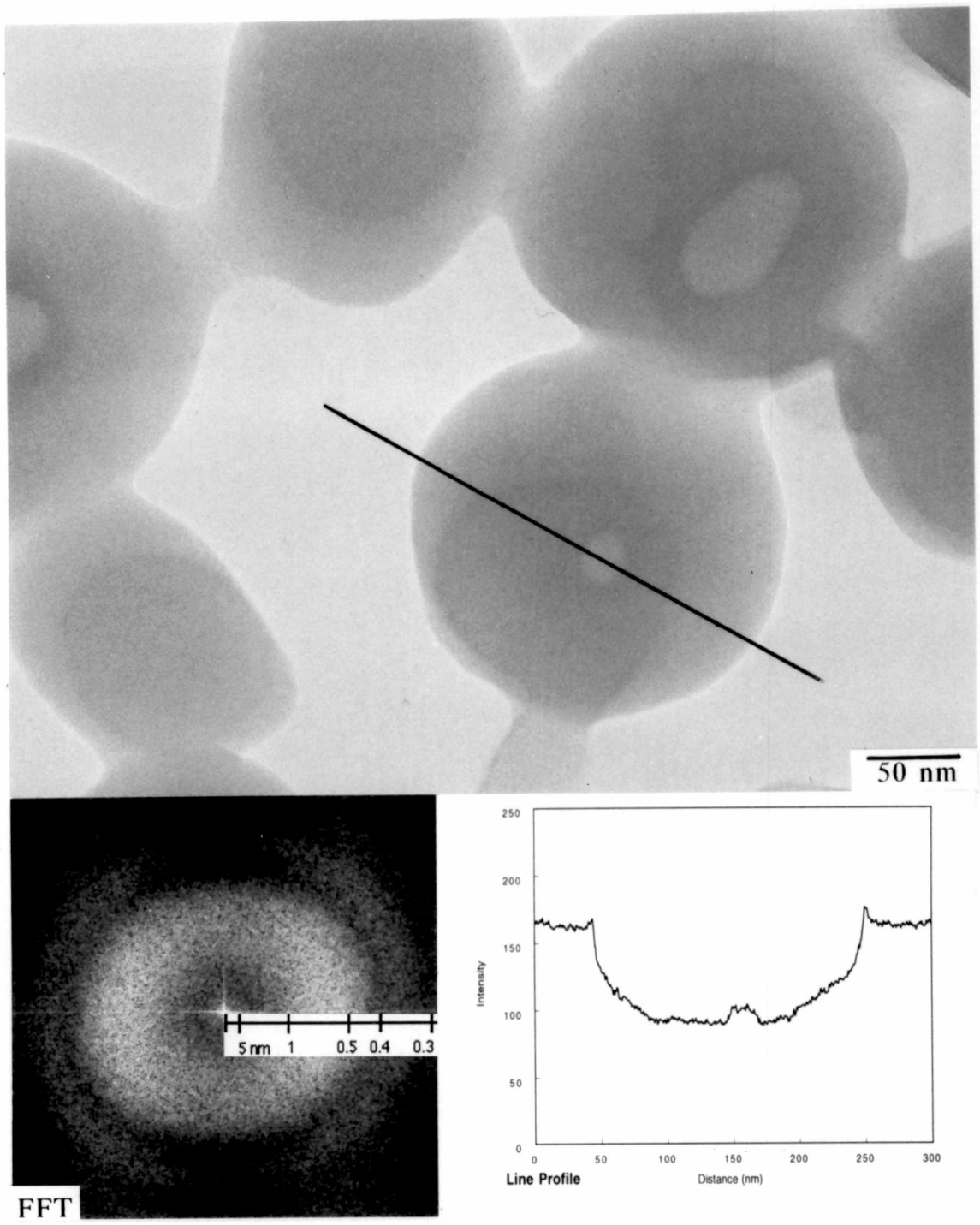

Figure 6.9. TEM micrograph of porous latex taken using a 75 μm objective aperture, a 100 μm condenser aperture and a #4 CL1 setting and an objective lens approximately at Scherzer focus (-38.8 nm).

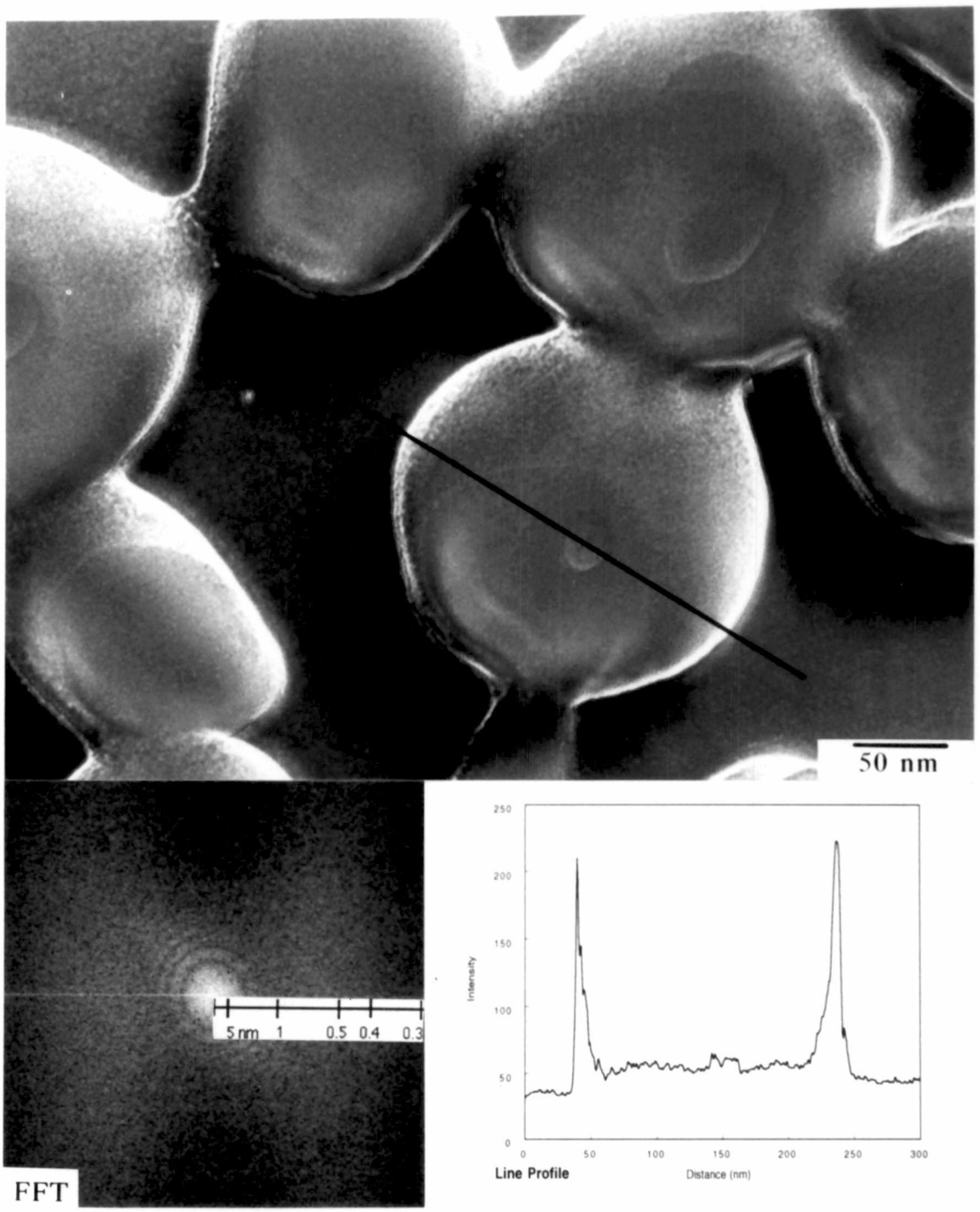

Figure 6.10. Phase contrast image of a porous latex taken using a contamination spot phase plate, a 30 μm condenser aperture and a #3 CL1 setting. The image was focused in bright field mode to approximately Scherzer focus (-38.8 nm).

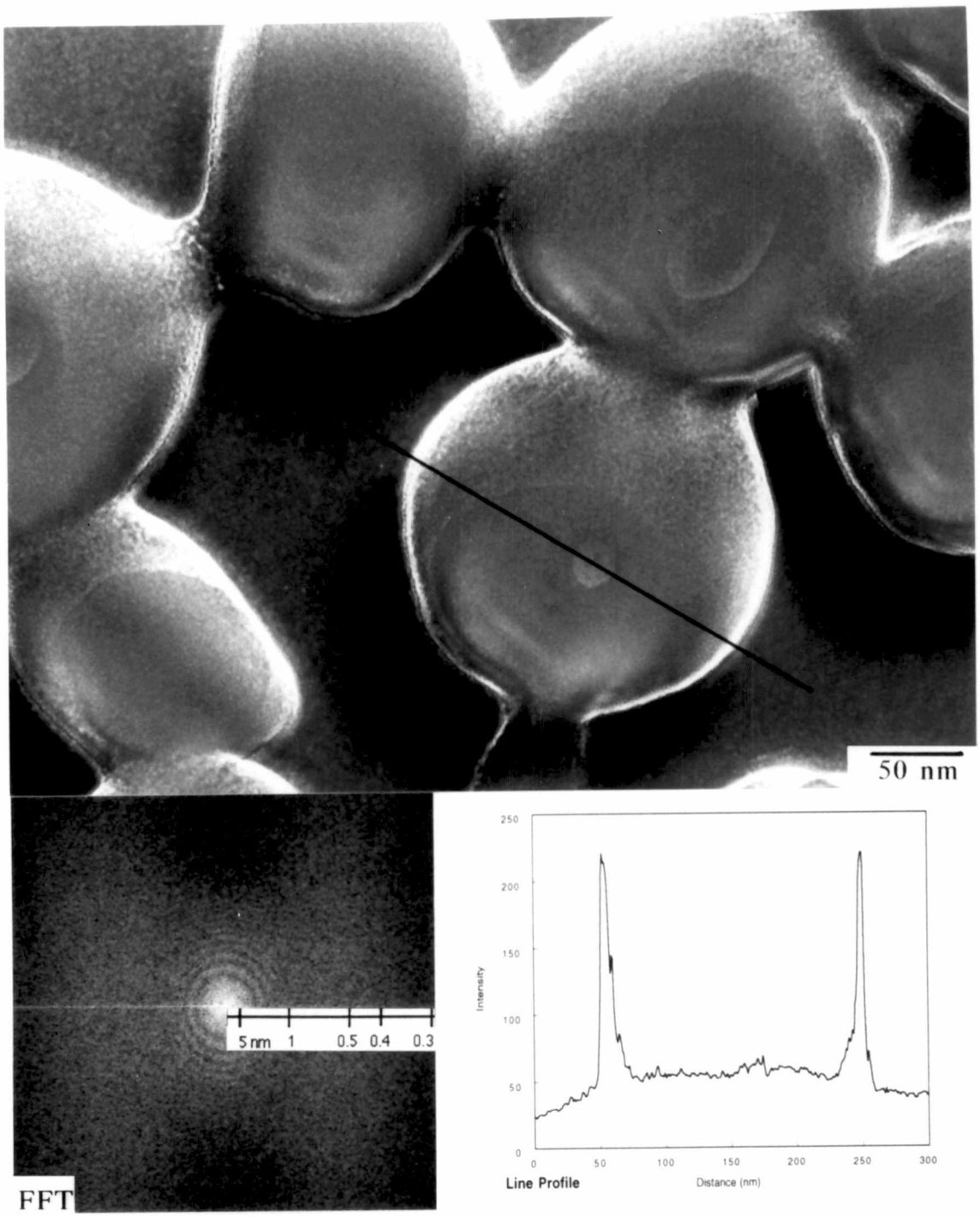

Figure 6.11. Phase contrast image of a porous latex taken using a contamination spot phase plate, a 30 μm condenser aperture, a #3 CL1 setting and an objective lens approximately -240 nm defocused.

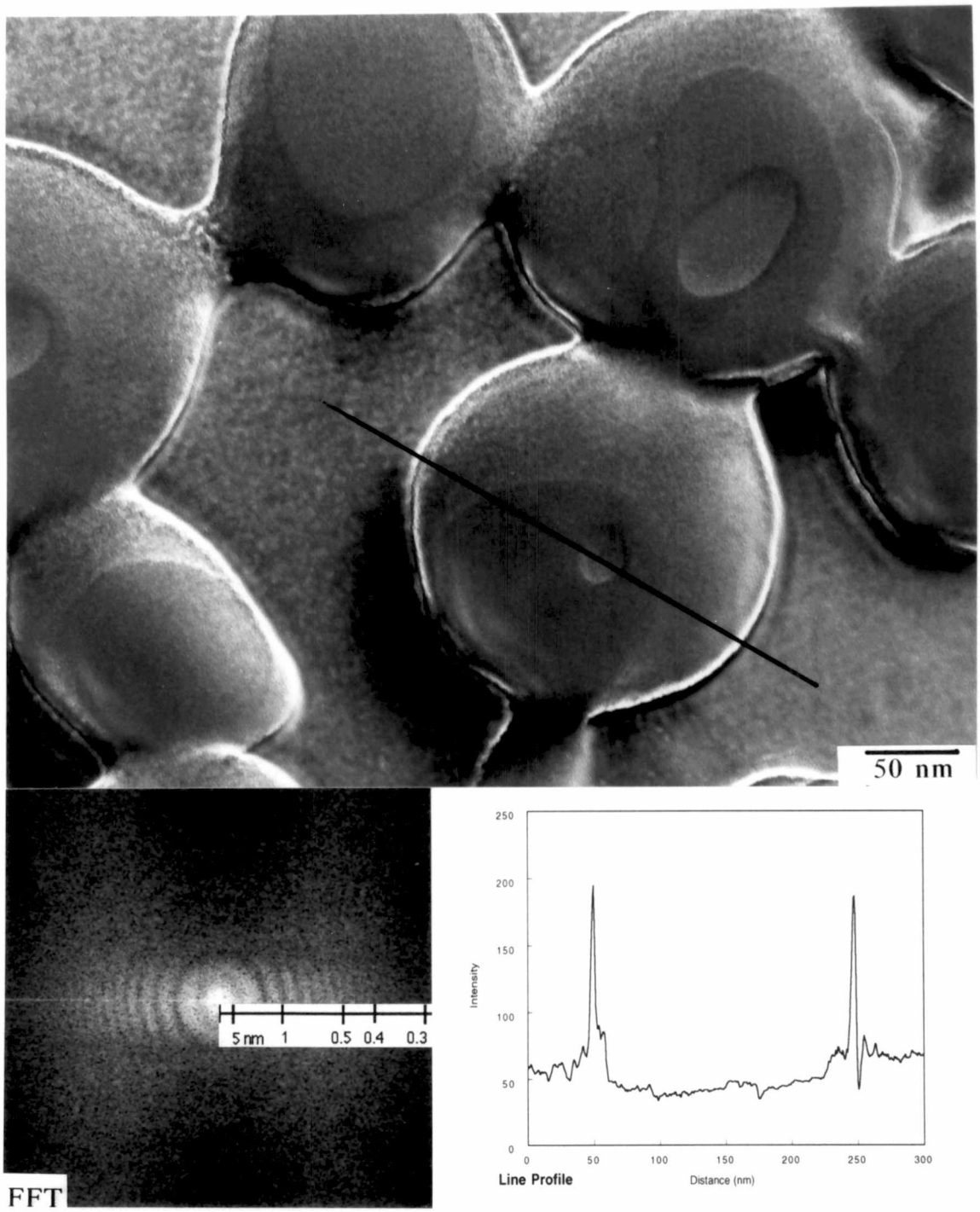

Figure 6.12. Phase contrast image of a porous latex taken using a contamination spot phase plate, a 30 μm condenser aperture, a #3 CL1 setting and an objective lens +160 nm defocused.

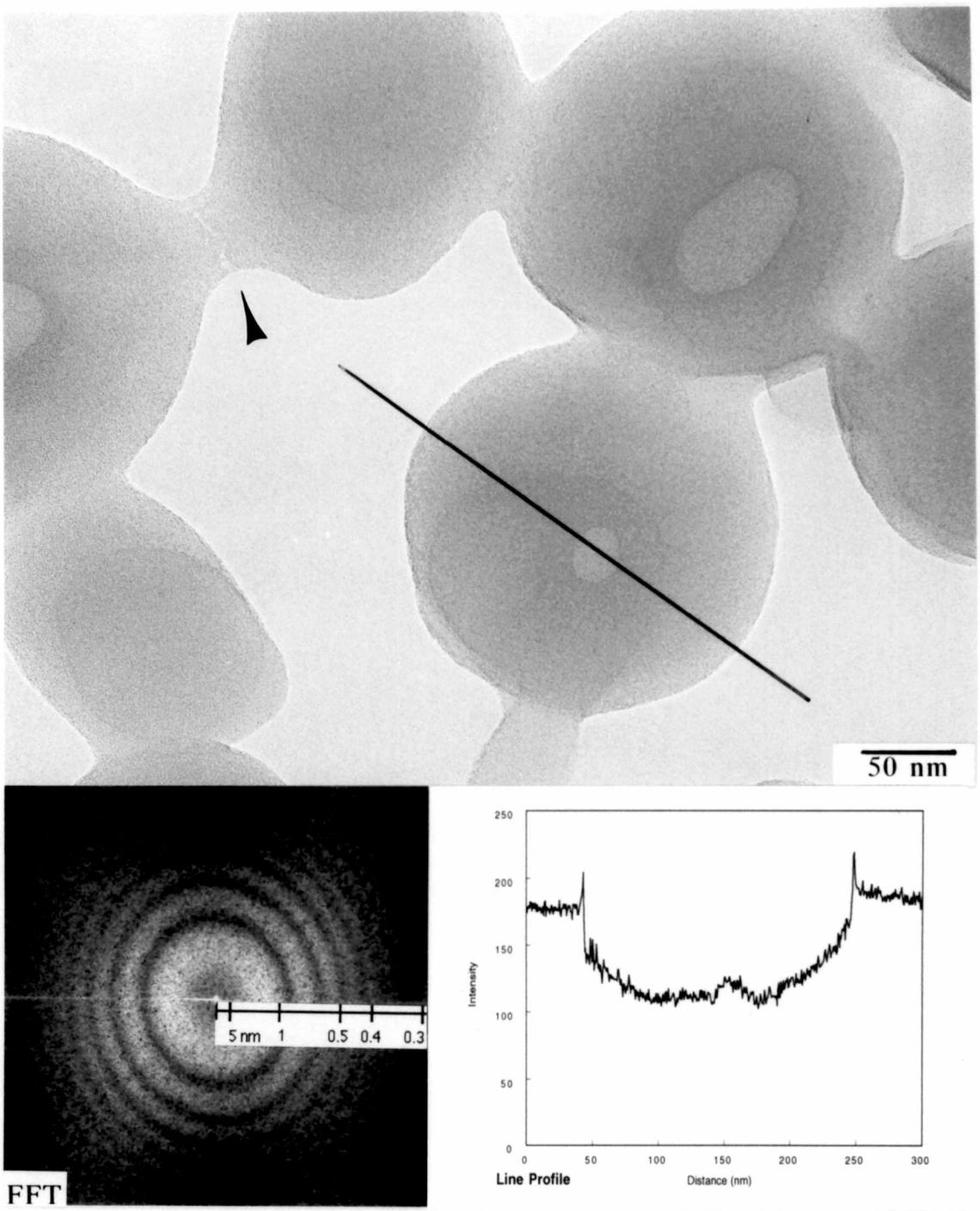

Figure 6.13. TEM micrograph taken using a 75 μm objective aperture, a 30 μm condenser aperture, a #3 CL1 setting and an objective lens -240 nm defocused.

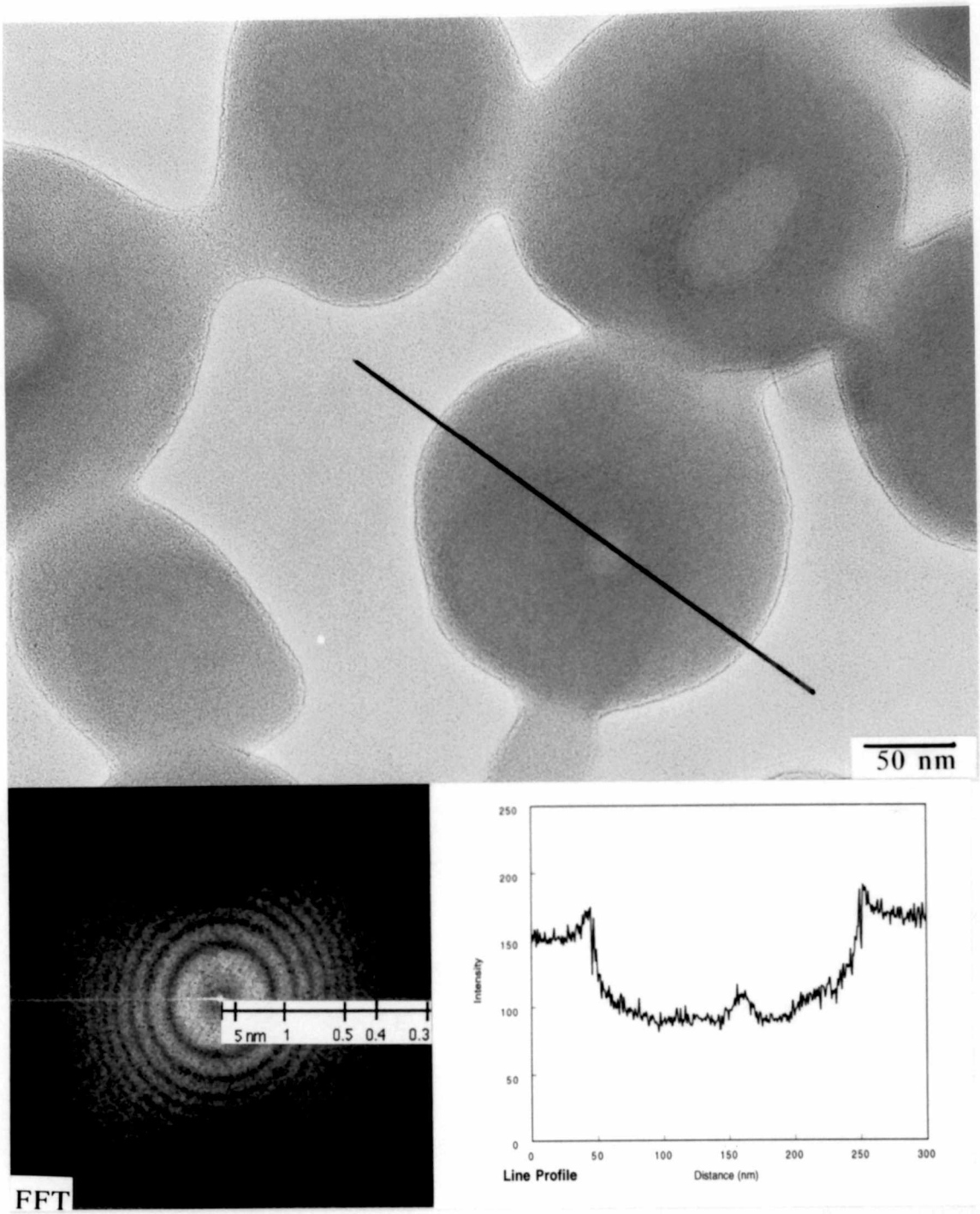

Figure 6.14 TEM micrograph taken using a 75 μm objective aperture, a 30 μm condenser aperture, a #3 CL1 setting and an objective lens +160 nm defocused.

generated for objects of homogeneous composition; and the device performance was not compromised even after 10 hours of use.

The quartz filament phase plate required careful control of the illumination conditions and, as for the contamination spot phase plate, near parallel illumination was necessary. Unlike the contamination phase plate that causes a phase shift by retarding the unscattered wave front through the intersection of its path with an amorphous mass, the quartz filament works by producing a point charge at its center (Unwin 1971). The charge generates an electrostatic field that causes the electrons passing close to the source of the field, where the field is stronger, to travel a longer distance than those more distant. In practice, the charge on the filament must be controlled to generate a field strength that gives maximum phase contrast without image distortion. Thicker or more highly scattering materials will cause more of the beam to be diffracted reducing the intensity of the unscattered beam striking the filament. The condenser aperture and the first condenser lens strength can also be altered to optimize filament charging.

Improper charge density results in a double image due to beam splitting (Figure 6.15) and for less severe conditions results in a ghosted image. The effect can be reduced by shifting the filament off center which reduces the number of electrons striking it, (Figure 6.16) but still results in enhanced contrast. Further translation of the filament, results in weaker contrast enhancement probably due to a reduction in the amount of attenuation of the unscattered wave front intensity and insufficient field strength (Figure 6.17). For this sample, conditions were not found that gave a properly charged filament, preventing the double image, with the filament centered and a reasonable exposure time.

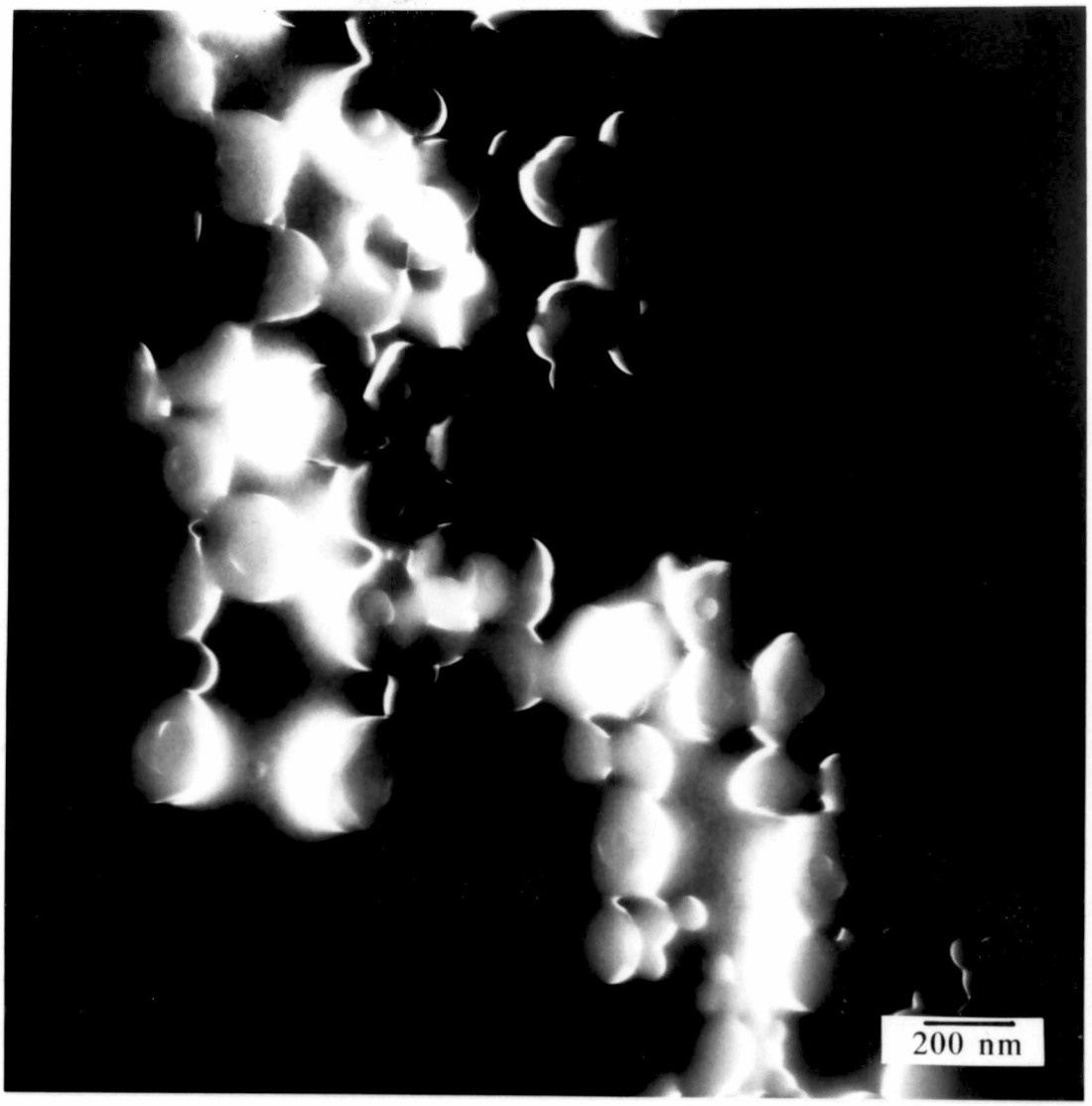

Figure 6.15. Phase contrast image of a porous latex taken using an overcharged electrostatic phase plate, a 100 μm condenser aperture, a #1 CL1 setting and an objective lens -38.8 nm defocused.

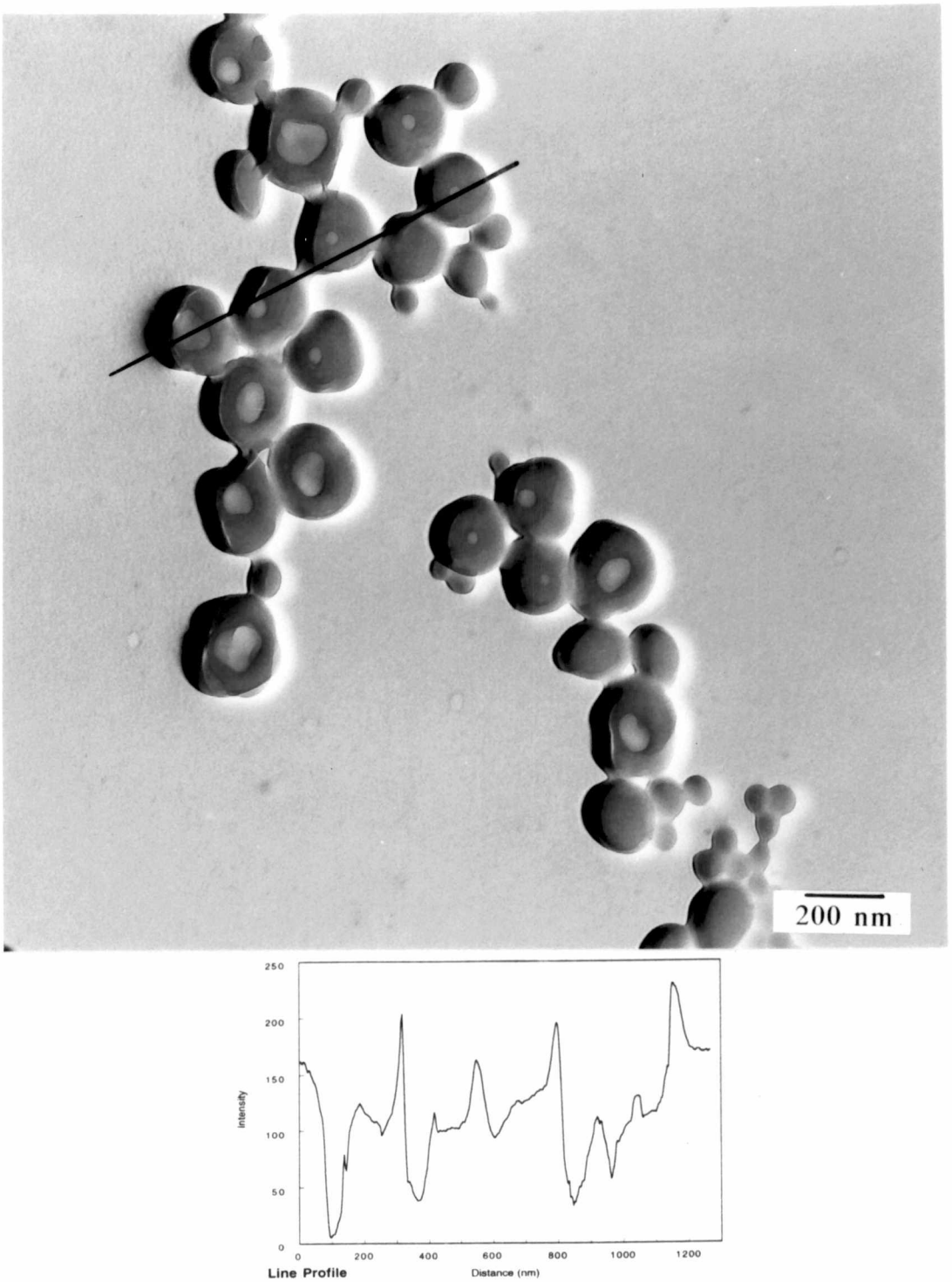

Figure 6.16. Phase contrast image of a porous latex taken using an off center electrostatic phase plate, a 100 μm condenser aperture, a #1 CL1 setting and an objective lens -38.8 nm defocused.

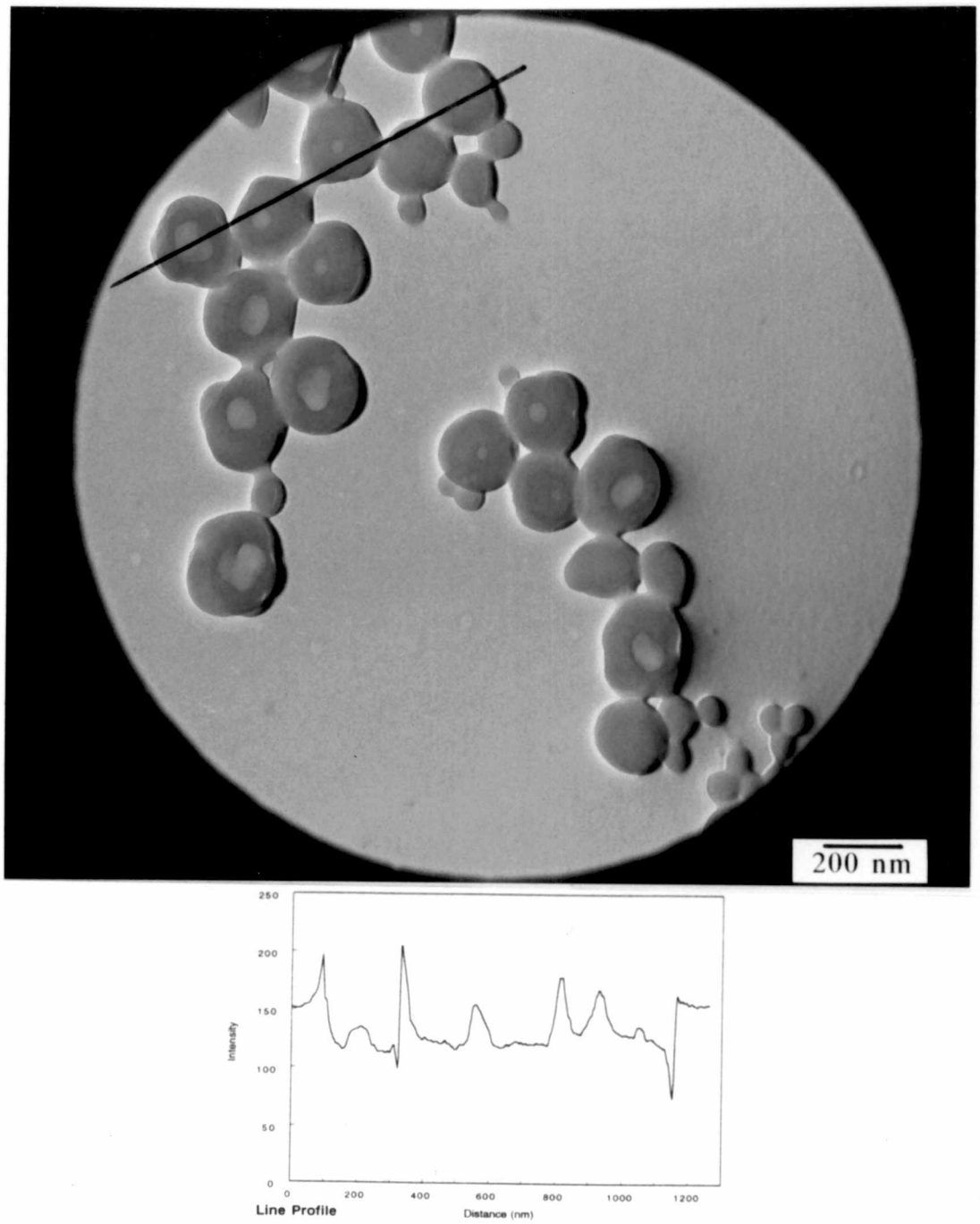

Figure 6.17. Phase contrast image of a porous latex taken using an off center electrostatic phase plate (farther off center than in figure 6.15), a 30 μm condenser aperture, a #1 CL1 setting and an objective lens -38.8 nm defocused.

Due to the restrictive conditions imposed by the use of the electrostatic phase plate, a method for increasing the range of conditions that would generate a useful image was sought. The incorporation of a mechanism to control the field, independent of the condenser setting, by electrically floating the aperture and providing a uniform charge to the conductive aperture was deemed the best approach.

The effect of charging the aperture can be seen by comparing micrographs with and without field compensation. Operating the microscope with high beam current, with a 100 μm condenser aperture and a number 4 C1 lens setting, provides short exposure times of 0.4 sec, but results in an overcharged phase plate that generates a double image (Figure 6.18). This is clearly seen for both the latex particles and the carbon support film when no external bias is applied. Charging the aperture to a potential of -390 volts avoids the double image and results in a high contrast image (Figure 6.19) where internal porosity is easier to see than in the image taken using the 75 μm objective aperture (Figure 6.20).

A difficult class of materials to image includes thin sections of materials where domains are present that do not differ significantly in composition. One such example is a biological thin section that has not received heavy metal staining during fixation or post sectioning such as bacteria fixed in glutaraldehyde, dried and embedded in LR White Resin. Some cellular features, such as vacuoles, can be seen on a printed micrograph using a standard 75 μm objective aperture, (Figure 6.21) but these are difficult to distinguish on the fluorescent screen. The use of a phase plate dramatically improves contrast making it easy to identify vacuoles, organelles, and cell walls (Figures 6.22 and 6.23). Both of these images were taken using the adjustable electrostatic device

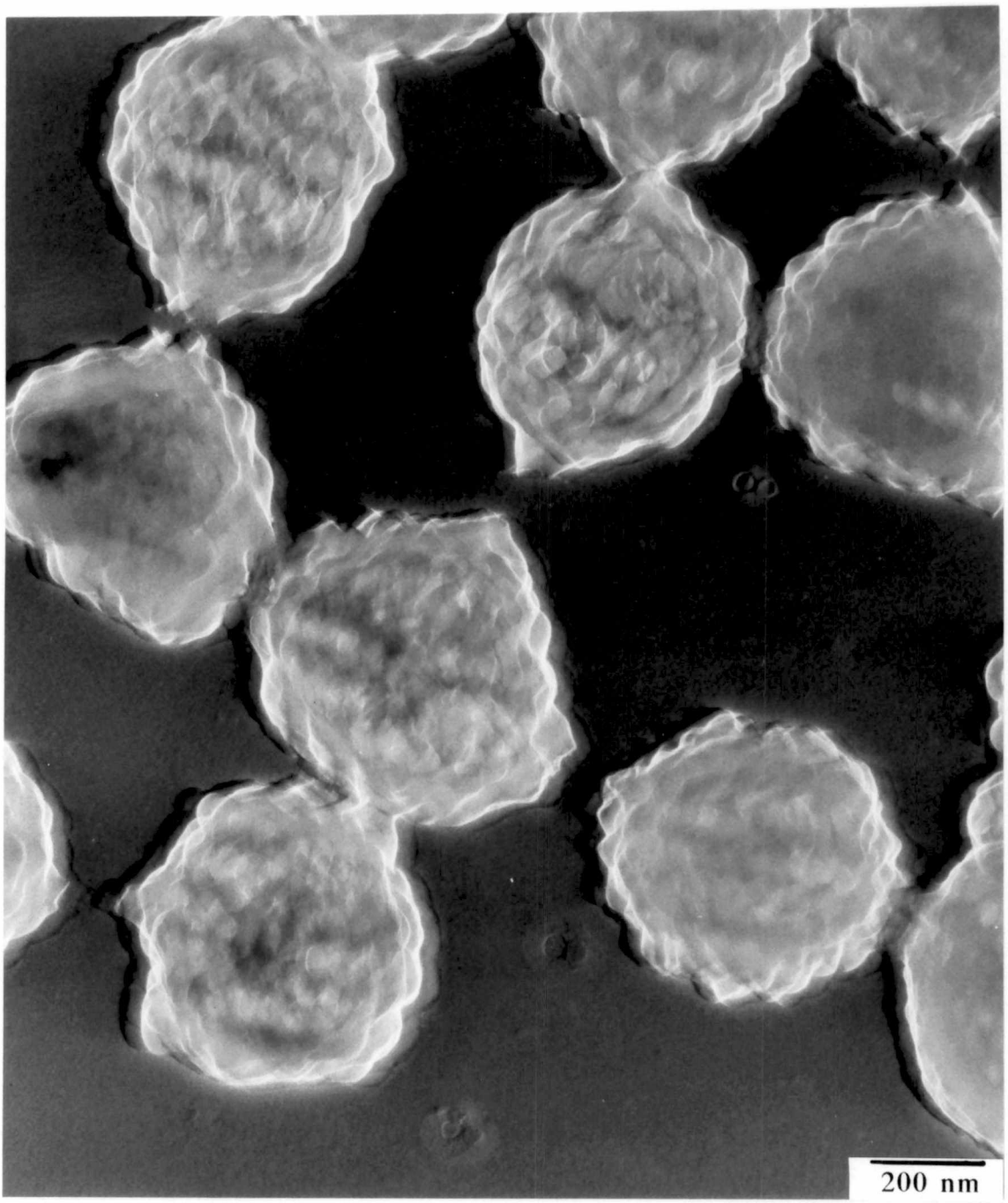

Figure 6.18. Phase contrast image of a porous latex taken using a compensated electrostatic phase plate, a 100 μm condenser aperture, a #4 CL1 setting, objective lens -38.8 nm defocused and a potential of 0 volts on the aperture.

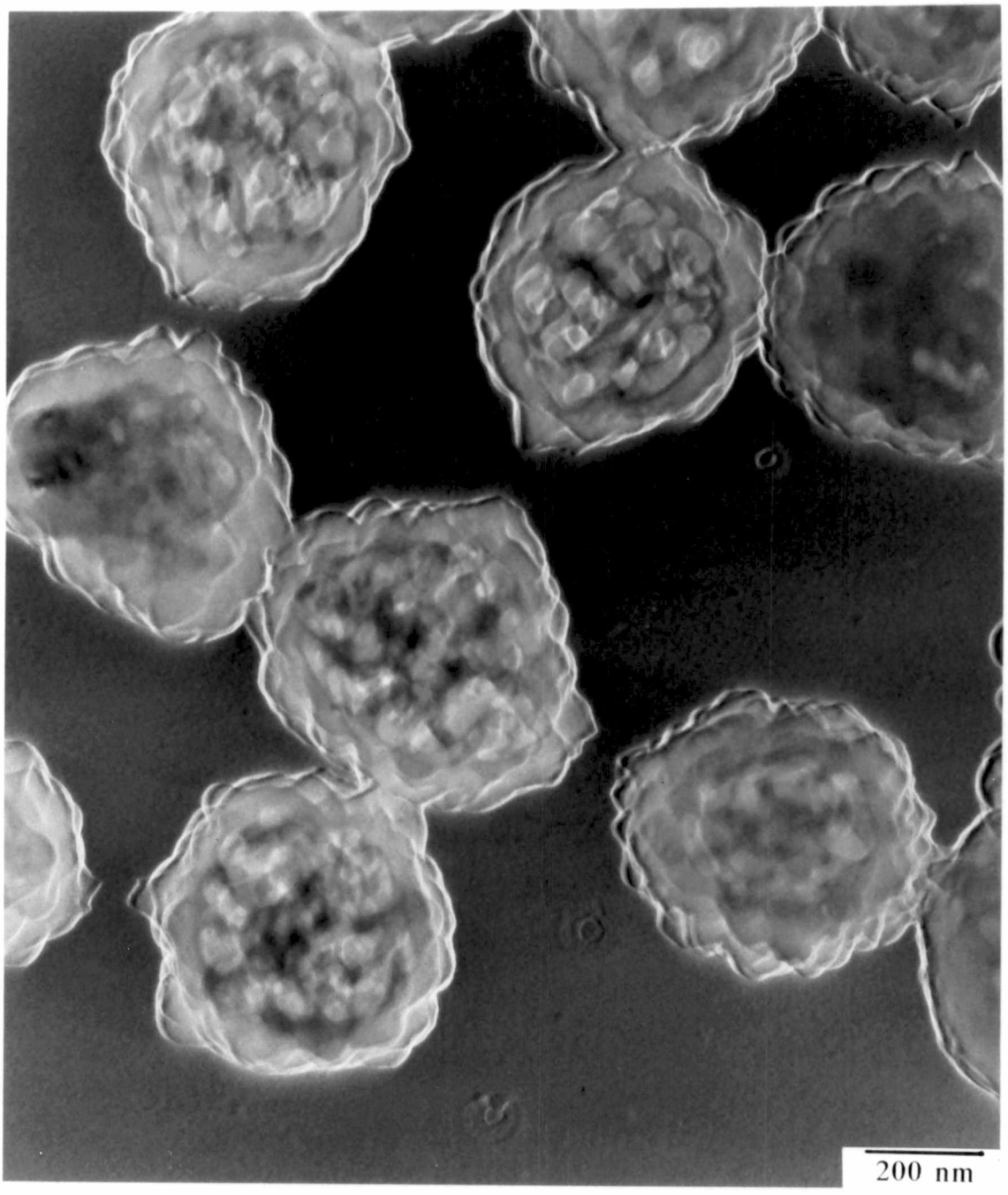

Figure 6.19. A phase contrast image of a porous latex taken using a compensated electrostatic phase plate, a 100 μm condenser aperture, a #4 CL1 setting, objective lens -38.8 nm defocused and a potential of -390 volts on the aperture.

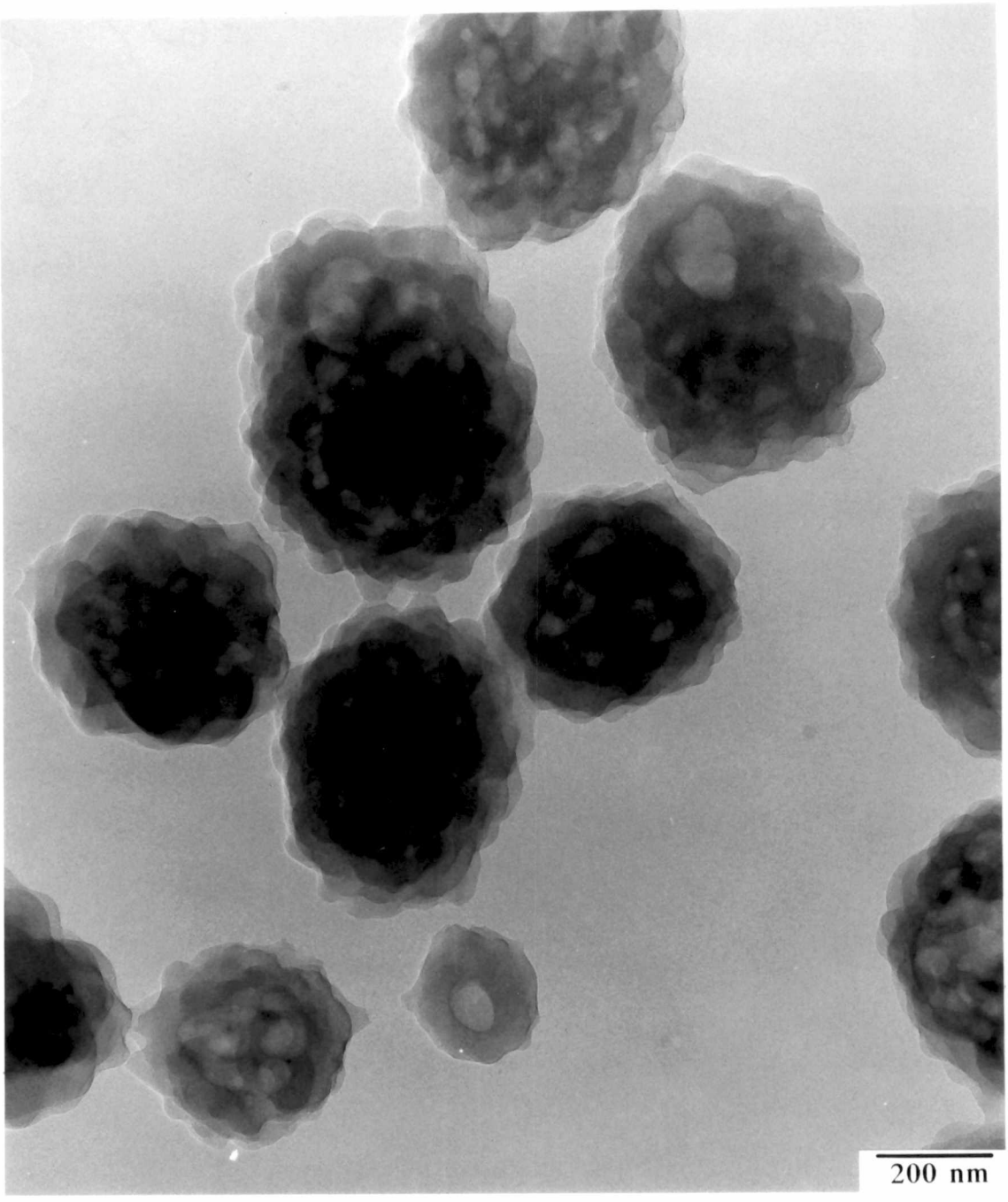

Figure 6.20. TEM micrograph of a porous latex taken using a 75 μm objective aperture, a 100 μm condenser aperture, a #3 CL1 setting and an objective lens -38.8 nm defocused.

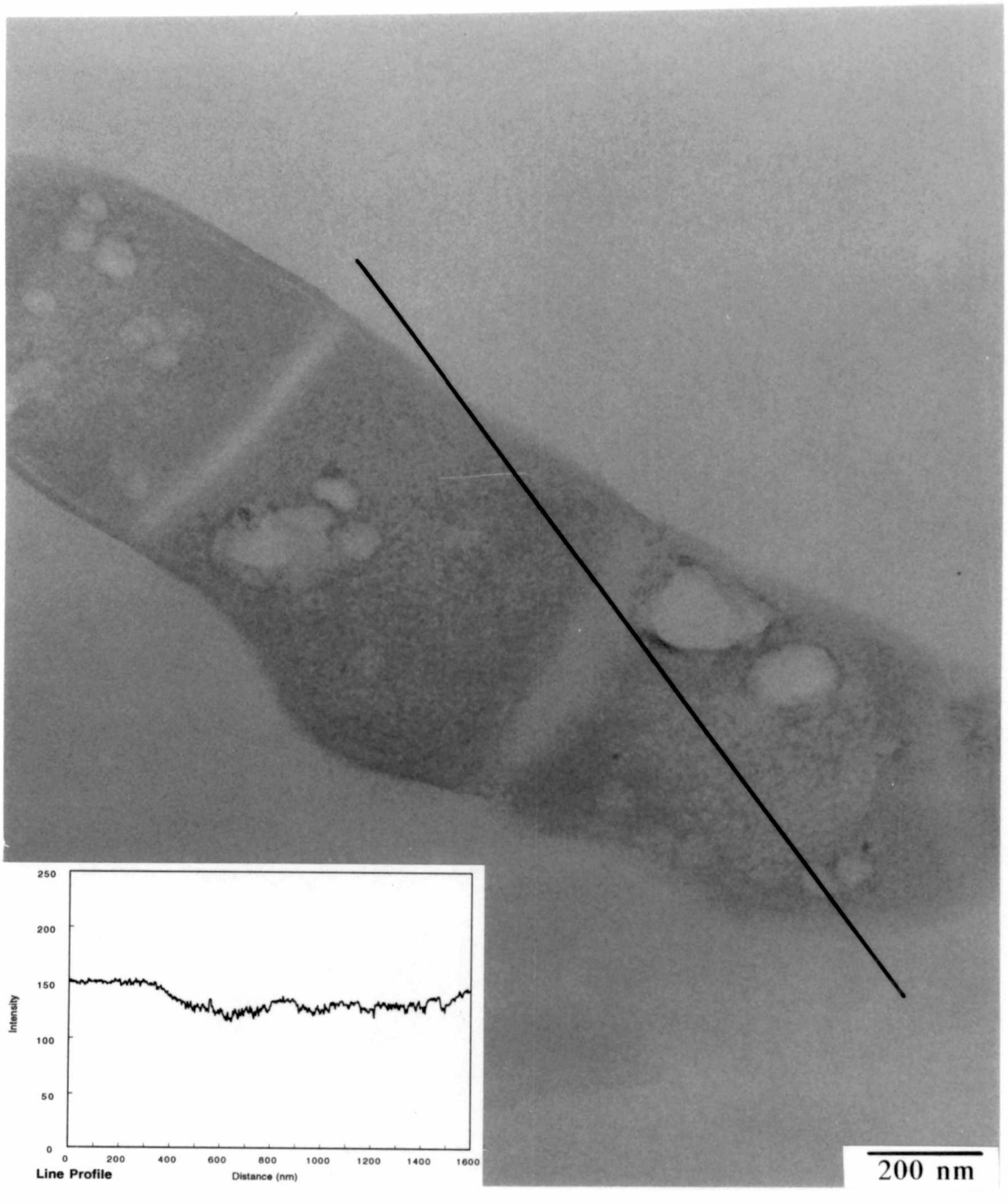

Figure 6.21. TEM micrograph of an unstained, epoxy embedded, ultramicrotomed, bacteria taken using a 75 μm objective aperture, a 100 μm condenser aperture, a #2 CL1 setting and an objective lens approximately -38.8 nm defocused.

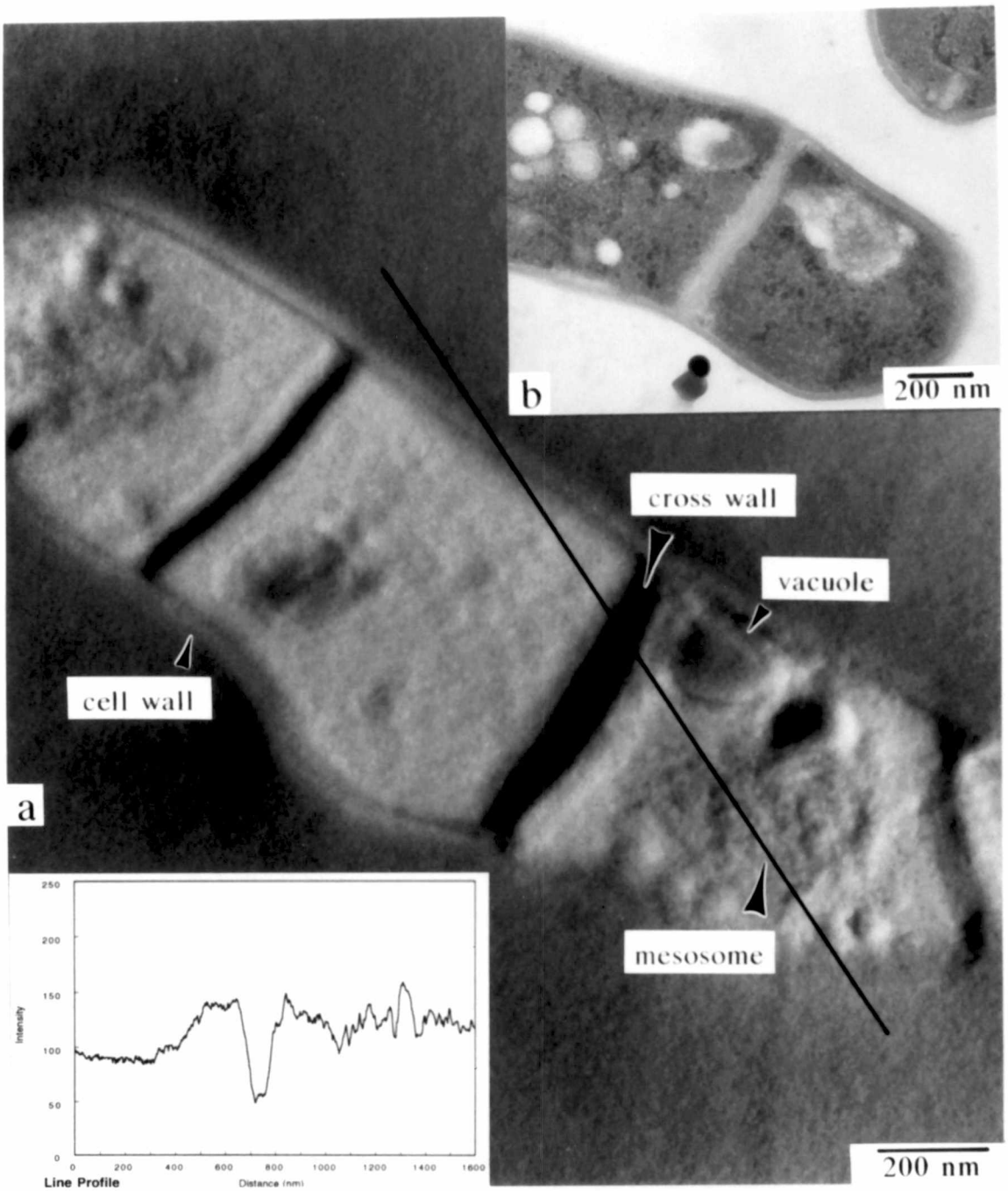

Figure 6.22. a) A phase contrast image of an unstained, epoxy embedded, ultramicrotomed, bacteria taken using a compensated electrostatic phase plate, a 100 μm condenser aperture, a #2 CL1 setting, objective lens -38.8 nm defocused and a potential of +300 volts on the aperture and b) conventionally stained and imaged.

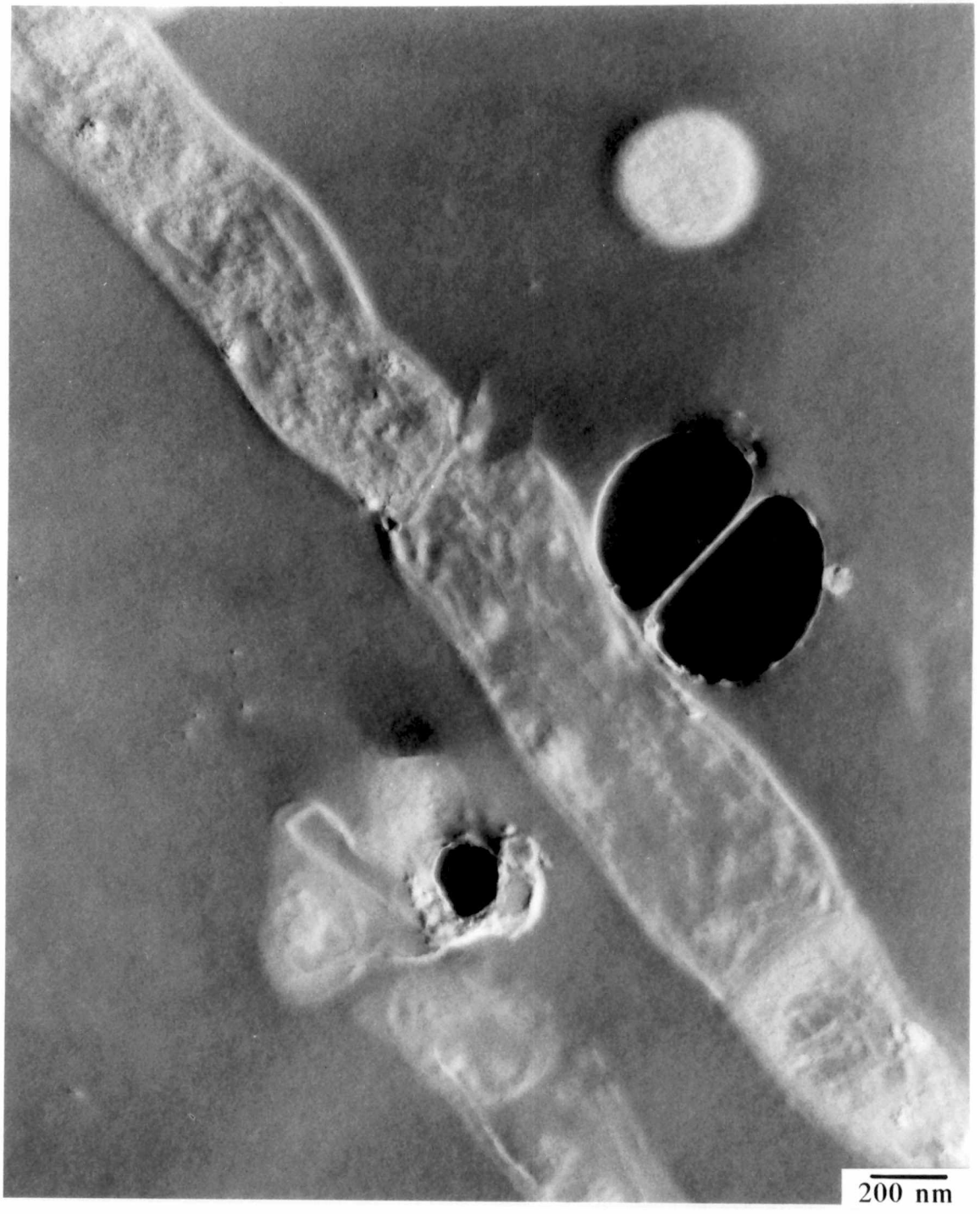

Figure 6.23. A phase contrast image of an unstained, epoxy embedded, ultramicrotomed, bacteria taken using a compensated electrostatic phase plate, a 100 μm condenser aperture, a #3 CL1 setting, objective lens -38.8 nm defocused, and a potential of +100 volts on the aperture.

with a positive potential on the aperture. While dark field imaging will generate a high contrast image, cell wall features are not visible, resolution is reduced and exposure times are increased by an order of magnitude (Figure 6.24). It is believed that a phase plate would be helpful in the examination and analysis of biological thin sections preserved by cryofixation, cryomicrotomed and cryotransferred to the analytical transmission electron microscope for cell constituent analysis using electron energy loss spectroscopy and/or energy dispersive x-ray analysis.

Man-made organic polymer blends are frequently as difficult to image as naturally occurring biological materials. Heavy metal staining is frequently employed in the microscopic analysis of these materials, but it is difficult to find a stain that is specific for one of the polymer phases. Additionally, the use of thin 40-50 nm thin sections for molecular microanalysis employing electron energy loss spectroscopy would be compromised by the presence of heavy metal stains. It would be advantageous in such instances to improve contrast without the use of stains. The contamination spot phase plate was used to enhance the contrast of cryo-ultramicrotomed (-120°C) sections of a polystyrene/polyethylene/ ethylene styrene copolymer (PS/PE/E-S) blend making the various phases clearly visible (Figure 6.25). This image can be compared to the normal bright field image (Figure 6.26) and a bright field scanning transmission electron microscope (STEM) image produced on a VG 601 FEG STEM (Figure 6.27). STEM has the advantage that contrast can be enhanced through electronic gain amplification. The contrast is comparable for the STEM image and the phase contrast image. Off axis electron holography was used to image a boundary between the PS and PE resulting in recognizable contrast at the interface when the electron hologram (Figure 6.28a) was reconstructed to generate a

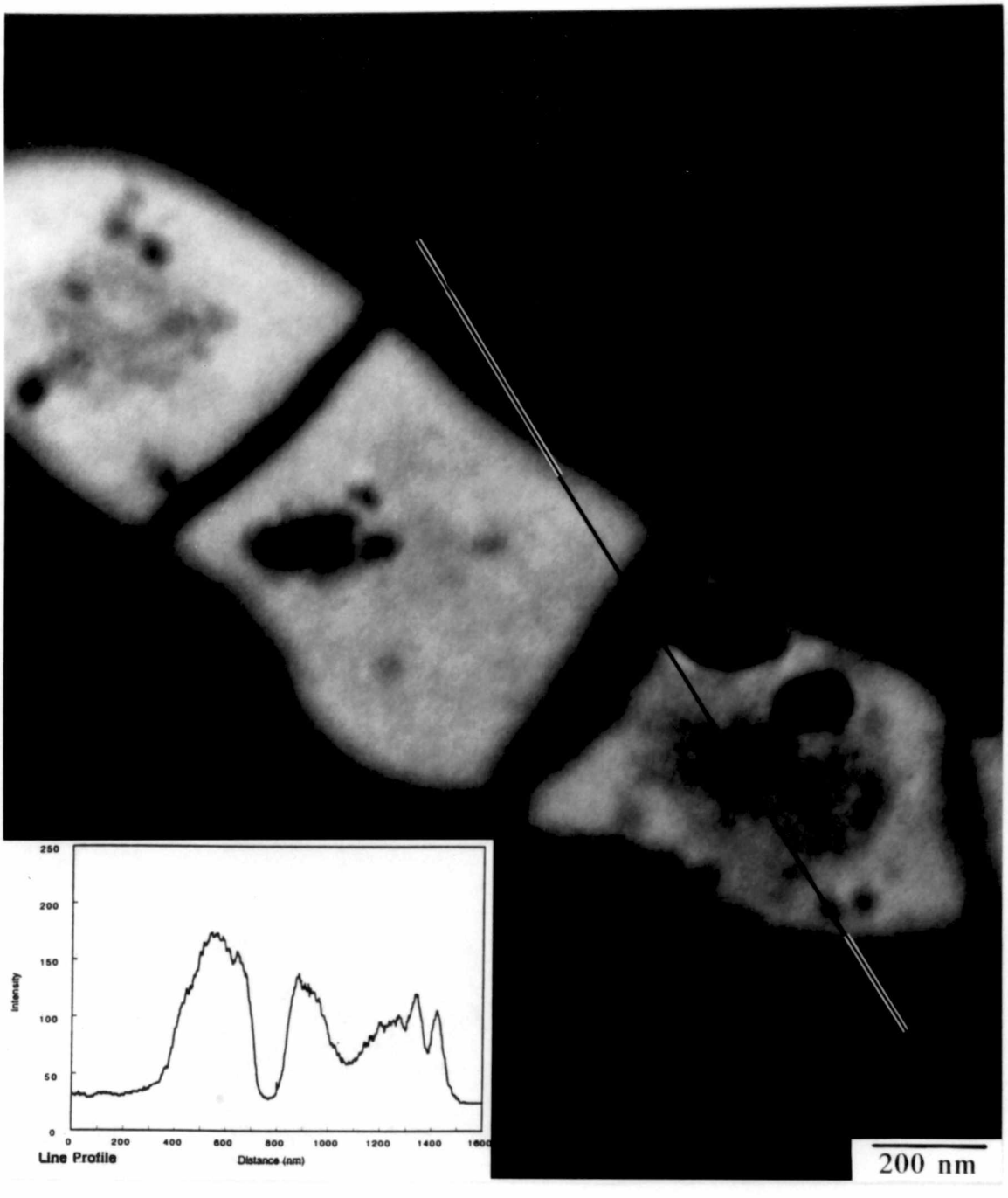

Figure 6.24. A dark field TEM micrograph of an unstained, epoxy embedded, ultramicrotomed, bacteria taken using a 75 μm objective aperture, a 100 μm condenser aperture, a #2 CL1 setting and an objective lens -38.8 nm defocused.

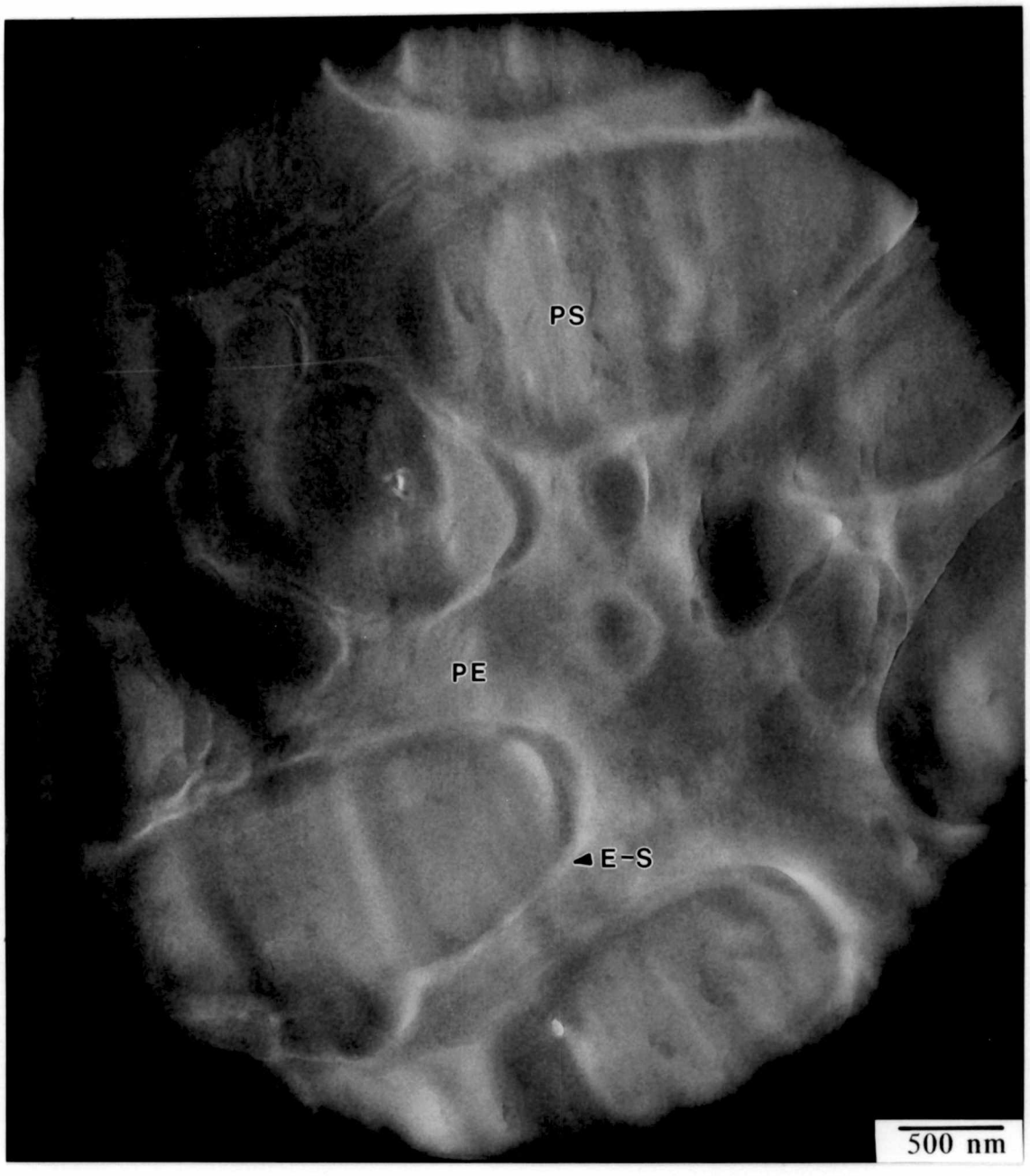

Figure 6.25. A phase contrast image of an unstained, ultramicrotomed thin section of PS/PE/E-S copolymer taken using a contamination spot phase plate, a 100 μm condenser aperture, a #0 CL1 setting and an objective lens approximately -38.8 nm defocused.

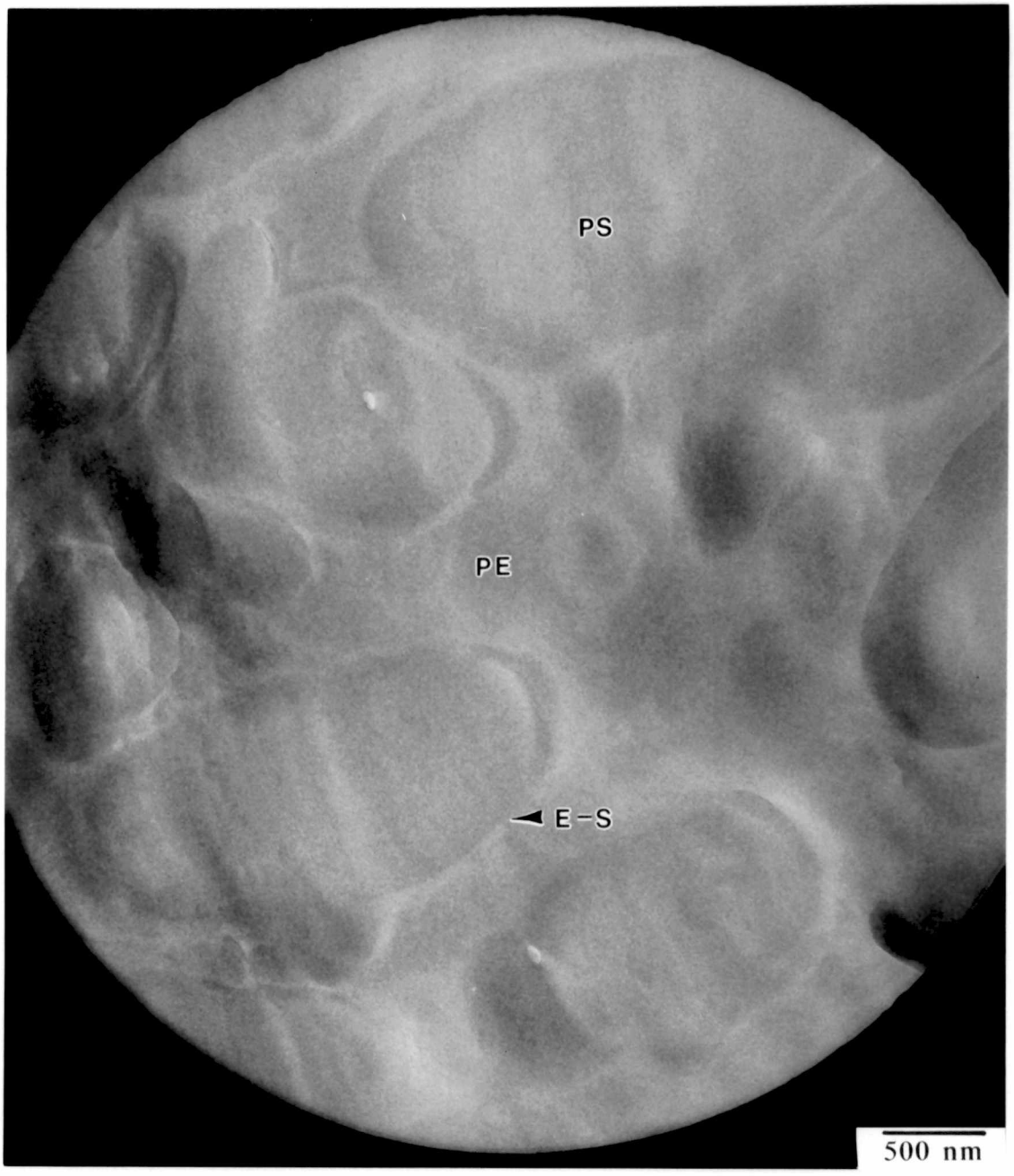

Figure 6.26. A TEM micrograph of an unstained, ultramicrotomed thin section of PS/PE/E-S copolymer taken using a 75 μm objective aperture, a 100 μm condenser aperture, a #2 CL1 setting and an objective lens approximately -38.8 nm defocused.

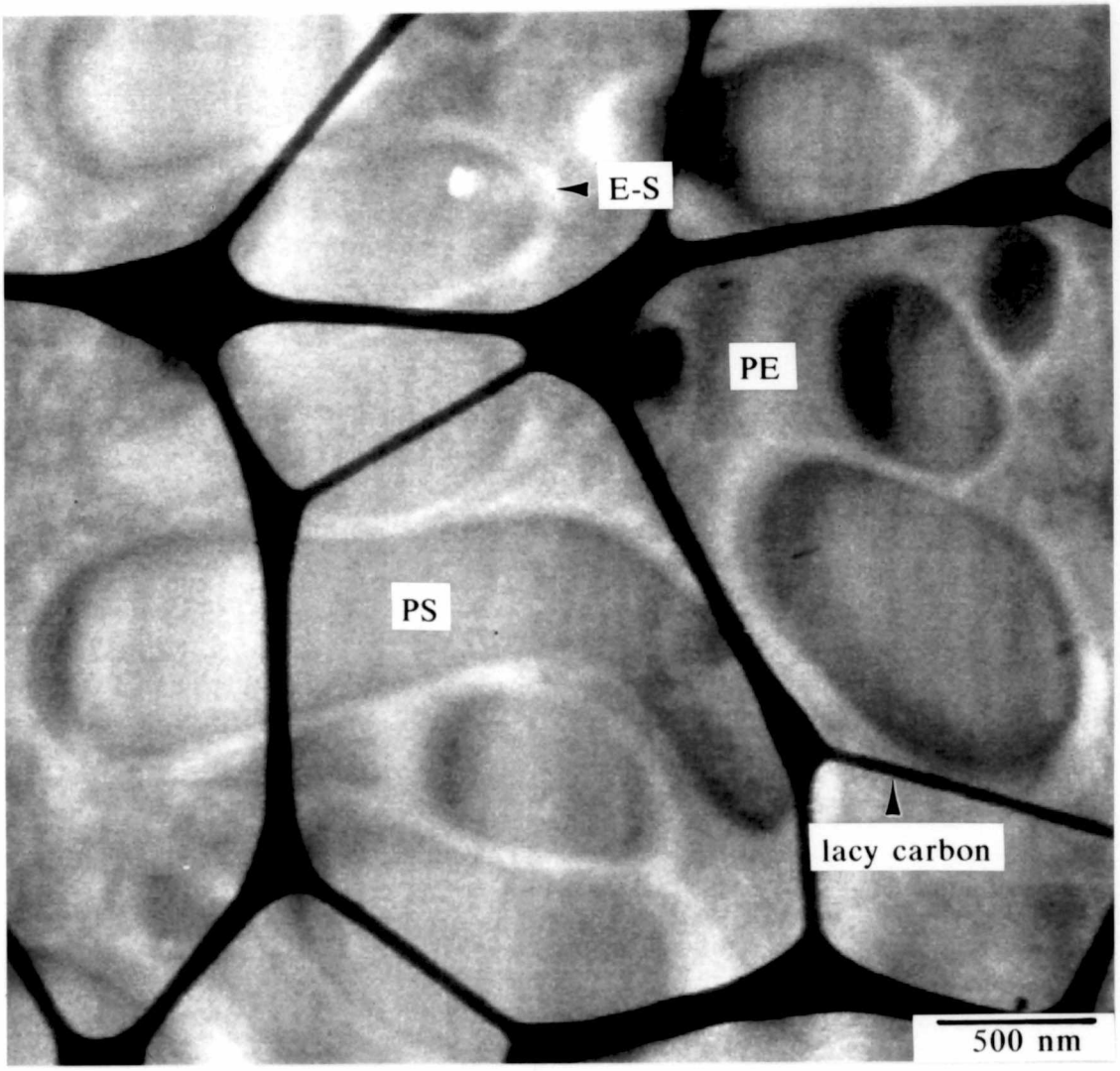

Figure 6.27. A bright field STEM micrograph of an unstained, ultramicrotomed thin section of PS/PE/E-S copolymer.

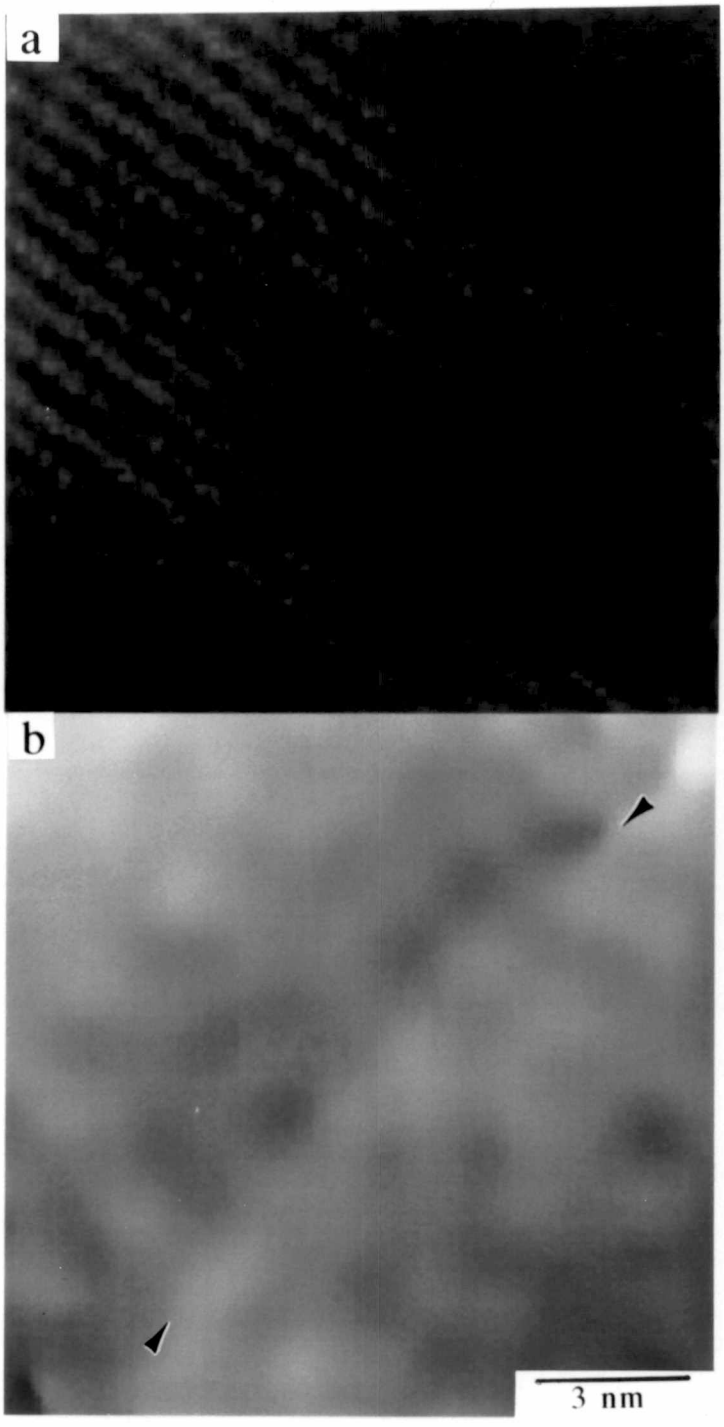

Figure 6.28. a) An electron hologram and b) a reconstructed continuous phase image of an unstained, ultramicrotomed thin section of PS/PE/E-S copolymer (arrows mark a PS/PE boundary).

continuous phase image (Figure 6.28b). A plot of the phase shift versus position shows an approximately 10 nm interface at the boundary that is believed to be the ethylene styrene copolymer (Figure 6.29). The phase shift generated by the PS is between 0.3 and 0.4π relative to the PS. If the mean inner potential is assumed to be the same for the PS and PE, this phase shift corresponds to a thickness difference of approximately 20 nm (Equation 2.15).

Parallel electron energy loss spectroscopy (PEELS) performed on a VG 601 dedicated FEG STEM confirms the thickness difference between the two phases which is generated during sectioning. The -120°C sectioning temperature represents a compromise between the ideal temperature for sectioning PE (-160°C) and that for PS (20°C). As a result, the PS is more brittle than desired and is cleaved during sectioning generating chatter clearly seen in the image recorded using the phase plate (Figure 6.25) and the PE is too ductile and compresses during sectioning. This results in the PE thickness being greater than the PS thickness and causes some overlap of the PS and PE at the leading edge of the PS particles when the PE is smeared during sectioning. This is seen as dark bands in the phase contrast image (Figure 6.25). Molecular microanalysis using PEELS performed on sections cooled to -160°C confirmed the composition of the various phases and gave an indication that the copolymer is present as a compatibilizer at the interface (Figure 6.30). The carbon core edge spectra acquired with a zero loss FWHM energy resolution of 0.6 eV is useful as a fingerprint to identify the polymeric structure. The carbon core edge fine structure is representative of the various bonding states of the carbon atoms present in the molecule (Blackson et al. 1994).

Another example of a polymer imaging problem, that is aided by phase contrast enhancement is a sectioned PS latex film. Using a 75 μm aperture, the

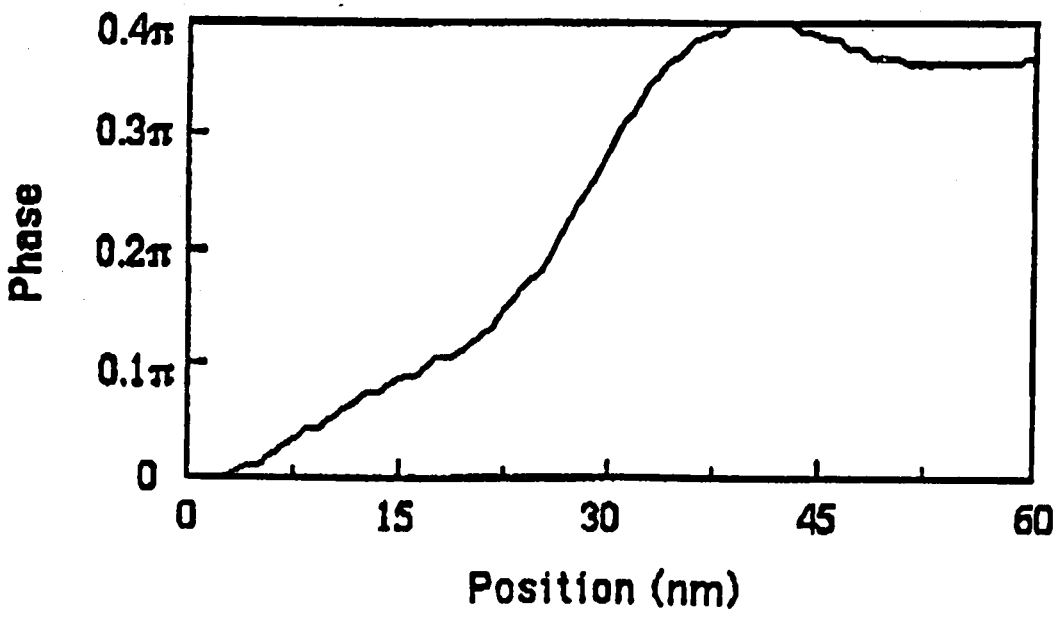

Figure 6.29. A line profile across the PS/PE boundary represented in figure 6.28 showing the relative phase change.

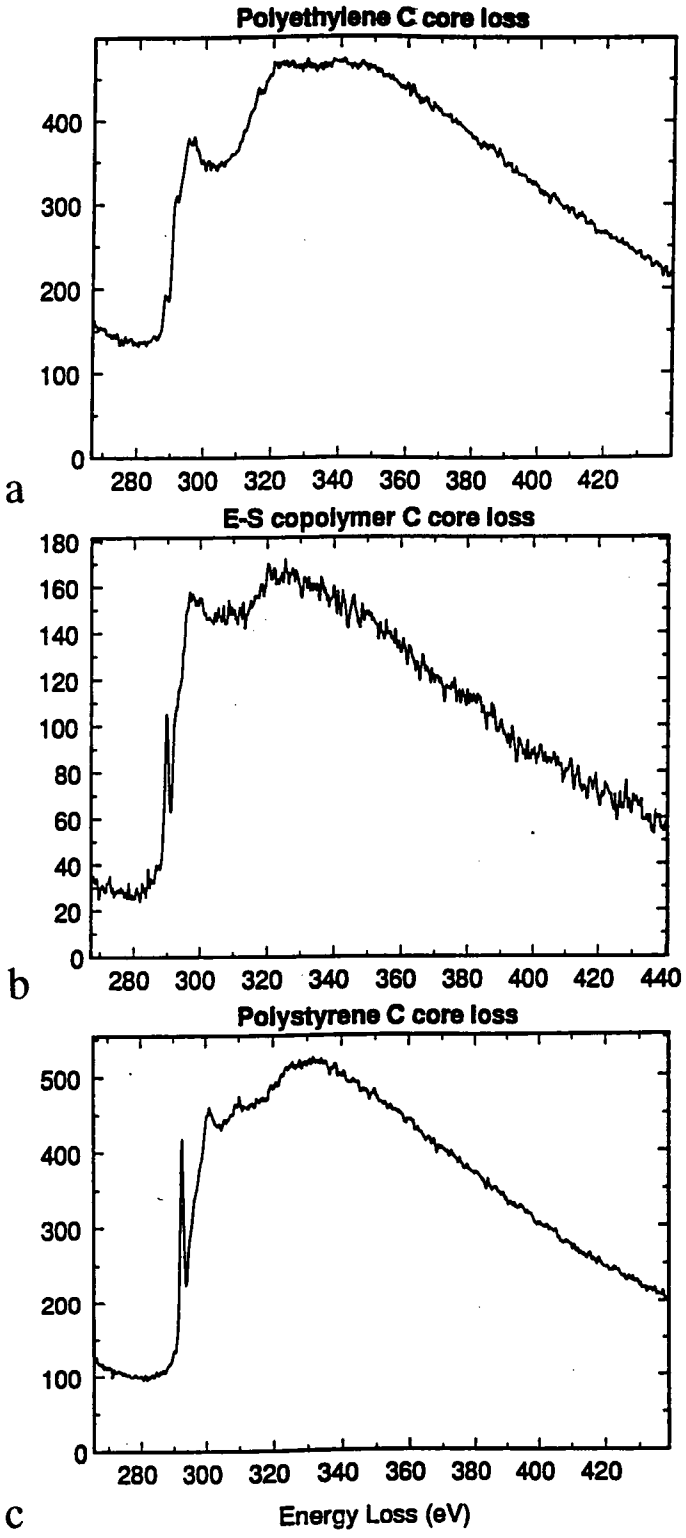

Figure 6.30. Carbon core edge PEELS spectra of a) PE, b) E-S and c) PS.

latex particles are not recognizable (Figure 6.31). With a defocus of -400nm, the void space between the latex particles becomes apparent but the individual particles are still difficult to distinguish (Figure 6.32). When the contamination spot phase plate is used, particle detail is clearer and of high contrast (Figure 6.33). In this case, a 140 nm diameter contamination spot was used which is smaller than in the previous example where a 700 nm diameter contamination spot was used. The contamination spot is clearly seen as a dark shadow in the center of figure 6.33. The quartz filament electrostatic phase plate also generates a high contrast image (Figure 6.34) elucidating detail comparable to that seen in the micrograph taken using the contamination spot (Figure 6.33).

Thin inorganic materials represent another example where phase contrast microscopy is beneficial. In one case, large pores greater than approximately 2.5 nm are clearly seen in a specially treated mordenite (zeolite) when the phase plate is used (Figure 6.35). Many of these pores are not visible in the conventional bright field image (Figure 6.36). This same material was examined using off axis electron holography, enabling another comparison of this technique to phase plate microscopy, and high resolution scanning electron microscopy. Conditions used for electron holography that resulted in a portion of the crystal being imaged failed to reveal the porosity (Figure 6.37). By plotting the phase intensity against position, a three dimensional representation of the phase can be obtained (Figure 6.38). If it is assumed that the composition of the crystal does not vary, then the three dimensional plot should be a good approximation of the thickness variations. A similar approach can be applied to the phase plate image, however the image produced using the phase plate is a convolution of both the phase and amplitude contrast which are not easily separated. The high resolution field emission gun scanning electron microscope

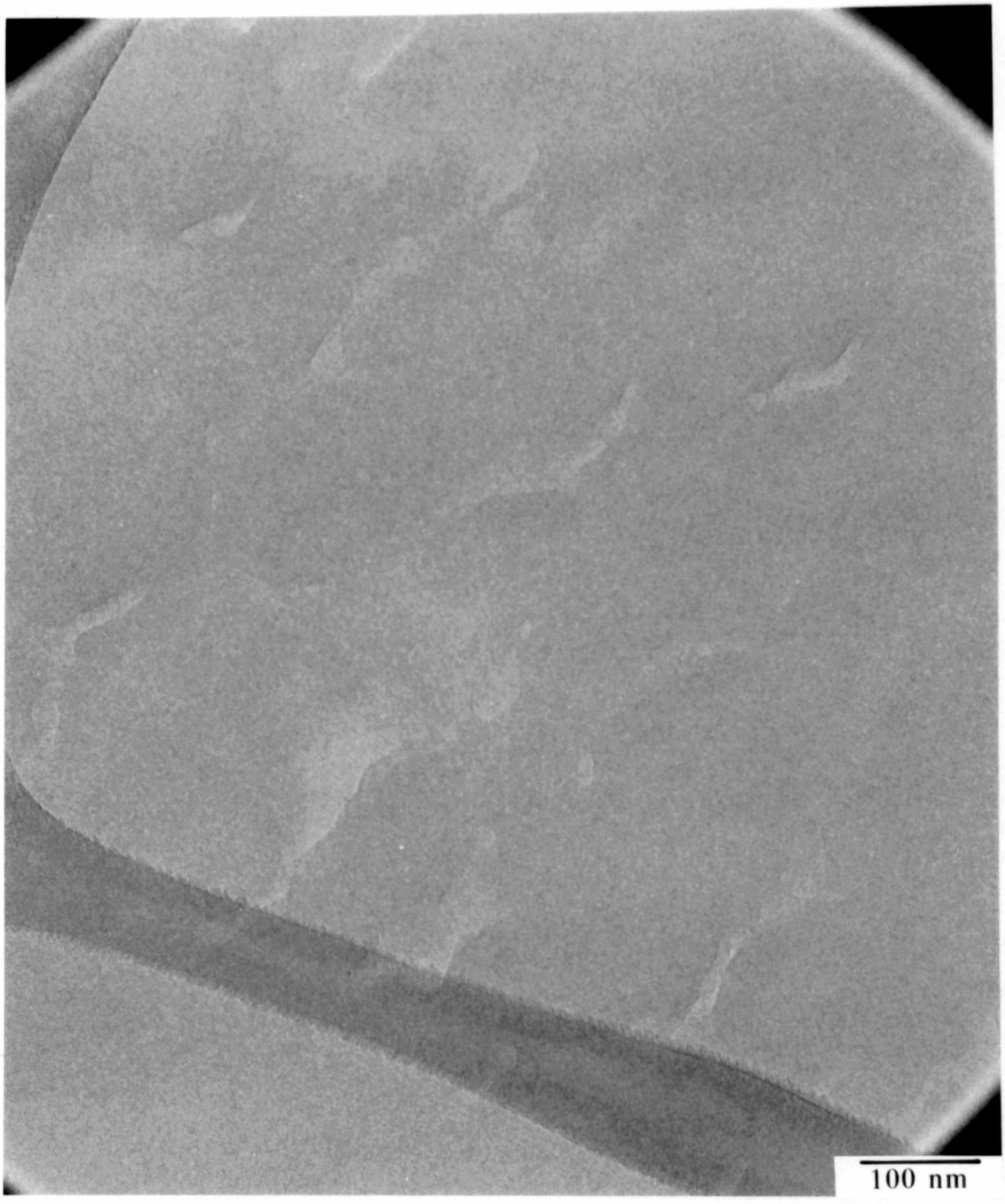

Figure 6.31. A TEM micrograph of an ultramicrotomed thin section of a latex film taken using a 75 μm objective aperture, a 30 μm condenser aperture, a #1 CL1 setting and an objective lens approximately -38.8 nm defocused.

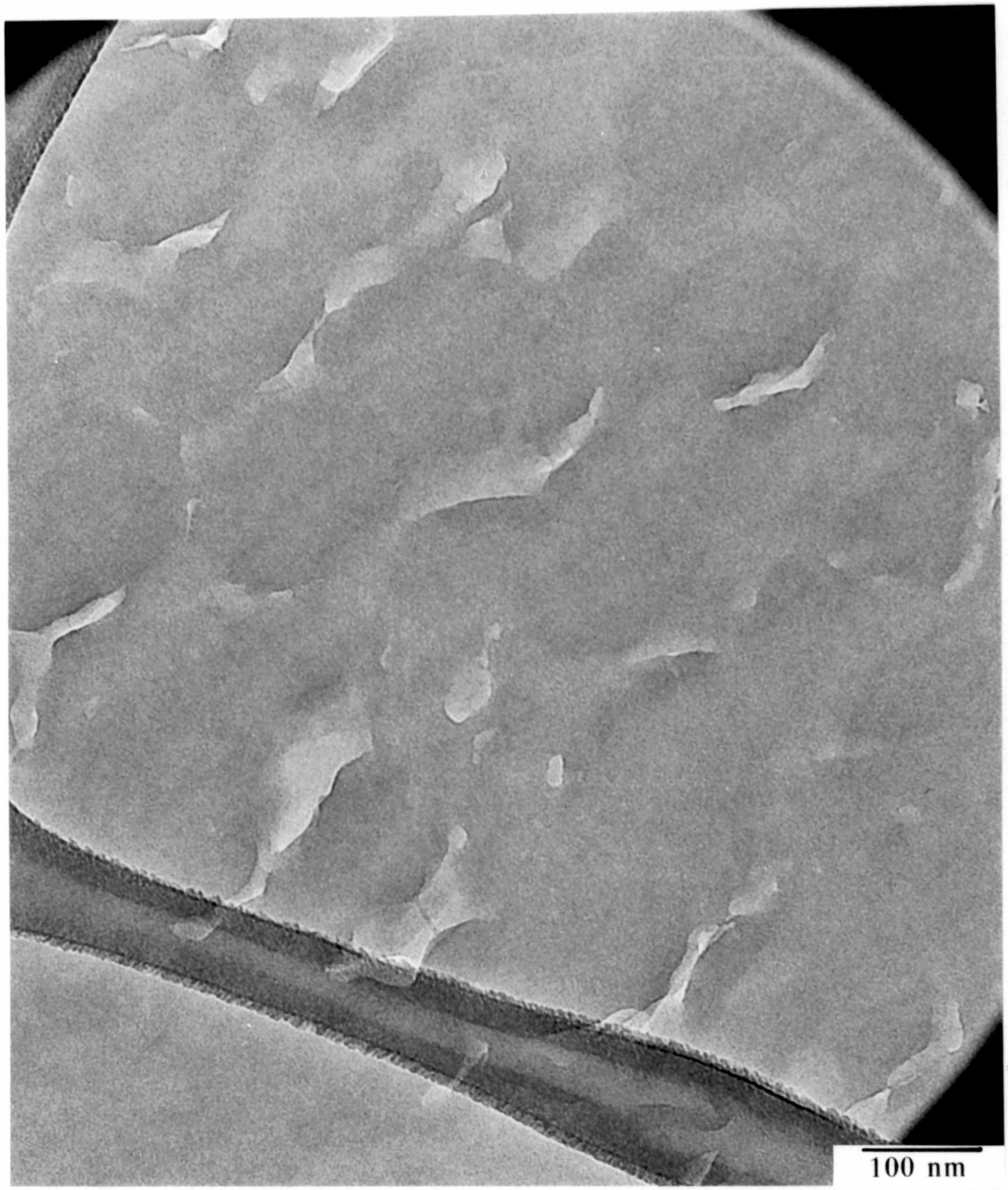

Figure 6.32. A TEM micrograph of an ultramicrotomed thin section of a latex film taken using a 75 μm objective aperture, a 30 μm condenser aperture, a #1 CL1 setting and an objective lens -400 nm defocused.

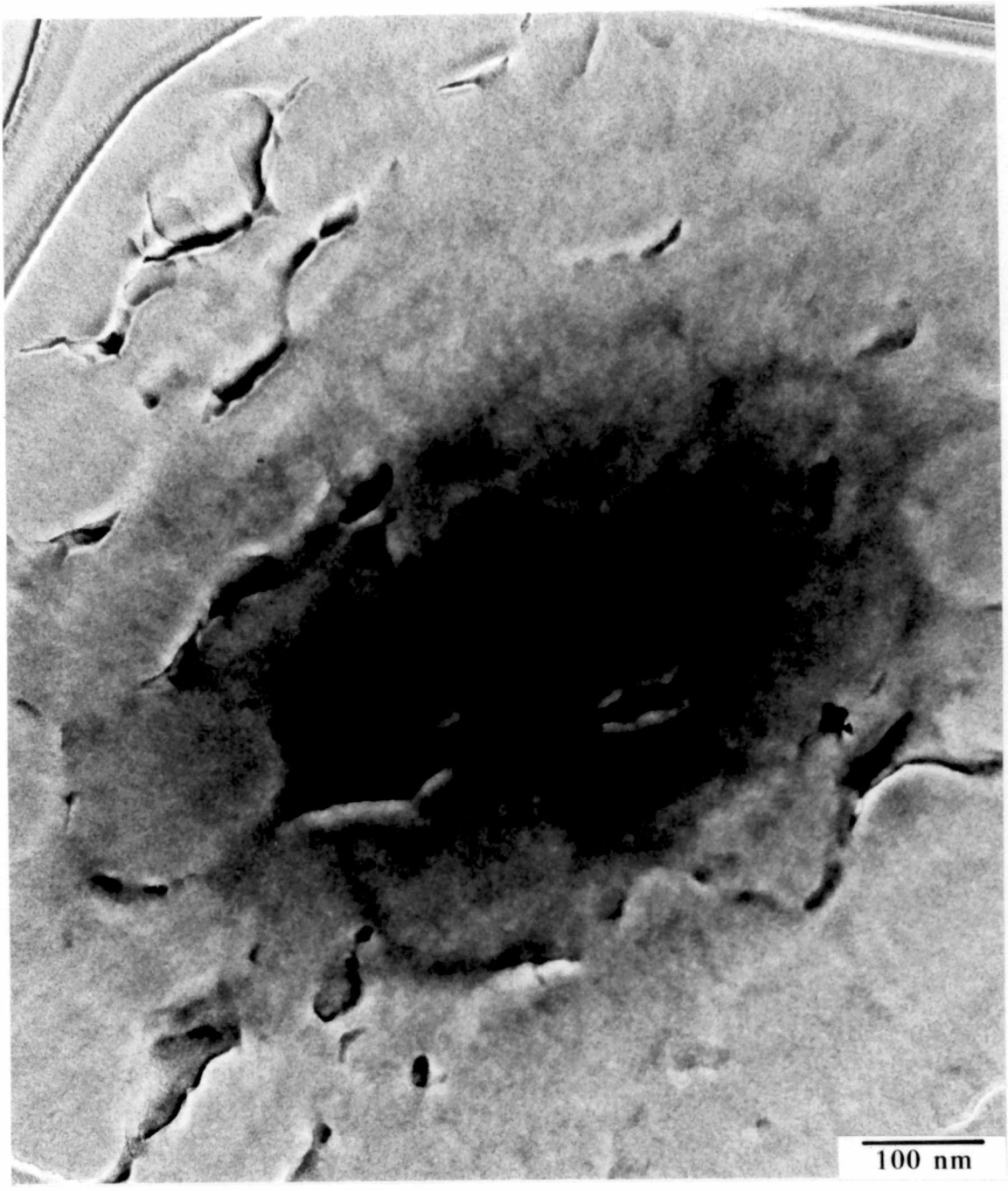

Figure 6.33. A phase contrast image of an ultramicrotomed thin section of a latex film taken using a contamination spot phase plate, a 30 μm condenser aperture, a #1 CL1 setting and an objective lens approximately -38.8 nm defocused.

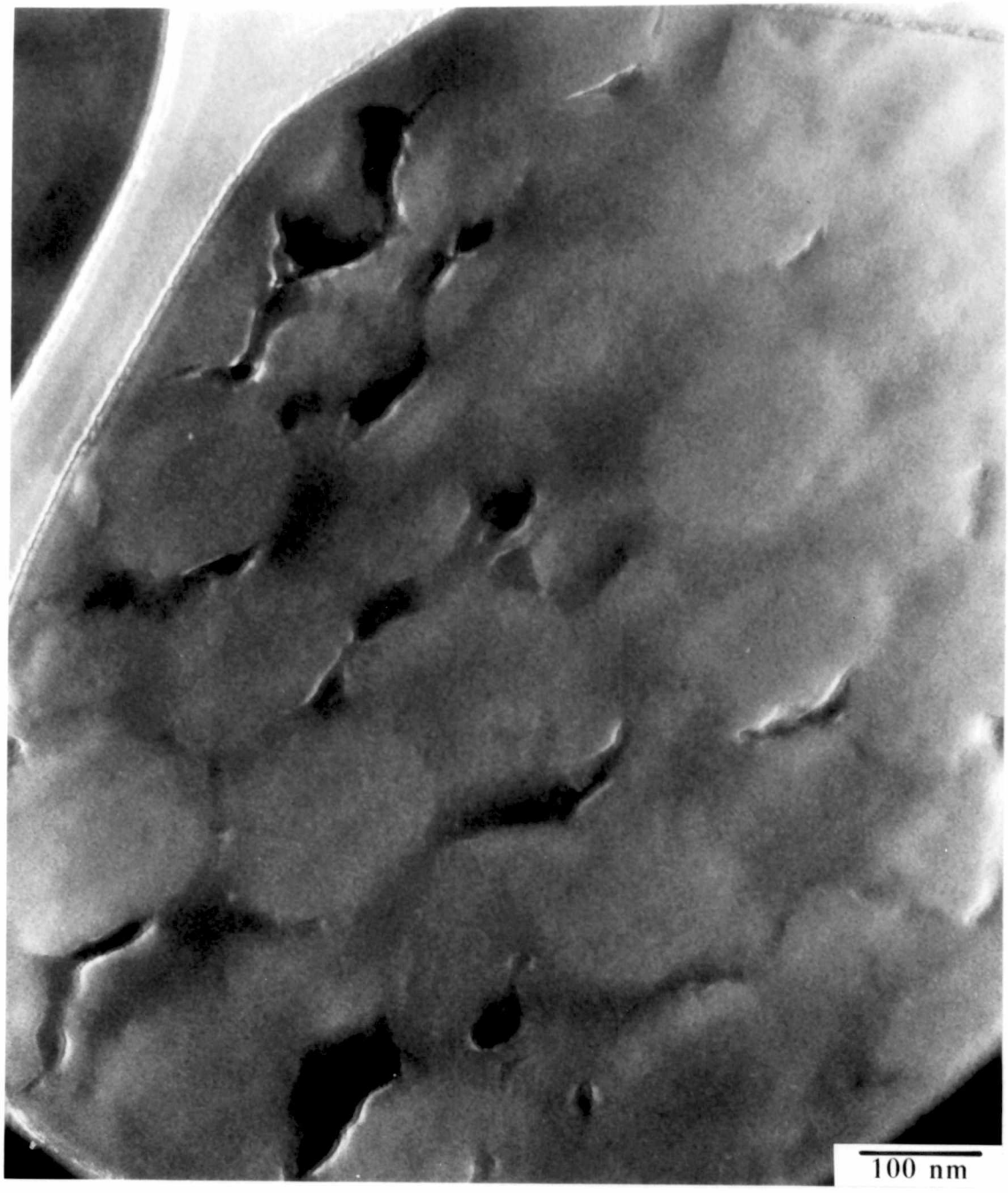

Figure 6.34. A phase contrast image of an ultramicrotomed thin section of a latex film taken using an electrostatic phase plate, a 30 μm condenser aperture, a #1 CL1 setting and an objective lens approximately -38.8 nm defocused.

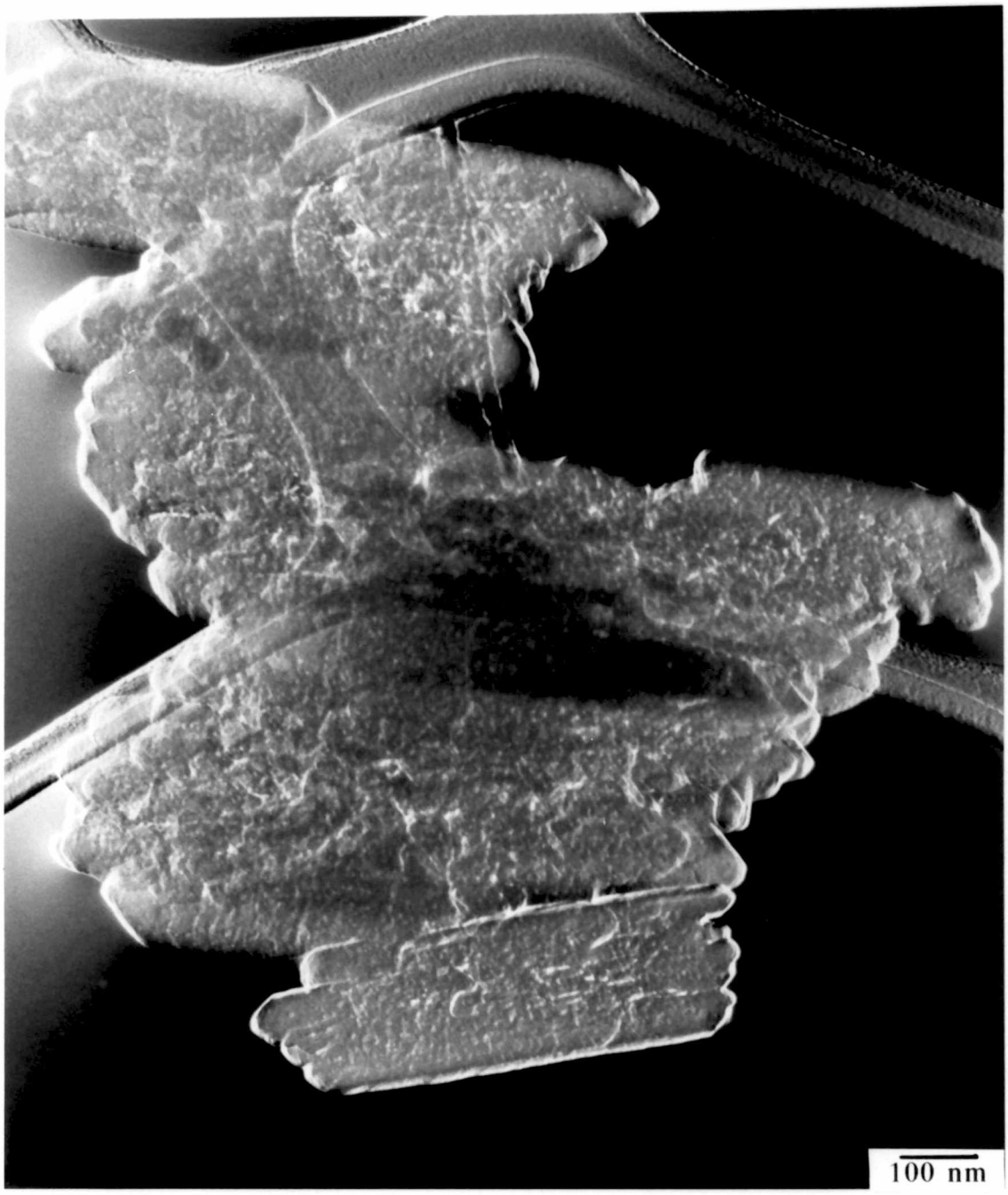

Figure 6.35. A phase contrast image of mordenite taken using a compensated electrostatic phase plate, a 30 μm condenser aperture, a #1 CL1 setting, an objective lens approximately -38.8 nm defocused and a potential of -440 volts on the aperture.

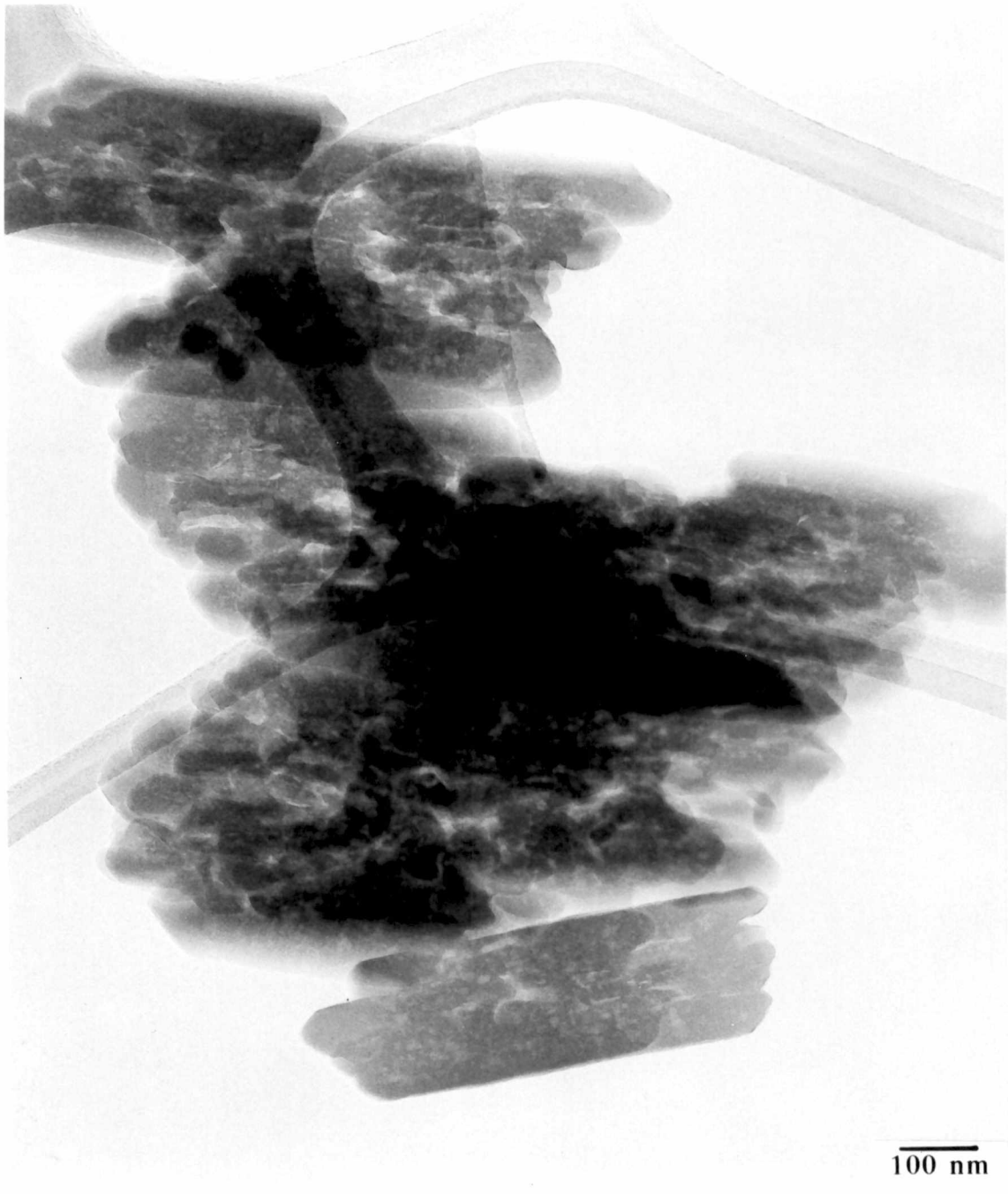

Figure 6.36. A TEM micrograph of mordenite taken using a 75 μm objective aperture, a 100 μm condenser aperture, a #3 CL1 setting and an objective lens approximately -38.8 nm defocused.

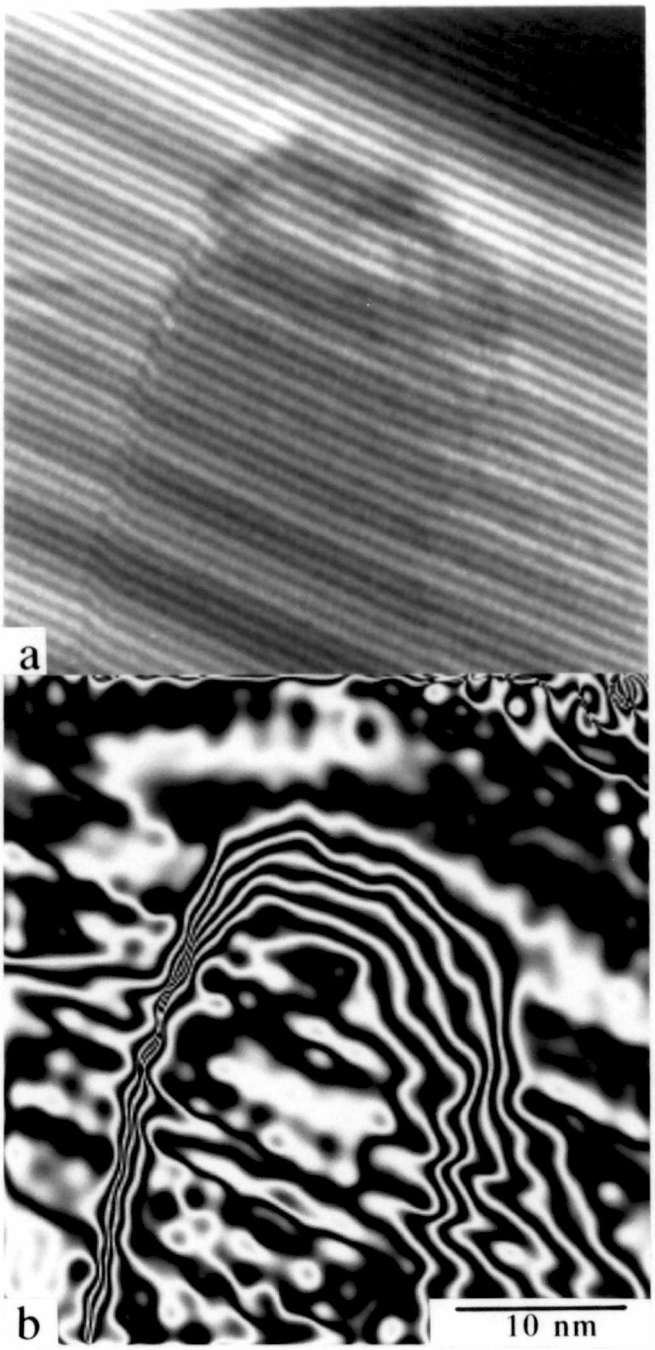

Figure 6.37. a) An electron hologram and b) an 8X amplified phase reconstruction of mordenite.

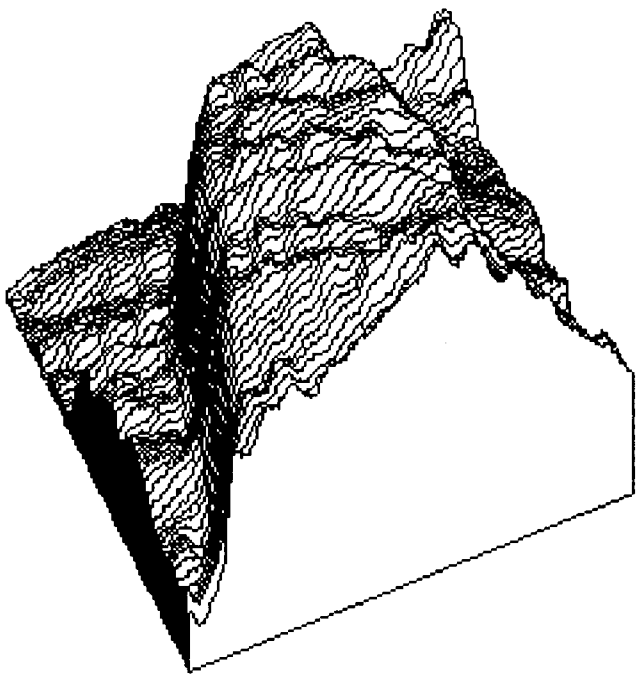

Figure 6.38. A 3D plot of figure 6.37b.

images of the mordenite crystals suspended over a lacy carbon grid clearly show the three dimensional nature of the material. Surface pores are visible down to 3 nm; however the SEM does not reveal anything about the internal porosity. (Figure 6.39)

It is clear from this comparison that the phase contrast enhancement provided by the phase plate is superior in its rendering of the large pores of this material when compared to the off axis holograms. Much of the surface detail, contained in the SEM micrographs, is also contained in the phase contrast micrograph. The clear advantage of the SEM is in imaging the pores that come to the surface.

Ultra-high resolution transmission electron microscopy using diffraction contrast can be used to examine the micropores of the mordenite (Figure 6.40). In the case of the micropores, the pore structure is delineated by the ordered arrangement of the atoms making up the crystal structure. To examine this structure the crystal must be orientated so that a long axis of the pore structure is running parallel to the optic axis. Due to the sensitivity of the material to the electron beam, the micrographs must be taken using low dose imaging techniques. In this example, it is clear that conventional high resolution bright field imaging is capable of producing high contrast images of atomic structures; however features greater than 2.5 nm have weak contrast transfer and benefit from phase contrast microscopy. This can be seen from the contrast transfer function for the 002B microscope operated at Scherzer defocus where good contrast is available for features with periodicity between approximately 0.8 and 0.2 nm (Figure 1.1). Features larger than 0.8 nm will exhibit very weak contrast. If a greater defocus is employed, contrast of larger features is improved;

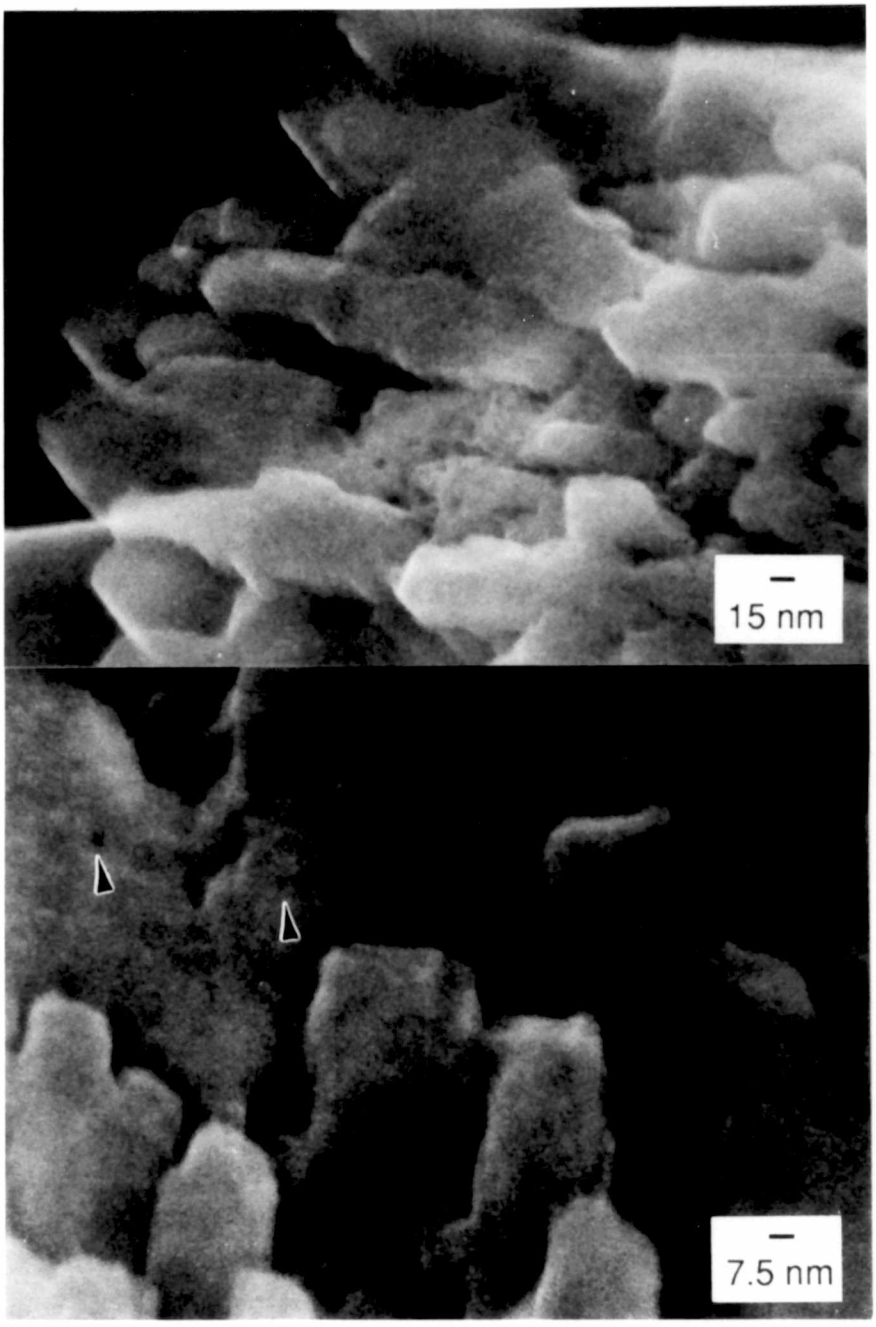

Figure 6.39. FEGSEM images of mordenite (arrows mark larger surface pores).

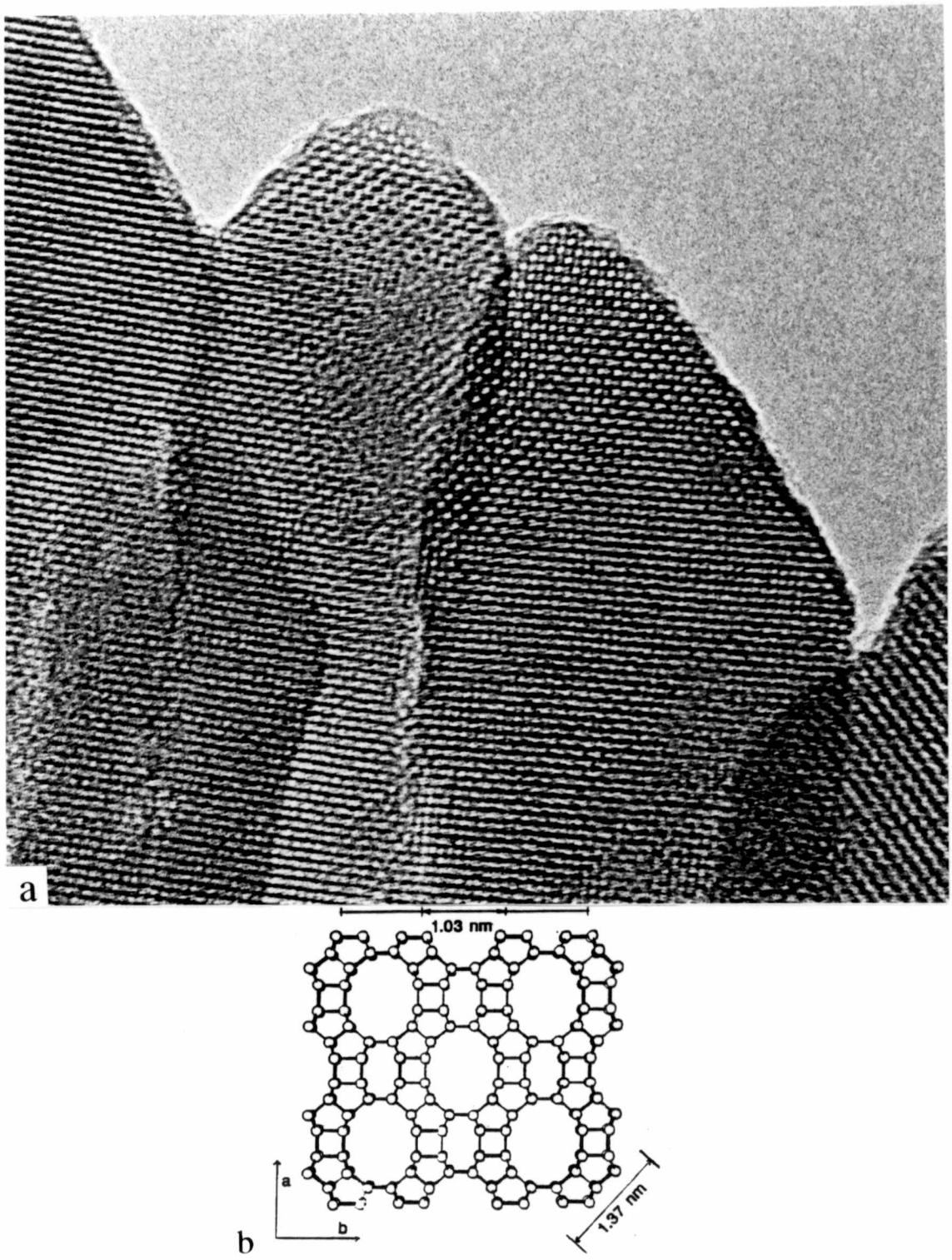

Figure 6.40. a) A high resolution TEM micrograph of mordenite showing the micropore structure and b) a schematic diagram of the molecular structure.

however finer structure contrast is marked by dramatic contrast inversions and frequent zeros making interpretation difficult (Figure 1.1).

A specimen containing both a weak phase material and a high atomic number crystalline metal was imaged using the phase plate to determine its effect on a mixed sample. For this test, a platinum catalyst on a carbon support was embedded and thin sectioned. The platinum particles ranged from approximately 1 nm to 5 nm in diameter and are easily seen in the bright field image taken with a 75 μm objective aperture (Figure 6.41). Contrast in the carbon support is low, making it difficult to resolve fine detail and to tell where the matrix carbon begins and ends. When the contamination spot phase plate is used, contrast in the carbon is dramatically improved making it easy to resolve areas of ordered structure and porosity (Figure 6.42). The high contrast in the carbon makes it difficult to identify the platinum particles that have inverted contrast when compared to the bright field image. In this mode, it would be difficult to identify the platinum particles without having the normal bright field image side by side for direct comparison with the image produced using the phase plate. For imaging mixed phase materials having components that are considered both weak and strong phase, it is advantageous to utilize both a phase plate and a conventional objective aperture. The phase plate is used to enhance contrast of the weak phase material and the objective aperture is used to enhance contrast of the strong phase or strongly diffracting material.

A contamination spot centrally deposited on a thin amorphous substrate suspended over a gold aperture proved to be useful for phase contrast enhancement. The significant contrast enhancement was quite different than that reported by Johnson and Parsons (1973). Their inability to enhance contrast is believed to be due to their failure to center the contamination spot in

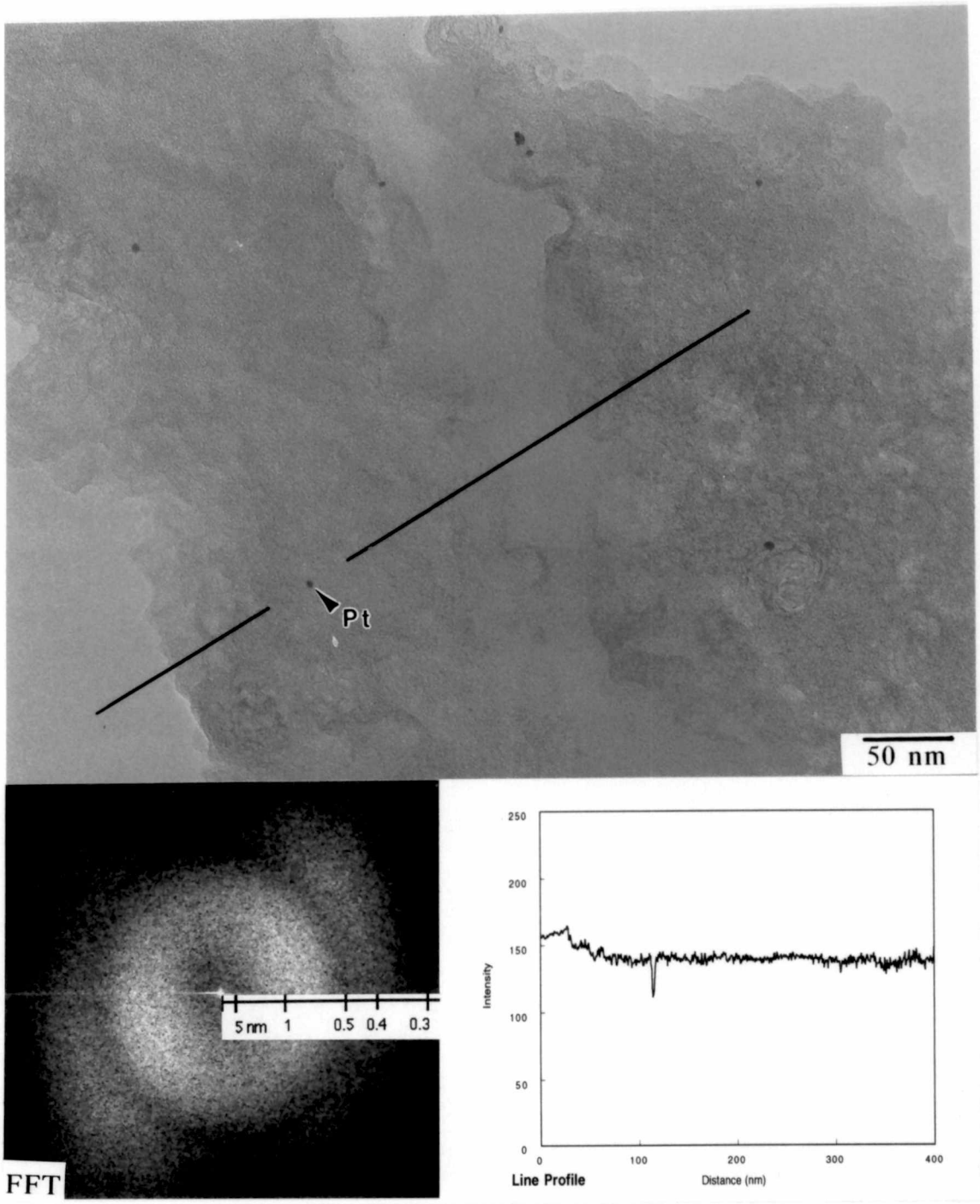

Figure 6.41. A TEM micrograph of an ultramicrotomed thin section of a platinum catalyst on a carbon support taken using a 75 μm objective aperture, a 100 μm condenser aperture, a #3 CL1 setting and an objective lens approximately -38.8 nm defocused.

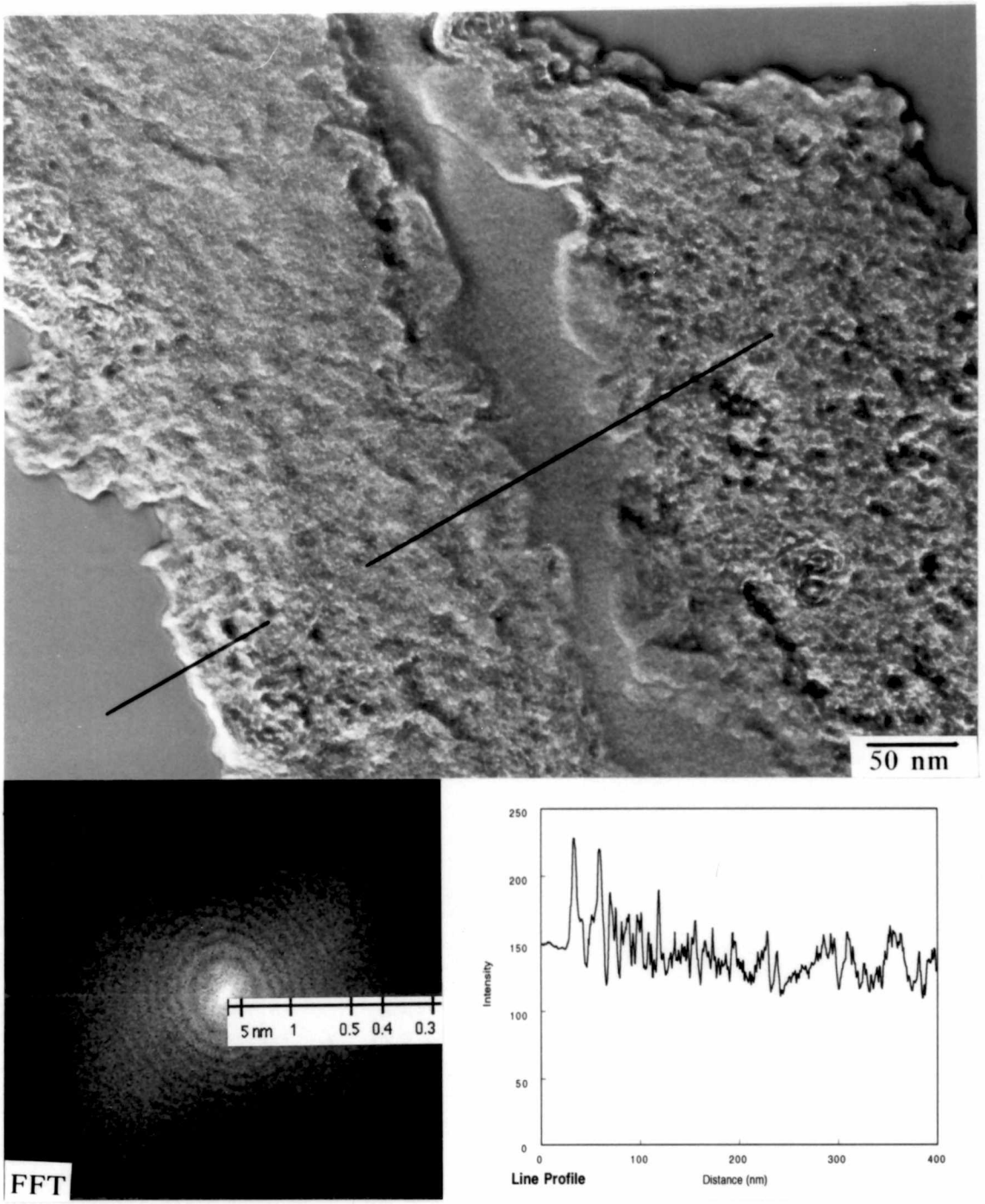

Figure 6.42. A phase contrast image of an ultramicrotomed thin section of a platinum catalyst on a carbon support taken using a contamination spot phase plate, a 100 μm condenser aperture, a #3 CL1 setting and an objective lens approximately -38.8 nm defocused.

an aperture and their use of a thicker supporting film. Both of these problems were overcome in the current study.

The shortcomings of Unwin's (1971; 1972; 1973; 1974) electrostatic device were overcome through the use of a cleaner microscope, more precise aperture translator and the use of a field compensation circuit. The ability to control the field strength independently of the illuminating conditions has resulted in a phase plate that can be practically used to generate and record phase enhanced images using short (2-4 second) exposure times. This is in contrast to the 40-60 second exposure times required without compensation.

This work has also demonstrated the advantages of phase contrast enhancement using phase plates when employed to image ultramicrotomed sections of both unstained biological materials and man made materials. Except for the work of Unwin (1971; 1972; 1973; 1974) most previous work was focused on the development and characterization of the phase plate. Unwin successfully used his electrostatic phase plate to image Tobacco Mosaic Virus revealing detail not seen before. The present work has been applied to the characterization of many materials not easily imaged using conventional TEM. The phase plate has revealed: the distribution of pores in porous latex particles and the large pores in a zeolite; cellular organelles in unstained bacteria sections; the position of latex particles in a latex film and; the location of polymer phases in a three component blend.

CHAPTER SEVEN

CONCLUSION

In conclusion, this work has demonstrated the utility of phase contrast transmission electron microscopy to study of weak phase materials including biological structures, polymers and thin amorphous and crystalline materials. Three devices were developed that are effective phase plates providing the necessary phase shift and intensity reduction of the unscattered electron wave front to generate substantial contrast enhancement. One, the contamination spot phase plate functions by retarding the unscattered electron wavefront through physical interaction with an amorphous mass. The other two designs are based upon a quartz filament drawn across an aperture and function by creating an electrostatic field generated by a point charge on the filament as a result of its interaction with the unscattered wavefront. The first design required that the illuminating conditions be precisely adjusted to generate the desired field for good contrast enhancement. The second incorporated a means to control the field strength by charging the aperture independently of the filament. This modification provided flexibility in the selection of illumination conditions.

The compensated electrostatic phase plate is more broadly applicable for general use due to the ability to record phase contrast images using short exposure times and it could be easily heated to reduce contamination build up. A disadvantage of this device compared to the contamination spot phase plate is the need to adjust the aperture bias to reduce double images and ghosting while still providing contrast enhancement.

With further refinement, the compensated electrostatic phase plate could be fitted to most commercially available TEM columns by exchanging the objective aperture holder for a holder designed to hold the phase plate. Many microscopes do not perform as clean as the one used in this present work making it desirable to heat the phase plate to reduce contamination resulting in a longer usable life. The electrical feed through for both the heater and compensator should be incorporated in the aperture holder to simplify the installation and eliminate the need for an additional port. The phase plate should be developed to occupy only one of the aperture slots with the remaining positions having a range of aperture diameters for conventional imaging. The most effective aperture size for phase plate construction should be evaluated for the common microscope accelerating voltages.

Alternative methodologies of fabrication should be explored that would make mass production possible. Micromachining or lithographic techniques might provide some options. The aperture retaining mechanism would be modified to provide phase plate and aperture anchoring without the use of adhesives. A modular phase plate design that would enable easy exchange in the event of failure or excessive contamination would be desirable.

The placement of the phase plate at the plane of the selected area aperture should be evaluated. If the device is as effective at this location, it would provide several advantages including additional space for the device as the intermediate lens gap is not as small and the dimensions of the device need not be so restrictive. In addition, the device could be used in this location without affecting the performance of the energy dispersive x-ray detector. In most TEM's, significant x-ray contribution is generated due to scatter off the objective aperture.

It is believed that the technology exists to overcome these problems and that a device could be constructed that would have broad appeal for the microscopist who images weak phase materials. The device, when not in use, would not interfere in any way with the microscope's normal operation. The phase plate also provides the advantage of phase contrast enhancement without the need of an expensive field emission gun.

Additional work is required to test the usefulness of the device in imaging magnetic domains of ferroelectric materials and to develop methodologies to quantitate the phase shift between different elements of the image. This may be possible through post processing schemes where a pure amplitude contrast image is subtracted from the combined phase and amplitude contrast image. A standard having known thickness would be useful as a test sample. A spherical latex sphere or a folded carbon foil would be useful for this purpose.

LIST OF REFERENCES

LIST OF REFERENCES

Abbe E. 1873 Beitrage zur theorie des mikroskops und der mikroskopischen wahrnehmung, *M. Schutzes Archiv f. mikr. Anatonie* **9**:413-468.

Agar A. W., Revell R.S.M., Scott R.A. 1949 A preliminary report on attempts to realize a phase contrast electron microscope, *Proceedings of the Conf. on Elect. Micro,* Delft.. Netherlands Physical Society, Amsterdam, 52-54.

Badde H.G., Reimer L. 1970 Der Einfluβ einer streuenden phasenplatte auf das eletstronenmikroskopisck bild, *Zeitschrift fur naturforschung* **A 26(5)**: 760-765.

Balossier G., Bonnet N. 1981 Use of an electrostatic phase plate in TEM. Transmission electron microscopy: Improvement of phase and topographical contrast, *Optik* **58(6)**:361-376.

Barer R. 1952a A vector theory of phase contrast and interference contrast I. Positive phase contrast, *J. Roy Micr. Soc.* **72**:10-38.

Barer R. 1952b A vector theory of phase contrast and interference contrast II. Positive phase contrast, *J. Roy Micr. Soc.* **72**:81-98.

Barer R. 1953 A vector theory of phase contrast and interference contrast III. Negative phase contrast, *J. Roy Micr. Soc.* **73**:30-39.

Barer R. 1954 A vector theory of phase contrast and interference contrast IV. B type phase contrast, *J. Roy Micr. Soc.* **74**:206-215.

Barer R. 1955 A vector theory of phase contrast and interference contrast V. Interference contrast, *J. Roy Micr. Soc.* **75**:23-37.

Blackson, J.H. , Zhang X., Garces J.M., Joy D.C. 1994 Electron holography, high resolution scanning and high resolution transmission electron microscopy characterization of dealuminated mordenite, Proceedings of the 28th Microbeam Analysis Society, edited by John Friel, VCH Publishers, 181-182.

Boersch, H. 1947 Über die fontraste von atomen im elektronenmikroskop, *Z. Naturforschg* **2a**:615-633.

Bonnet N., Troyon M., Gallion P. 1978 Possible applications of Fraunhofer holography in high resolution electron microscopy. *Proc. 9th Int. Congr. Electron Micros, Toronto* **1**:222-223.

Bradley F.G., Joy D.C. 1991 Spreadsheet program for calculation secondary electron trayectorier in electrostatic fields, *Proc. 49 Ann. Meeting EMSA, San Jose,* edited by G.W. Bailey and E.L. Hall, San Francisco Press Inc., 534-535.

Brock J.M., Otten, M. T, deJong, M.J.C. 1992 Performance and applications of a field-emission gun TEM/STEM, *Proceedings 50th EMSA*, edited by G.W. Bailey, J. Bentley, J.A. Small, San Francisco Press Inc., 942-943.

Cowley, J. 1988 High resolution transmission electron microscopy and associated techniques, in *Imaging,* edited by Buseck P.R., Cowley J.M. Eyring L., Oxford University Press, 3-37.

Cullis A., Maher D. 1974a High-resolution topographical imaging by direct transmission electron microscopy, *Phil Mag.* **30**:447-451.

Cullis A., Maher, D. 1974b High resolution observations of topographical contrast using transmission electron microscopy, *Proc. 32 Ann. Meeting EMSA, St. Louis,* edited by G.W. Dailey and E.L. Hall, San Francisco Press Inc., 394-395.

Cullis A., Maher D. 1975 Topographical contrast in the transmission electron microscope, *Ultramicroscopy* **1**:97-112.

Downing K.H., Siegel B.M. 1973 Phase shift determination in single-sideband holography, *Optik* **38**:21-28.

Downing K.H., Siegel B.M. 1975 Discrimination of heavy and light components in electron microscopy using single-sideband holographic techniques, *Optik* **42(2)**:155-175.

Dupouy G. , Perrier F., Enjalbert L., Lapchine L. and Verdier P. 1969 Accroissement du contrase des images d'objets amorphes en microscopie electronique, *C.r. hebd. Seanc. Acad Sci.*, Paris **B268**:1341-1345.

Dupouy G., Perrier F. and Verdier P. 1966 Sur une methode permettant d'ameliorer le contraste des images en microsocope electronique, *C.r. hebd. Seanc. Acad. Sci.*, Paris **B262**:1063-1068.

Faget J., Fagot M. and Fert C. 1960 Microscopie electronique en eclairage coherent: microscopie interferentielle, contraste de defocal isation, strioscopie et contraste de phase, *Proc. Eur. Conf. Electron Microscopy Delft.* Netherlands Physical Society, Amsterdam, **1**:18-24.

Faget J., Fagot M., Ferre J., Fert C. 1962 Microscopie electroniaue a contraste de phase, edited by A. Houwink & B. Spit, *5th International Congress for Electron Microscopy,* Academic Press Inc. **A7**.

Faget J., Ferre J., Fert C. 1960 Contraste de phase en microscopie electronique, *Academic Des Sciences* **251**:526-528.

Gabor D. 1948 A new microscopic principle., *Nature* **161**:777-778.

Gabor D. 1949 Microscopy by reconstructed wave-fronts, *Proc. Roy. Soc. London* **A197**:454-486.

Gabor D. 1951 Microscopy by reconstructed wave-fronts, *Proc. Roy. Soc. London* **B64**:449-469.

Haine M.E., Mulvey T.J. 1952 The formation of the diffraction image with electrons in the Gabor diffraction microscope, *Opt. Soc. Am.* **42**:763-773.

Hanszen K.J. 1969 Einseitenband-Holographie, *Z. Naturforsch* **24a**:1849.

Hanszen K.J. 1970 In-line holographic reconstruction methods in electron microscopy. *Proceedings 7th International Congress Electron Microscope, Grenoble*, edited by Favard, Soc. Francaise de Microsc. Electronique **1**:21-22.

Hanszen K.J. 1973 Contrast transfer and image processing in *Image Processing and Computer Aided Design in Electron Optics* edited by P. Hawkes, Academic Press, 16-53.

Hanszen K.J., Morgenstern B. 1965 Die phasenkontrast-und amplituden kontrast-Übertragung des elektronemmikroskopischen objektivs, *Z. angew Phys.* **19**:215-227.

Haydon G.B., Lemons R. 1972 Optical shadowing in the electron microscope, *J. of Microscopy* **95(3)**:483-491.

Heidenreich R. 1964 *Fundamentals of Transmission Electron Microscopy*, Interscience Publishers, New York 136-143.

Hoppe W. 1963 Fresnelsche zohenkorrekturplatten für das elektronenmikroskop, *Optik* **20**:599-606.

Hoppe W. 1970 Principles of electron structure research at atomic resolution using conventional electron microscopes for the measurement of amplitudes and phases, *Acta Cryst* **A26**: 414-26.

Hoppe W. 1971 Zur abbildung komplexer bildfunktionen in der elekronenmikroskopie, *Z. Naturforsch* **26a** :1155-1168.

Hoppe W., Langer R., Thon F. 1970 Verfahren zur rekonstruktion komplexer bildfunktionen in der elektronenmikroskopie, *Optik* **30**:538-545.

Johnson D.J., Crawford D. 1973 Defocusing phase contrast effects in electron microscopy, *J. of Microscopy* **98(3)**:313-324.

Johnson H.M., Parsons D.F. 1967 Four-stage E.M. for phase contrast and strioscopic microscopy. *Proc. 25th EMSA Meeting, Chicago* edited by J. Arceneaux, Claitor's Book Store, 236-237.

Johnson H.M., Parsons D.F. 1970 In-focus phase contrast electron microscopy, *Proceedings of the 7th International Congress on Electron Microscopy,* Gernoble, edited by Favard, Soc. Francaise de Microsc. Electronique **1**:71-72.

Johnson H.M., Parsons D.F. 1973 Enhanced contrast in electron microscopy of unstained biological material III In-focus phase contrast of large objects, *Journal of Microscopy* **98(1)**:1-17.

Joy D.C., Maher, D.M. 1977 Sensitivity limits for thin specimen x-ray analysis, *Proceedings of the Workshop on Analytical Electron Microscopy IIT Research Institute, Chicago, Ill.*, edited by O. Johari1:325-334.

Joy D.C., Bunn R.D. 1993 Software for the reconstruction of off-axis electron holograms, *Proc. 51st MSA Meeting* edited by G.W. Bailey and C.L. Rieder, San Francisco Press Inc., 550-551.

Kanaya K., Kawakatsu H., Ishikawa A. 1957 Preliminary experiment on the electron phase microscope, *Bulletin of the Electrotechnical Laboratory* **21(11)**:25-33.

Krakow W., Siegel B. 1975 Phase contrast in electron microscope images with an electrostatic phase plate, *Optik* **42(3)**:245-268.

Leclerc G., Sanche L. 1990 Spreadsheets for computing charged-particle trajectories in 3-D electrostatic fields, *Computer in Physics* Nov/Dec: 617-626.

Leith E.N., Upatnicks J.J. 1962 Reconstructed wavefronts and communication theory, *J. of Opt. Soc. Am.* **52(10)**:1123-1130.

Lenz F. 1963 Zonenplatten zur offnungsfehlerkorrektur und zur kontrasterholhung, *Z. Phys.* **172**:498-502.

Lichte H. 1991 Electron image plane off-axis holography of atomic structure, *Advances in Optical and Electron Microscopy* **12**:25-91.

Locquin M. 1954 L'influence des modifications pupillaires de L'objectif sur les contrastes en microscopie electronique, *Proc. 3rd Inf. Conf. on EM, London,* edited by R. Ross Royal Microscopy Society, London, 285-289.

Möllenstedt G., Duker H. 1956 Beobachtungen und Messungen an biprisma-interferenzen mit elektronenwellen, *Zeitschrift fur Physik*, **145**:377-397.

Möllenstedt G., Speidel R., Hoppe W., Langer R., Katerbau K., Thon F. 1968 Electron microscopical imaging using zonal correction plates, *4th European Regional Conference on Electron Microscopy, Rome*, 125-126.

Müller K.H. 1970 Micro-recording by use of the Elmiskop 101, *Proceedings 7th International Congress on Electron Microscopy, Grenoble,* edited by Favard Soc. Francaise de Microsc. Electronique, **1**:183-184.

Müller K.H. 1976 Phasenplatten fur elektronenmikroskope, *Optik* **45(1)**:73-85.

Müller K.H, Rindfleisch V. 1971 Applications of a micro-recording device, *Proc. 29 EMSA Meeting, Boston,* edited by J. Arceneaux, Claitor's Publishing Division, 48-49.

Munch J. 1975 Experimental electron holography, *Optik* **43(1)**:79-79.

Nakahara S., Cullis A., Maher D. 1975 Theory of topographical image contrast, *Proceedings of the 33rd Meeting of EMSA, LasVegas*, edited by G.W. Bailey Claitor's Publishing Division: 188-189.

Nakahara S., Cullis A.G. 1977 Half-plane and topographical contrast in the TEM--theoretical considerations, *Inst Phys. Conf. Ser.* **36**:263-266.

Orchowski A., Rau W.D., Lichte, H. 1995 Electron holography surmounts resolution limit of electron microscopy, *Phys. Rev. Letters* **74(3)**:399-402.

Parsons D.F., Johnson H.M. 1972 Possibility of a phase contrast electron microscope, *Applied Optics* **11(12)**:2840-2843.

Parsons J.R. 1976 High resolution bright-field phase contrast microscopy, *Microscopical Society of Canada,* **111**:2-5.

Pluta M. 1989 *Advanced Light Microscopy,* Polish Scientific Pub., Amsterdam, **2**:1-66.

Reimer L. 1993 *Transmission Electron Microscopy Physics of Image Formation and Microanalysis,* Springer-Verlag.

Reimer L., Badde H.G. 1970 Einfluss der elektronenstreuung in einer phasenplatte auf die abbildung von einselatomen, *Proceedings of the 7th International Congress on Electron Microscopy, Paris*, 15-16.

Ruska E. 1966 Past and present attempts to attain the resolution limit of the transmission electron microscope in *Optical and Electron Microscopy* edited by Barer and Cosslett Academic Press, 116-178.

Scales D.J. 1974 A Fourier approach to optical shadowing with a transmission electron microscope, *J. Microsc.* **102**:49-58.

Scherzer O. 1949 The theoretical limit of the electron microscope, *Journal Appl. Physics* **20**:20-29.

Shi S.L., Sun S.Q., Nash T.E., Leapman R.D. 1994 Characterization of cryosectioned cell suspensions by STEM, *Proceedings 52 Annual Metting Microscopy Society of America, New Orleans,* edited by Bailey G.W. and Garratt-Reed A.J., San Francisco Press Inc., 136-137.

Shushurin S.F. 1971 On the history of holography. *Usp. Fix. Nauk*, **105**:145-148.

Thon F., Siegel B.M. 1970 Zonal filtering in optical reconstruction of high resolution phase contrast images. *Microscopie Electronique, Paris* **1**:13-14.

Thon F., Willasch D. 1970 Hochauflosungs-elektronenmikroskopie mit spezialaperturblenden und phasenplatten, *Proceedings of the 7th International Congress on Electron Microscopy, Grenoble*, edited by Favard Soc. Francaise de Microsc. Electronique **1**:3-4.

Thon F., Willasch D. 1971a High resolution electron microscopy using phase plates, *Proceedings of the 29th Meeting of EMSA, Boston*, edited by J. Areneaux, Claitor's Publishing Division, 38-39.

Thon F., Willasch D. 1971b A calibration method usable in the production of phase plates for high resolution electron microscopy, *Proceedings of the 29th Meeting of EMSA, Boston*, edited by J. Areneaux, Claitor's Publishing Division, 46-47.

Thon F., Willasch D. 1972 Recent results in high resolution microscopy with special apertures, *Proceedings Fifth European Congress on Electron Microscopy, Manchester*, Inst. Phys. London, 650-651.

Tochigi H., Nakatsuka H., Fukami A., Kanaya K. 1970 The improvement of the image contrast by using the phase plate in the transmission electronmicroscope, *Septieme Congress International De Microscopie Electronique, Gernoble,* edited by Favard, Francaise de Microscopie Electroniques, 73-74.

Tonomura A. 1987 Applications of electron holography, *Rev. Mod. Phys.* **59(3)**:639-669.

Tonomura A., Fukuhara A., Watanabe H., Komoda T. 1968 Optical reconstruction of image from Fraunhofer electron-hologram, *Japan J. Appl. Phys.* **7**:295.

Unwin P.N.T. 1971 Phase contrast and interference microscopy with electron microscope, *Phil. Trans. Roy. Soc. London* **B261**:95-104.

Unwin P.N.T. 1972 Electron microscopy of biological specimens by means of an electrostatic phase plate, *Proceedings of the Royal Society of London* **A329(1578)**:327-359.

Unwin P.N.T. 1973 Phase contrast electron microscopy of biological materials, *J. of Microscopy* **98(3)**:299-312.

Unwin P.N.T. 1974 A new electron microscope imaging method for enhancing detail in thin biological specimens, *Z. Naturforsch* **29A**:158-163.

Vanzi M. 1984 Theoretical model for studying electrostatic potenials by means of Lorentz Microscopy, *Optik* **68(4)**:319-333.

Völkl E., Lichte H. 1990 Electron holograms for subagstrom point resolution. *Ultramicroscopy* **32**:177-180.

Willasch D. 1975 High resolution electron microscopy with profiled phase plates, *Optik* **44(1)**:17-36.

Wolfke, M. 1920 Über die Moglichkeit der optischen abbildung von molkulargittern, *Physikalische Zeitschrift* **21**:495-497.

Zhang X. 1992 New electron beam methods for materials microcharacterization, *Dissertation Univ. of Tennessee Knoxville.*

Zernike F. 1935a Das phasenkontrast verfahren bei der mikroskopschen beobachtung, *Phys. Zeitschrift* **23**:848-851.

Zernike F. 1935b Das phasenkontrast verfahren bei der mikroskopischen beobachtung, *Z. Techn. Physik* **16**:454-457.

Zernike F. 1942a Phase contrast, a new method for the microscopic observation of transparent objects, part 1, *Physica* **9(7)**:686-693.

Zernike F. 1942b Phase contrast, a new method for the microscopic observation of transparent objects, part 2, *Physica* **9**:974-986.

VITA

John Henry Blackson was born in Wyandotte, Michigan on May 12, 1956 to Stanley and Doris Blackson. He attended elementary and secondary schools in the Wyandotte Public Schools and graduated from the Wyandotte Roosevelt High School in June 1974. The following September he started at Michigan State University where he graduated with two Bachelor of Science degrees, one in Botany and one in Biology, and a Michigan secondary school teaching certificate in March 1979. The following September he started back at Michigan State University and earned a Masters of Science degree in Botany in June 1991. The thesis was entitled Cytological, Statistical and Transmission Electron Microscopy Studies of Secondary Association in the Genus *Phaseolus*. While working on his Masters degree he also earned an Associate Degree of Science specializing in photography from Lansing Community College on August 1980. Upon graduation John accepted a 9 month position with the Bowling Green State University Electron Microscopy Center as the Technical Director. Next he accepted a position as the Manager of the University of Southwestern Louisiana Electron Microscopy Center where he served for 2 1/2 years. John then began his career at The Dow Chemical Company where he works in the Microscopy and Microanalysis group, a position he has had since December, 1994. John is currently a Research Leader at Dow and has received many Dow awards and honors. While at Dow he pursued a Doctor of Philosophy degree in Zoology which he earned in December 1995.

John has published in the areas of electron microscopy, geology and polymer science. He is a member of the Microscopy Society of America, Microbeam Analysis Society, and is currently the President of the Michigan Electron Microscopy Society.